

Weak decays of B_c involving vector mesons in self-consistent covariant light-front approach

Thejus Mary S.^{1*}, Avijit Hazra^{1†}, Neelesh Sharma^{2‡}, and Rohit Dhir^{1§}

¹*Department of Physics and Nanotechnology,*

SRM Institute of Science and Technology, Kattankulathur 603203, India.

²*Paradigm of Science Cultivation and Ingenious, Kangra 176032, India.*

Abstract

We present a comprehensive analysis of weak transition form factors, semileptonic decays, and nonleptonic decays of B_c meson involving pseudoscalar (P) and vector (V) meson for bottom-conserving and bottom-changing decay modes. We employ self-consistent covariant light-front quark model (CLFQM), termed as Type-II correspondence, to calculate the B_c to $P(V)$ transition form factors. The Type-II correspondence in the CLF approach gives self-consistent results associated with the $B_j^{(i)}$ functions, which vanish numerically after the replacement $M^{(i)} \rightarrow M_0^{(i)}$ in traditional Type-I correspondence, and the covariance of the matrix elements is also restored. We investigate these effects on bottom conserving $B_c \rightarrow P(V)$ form factors that have not yet been studied in CLFQM Type-II correspondence. In addition, we quantify the implications of self-consistency propagating to weak decays involving both bottom-conserving and bottom-changing B_c transition form factors. We use two different parameterizations, the usual three-parameter function of q^2 and the model-independent z -series expansion, to establish a clear understanding of q^2 dependence. Using the numerical values of the form factors, we predict the branching ratios and other physical observables, such as, forward-backward asymmetries, polarization fractions, etc., of the semileptonic B_c decays. We extend our analysis to predict the branching ratios of two-body nonleptonic weak decays using the factorization hypothesis in self-consistent CLFQM. We also compare our results with those of other theoretical studies.

* thejusmarys@gmail.com

† hazra.avijit@outlook.com

‡ nishu.vats@gmail.com

§ Corresponding author: dhir.rohit@gmail.com

I. INTRODUCTION

The B_c meson is a quark-antiquark bound-state composed of two heavy quarks (b and c) with distinct flavors that decays solely via weak interactions [1]. The study of B_c meson decays provide valuable insights into the fundamental aspects of the Standard Model (SM) and offers a unique platform to explore the underlying heavy flavor dynamics, which is of immense experimental and theoretical significance. A peculiarity of B_c decays, compared to B and B_s decays, is that both constituent quarks are involved in weak decays, *i.e.*, b quark decays with c quark as spectator, and c quark transitions with spectator b quark, in addition to weak annihilation of constituent quarks. The weak annihilation processes decay to leptons or lighter mesons that are relatively suppressed, and are, therefore, ignored in the current analysis. The phase space available for c quark decays is significantly smaller compared to b quark decays, but the Cabibbo-Kobayashi-Maskawa (CKM) matrix elements strongly favor c quark decays [1, 2]. The study of heavy flavor weak decays is a powerful tool to test SM and search for new physics (NP) beyond SM. The semileptonic decays are governed by tree-level processes in the SM, which provides a relatively simple theoretical description to capture the effects of the weak interaction in terms of Lorentz invariant form factors. In addition, these decays are of immense importance for extracting the CKM matrix elements (and their phases), and studying lepton flavor universality (LFU). On the other hand, the study of two-body weak decays of B_c mesons offers an excellent opportunity to explore quantum chromodynamics (QCD) in both perturbative and nonperturbative regimes to understand the interplay of strong and electroweak interactions. Additionally, these decays allows for testing QCD-motivated effective theories and models within and beyond the SM.

Currently, modern experimental collaborations such as LHCb, CMS, ATLAS, and CDF have been exploring the B_c meson to provide valuable insights into heavy flavor physics in the SM and NP. The Large Hadron Collider (LHC) and Relativistic Heavy Ion Collider (RHIC) are expected to produce sizable number of B_c meson events (about 10^6) via the proton-nucleus and nucleus-nucleus collision modes [3]. Therefore, in the near future it would be possible to study the B_c meson properties by using more collision modes other than the usually considered proton-proton collision mode. In the recent past, the LHCb has reported precise measurement of B_c meson mass and lifetime as $M_{B_c} = 6274.47 \pm 0.27 \pm 0.17$ MeV and $\tau_{B_c} = 0.5134 \pm 0.011 \pm 0.0057$ ps, respectively [4, 5]. Although the spectroscopy and decays of B_c meson are being probed extensively, their experimental observations and measurements are scarce [6–8]. So far, the LHCb has reported the observation of two-body nonleptonic $B_c^+ \rightarrow B_s^0 \pi^+$ decay [9] and their experimental efforts have resulted in the observation of B_c decays involving two charm mesons, such as, $B_c^+ \rightarrow D_{(s)}^{(*)+} \bar{D}^{(*)0}$ and $B_c^+ \rightarrow D_{(s)}^{(*)+} D^{(*)0}$ [10–12]. Recently, LHCb and ATLAS reported the ratios of branching fractions of two-body nonleptonic B_c decays involving a J/ψ meson in the final state, *i.e.*, $\frac{\mathcal{B}(B_c^+ \rightarrow J/\psi D_s^{(*)+})}{\mathcal{B}(B_c^+ \rightarrow J/\psi \pi^+)}$, $\frac{\mathcal{B}(B_c^+ \rightarrow J/\psi D_s^{*+})}{\mathcal{B}(B_c^+ \rightarrow J/\psi D_s^+)}$, and $\frac{\mathcal{B}(B_c^+ \rightarrow J/\psi K^+)}{\mathcal{B}(B_c^+ \rightarrow J/\psi \pi^+)}$ [13–16]. Even though there exist observations of a few semileptonic and nonleptonic decays of the B_c meson, more efforts are required for precise experimental measurements. Interestingly, the LHCb collaboration reported the LFU ratio for J/ψ in the final state as $\mathcal{R}_{J/\psi} = 0.71 \pm 0.18 \pm 0.17$ [17]. However, this ratio significantly exceeds the theoretical estimates, including the lattice QCD (LQCD) results [18]. Such discrepancies between theory and

experiment garner significant attention to physics beyond the SM.

Considering the imminent advancements in precision measurements of the B_c meson at hadron colliders and B -factories, several theoretical models, such as LQCD, QCD sum rules (QCDSR), Bethe-Salpeter (BS) model, covariant light-front quark model (CLFQM), relativistic quark model (RQM), relativistic constituent quark model (RCQM), relativistic independent quark model (RIQM), perturbative QCD (pQCD) approach, QCD factorization (QCDF) approach, etc., studied the semileptonic and nonleptonic B_c meson decays involving pseudoscalar (P) and vector (V) mesons [19–40]. In this work, we study the semileptonic and nonleptonic decays using the covariant light-front (CLF) approach. The CLFQM, apart from providing a relativistic treatment of physical quantities, has several advantages over the traditional light-front quark model (LFQM) [41–45]. In the traditional LFQM, the Lorentz covariance of the matrix element is violated due to the spurious contributions, and it does not provide any systematic approach to determine the zero-mode contributions [41, 45]. Jaus [46] proposed the CLFQM to provide resolution of these ambiguities by using the manifestly covariant BS approach [47, 48]. The CLFQM ensures covariance of the matrix elements by the inclusion of zero-mode contributions, which make the spurious contributions proportional to the light-like four-vector $\omega^\mu = (0, 2, 0_\perp)$ irrelevant [41, 46, 49]. Following this, CLFQM has been extensively used to investigate the semileptonic and nonleptonic decays of bottom mesons [28–30, 50–62].

In this study, we employ the recent advancements in CLFQM, termed as self-consistent CLFQM, to calculate the B_c to P and V meson transition form factors. The B_c meson decays involve c quark transitions, $c \rightarrow s(d)$ and b quark transitions, $b \rightarrow c(u)$. These quark-level transitions are categorized as bottom-conserving ($\Delta b = 0$) and bottom-changing ($\Delta b = -1$) CKM-favored and -suppressed modes (their selection rules are defined in Sec. II and III), respectively. It should be noted that the self-consistent CLFQM is termed as Type-II correspondence in CLFQM on account of the challenges associated with Type-I correspondence [46, 50, 51]. In the traditional Type-I scheme, the CLF predictions for the P to V transition form factors suffer from the self-consistency problem, for example, the results obtained via the longitudinal ($\lambda = 0$) and transverse ($\lambda = \pm$) polarization states are different from each other, due to the additional contributions characterized by the coefficients $B_1^{(2)}$ and $B_3^{(3)}$. These additional contributions affect $f(q^2)$ and $a_-(q^2)$ form factors only¹. Moreover, the manifest covariance of the matrix element in CLFQM is also violated within the Type-I scheme due to the residual ω -dependencies associated with $B_j^{(i)}$ functions that are independent of zero-mode contributions. Therefore, both these issues originate from the same source, which can be remarkably resolved by incorporating Type-II correspondence [59]. The CLFQM with Type-II correspondence can, however, give self-consistent results because integration over the terms associated with the coefficient $B_j^{(i)}$ vanish numerically after the replacement $M^{(\prime\prime)} \rightarrow M_0^{(\prime\prime)}$ and the covariance of the matrix elements is also restored. It should be noted that Type-II correspondence scheme has been employed to calculate the bottom-changing $B_c \rightarrow D_{(s)}^*(J/\psi)$ transition form factors [59]; however, the bottom-conserving $B_c \rightarrow B_{(s)}^*$ form factors have not yet been studied. Furthermore, the implications of self-consistency have not been investigated on the decays involving both bottom-conserving as well as bottom-changing B_c transition form

¹ The form factors $f(q^2)$ and $a_-(q^2)$ can be related to the Bauer-Stech-Wirbel (BSW) form factors $A_1(q^2)$ and $A_0(q^2)$, respectively, and their transformation relations are given in Eq. (17).

factors. It should be emphasized that the study of semileptonic and nonleptonic weak decays is necessary to quantitatively assess the effect of self-consistency on these decays. The self-consistency issues originating from form factors $A_0(q^2)$ and $A_1(q^2)$, affects the semileptonic decays of the B_c meson. On the other hand, $B_c \rightarrow PV$ decays explicitly involve $A_0(q^2)$ (other than $F_1(q^2)$) form factor and provide an excellent scenario for quantitative analysis of self-consistency issues that are expected to be more serious in these decays. We further investigate the implication of q^2 dependence on the B_c to $P(V)$ transition form factors over the available momentum range. In order to establish a clear understanding of q^2 dependence, we utilize two different parameterizations, *i.e.*, the usual three-parameter function of q^2 influenced by vector meson dominance (VMD) and model-independent z -series expansion. Furthermore, we plot these B_c to $P(V)$ transition form factors to analyze their behavior with respect to available q^2 range. Using the numerical values of the form factors, we predict the physical observables, such as branching ratios, forward-backward (FB) asymmetries, polarization fractions, etc., of the semileptonic B_c decays. In addition, we analyze the q^2 dependence of these physical observables by plotting them. Later, we extend our analysis to predict the branching ratios of two-body nonleptonic weak decays using the factorization hypothesis in self-consistent CLFQM. In addition, we also compare our results with existing results from other models.

Our paper is organized as follows. In Sec. II, we present the methodology for the calculation of form factors and its q^2 dependence in self-consistent CLFQM. In addition, we provide the decay rate expressions for semileptonic B_c to $P(V)$ and nonleptonic B_c to PV decays. In Sec. III, we give the numerical results and detailed discussions of the form factors, as well as decay rates of semileptonic and nonleptonic B_c to PV decays. We summarize and conclude in Sec. IV.

II. METHODOLOGY

A. Self-consistent covariant light-front approach

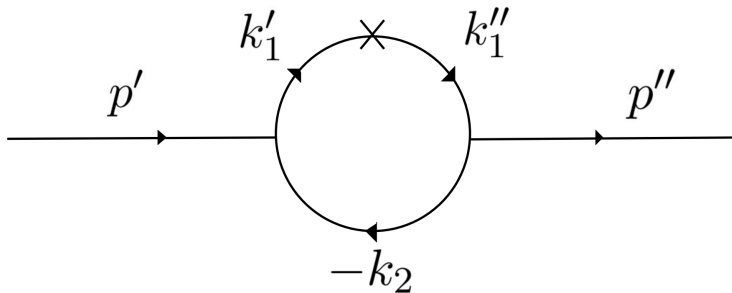


Figure 1: Feynman diagram for meson transition amplitudes, where \times denotes the vector or axial vector current vertex

In this work, we focus on the self-consistent CLF approach [46, 50, 51, 58–60] and summarize the theoretical framework to calculate the B_c to $P(V)$ form factors. In CLFQM, a meson transition, as shown in Figure 1, is represented in terms of the four momenta of the parent and daughter

mesons, *i.e.*, $p' = k'_1 + k_2$ and $p'' = k''_1 + k_2$, respectively. Here, k''_1 and k_2 represent the momenta of the quark and the antiquark of the incoming (outgoing) meson with masses, m''_1 and m_2 , respectively. These momenta can further be expressed using internal variables, namely, momentum fraction ($x_{1(2)}$) and transverse momentum (\mathbf{k}'_{\perp}) of the quark, as follows:

$$k''_{1(2)} = x_{1(2)} p'^+, \quad \mathbf{k}'_{1(2)\perp} = x_{1(2)} \mathbf{p}'_{\perp} \pm \mathbf{k}'_{\perp}, \quad (1)$$

where they must satisfy the relation $x_1 + x_2 = 1$. The meson momentum is defined as $p' = (p'^-, p'^+, \mathbf{p}'_{\perp})$ with $p'^{\pm} = p'^0 \pm p'^3$, such that $(p')^2 = p'^+ p'^- - p'^2_{\perp} = M'^2$, where M' is the mass of the parent meson. The transverse momenta of the quark and meson are given by $\mathbf{k}'_{\perp} = (k'^x, k'^y)$ and $\mathbf{p}'_{\perp} = (p'^x, p'^y)$, respectively. The definition of the internal quantities for the outgoing meson can be obtained by replacing the prime notation with a double-prime.

Conventionally, a meson bound-state (q'_1, \bar{q}_2) can be represented as

$$|M(p, {}^{2S+1}L_J, J_z)\rangle = \int \{d^3\tilde{k}_1\} \{d^3\tilde{k}_2\} 2(2\pi)^3 \delta^3(\tilde{p} - \tilde{k}_1 - \tilde{k}_2) \\ \times \sum_{h_1, h_2} \Psi_{LS}^{JJ_z}(\tilde{k}_1, \tilde{k}_2, h_1, h_2) |q'_1(k'_1, h_1) \bar{q}_2(k_2, h_2)\rangle, \quad (2)$$

where L and J are orbital angular and total spin quantum numbers, respectively [50]. Further, $\tilde{p} = (p'^+, \mathbf{p}'_{\perp})$, and $\tilde{k}_{1,2} = (k'^{\pm}_{1,2}, \mathbf{k}'_{1,2\perp})$ represent the on-mass-shell LF momenta, and $\{d^3\tilde{k}\} \equiv \frac{1}{2(2\pi)^3} d^4k'^+ d^2\mathbf{k}'_{\perp}$. The wave function $\Psi_{LS}^{JJ_z}(\tilde{k}_1, \tilde{k}_2, h_1, h_2)$, which describes the distribution of momentum in space for ${}^{2S+1}L_J$ meson, satisfies the normalization condition

$$\sum_{h_1, h_2} \int \frac{dx_1 d^2\mathbf{k}'_{\perp}}{2(2\pi)^3} |\Psi_{LS}^{JJ_z}(x_1, \mathbf{k}'_{\perp}, h_1, h_2)|^2 = 1, \quad (3)$$

and can be written as

$$\Psi_{LS}^{JJ_z}(x_1, \mathbf{k}'_{\perp}, h_1, h_2) = R_{h_1 h_2}^{SS_z}(x_1, \mathbf{k}'_{\perp}) \psi_{LL_z}(x_1, \mathbf{k}'_{\perp}). \quad (4)$$

The radial wave function $\psi_{LL_z}(x_1, \mathbf{k}'_{\perp})$ characterizes how the constituent quarks' momenta are distributed in a bound-state that possesses orbital angular momentum L [50]. The spin-orbital LF wave function ($R_{h_1 h_2}^{SS_z}$) represents the definite spin state (S, S_z) corresponding to the LF helicity (h_1, h_2) eigenstates. Additional details for the treatment of spin, polarization, and complete normalization procedure are discussed in Refs. [42, 45, 50]. A suitable choice for the radial wave function is the phenomenological Gaussian-type wave function, *i.e.*,

$$\psi(x_1, \mathbf{k}'_{\perp}) = 4 \frac{\pi^{\frac{3}{4}}}{\beta^{\frac{3}{2}}} \sqrt{\frac{\partial k'_z}{\partial x_1}} \exp\left[-\frac{k'^2_z + k'^2_{\perp}}{2\beta^2}\right], \quad (5)$$

for s -wave mesons [42]. The shape parameter, β , in Eq. (5), describes the momentum distribution and is expected to be of the order Λ_{QCD} [57]. The relative momentum k'_z (in the z -direction) is given by

$$k'_z = \left(x_1 - \frac{1}{2}\right) M'_0 + \frac{m_2^2 - m_1'^2}{2M'_0}, \quad (6)$$

which yields [51]

$$\frac{\partial k'_z}{\partial x_1} = \frac{M'_0}{4x_1(1-x_1)} \left\{ 1 - \left[\frac{m_1'^2 - m_2^2}{M_0'^2} \right]^2 \right\}, \quad (7)$$

where,

$$M'_0 = \sqrt{\frac{m_1'^2 + k_\perp'^2}{x_1} + \frac{m_2'^2 + k_\perp'^2}{x_2}}, \quad (8)$$

is the kinetic invariant mass of the incoming meson. In addition, the kinetic invariant mass of the outgoing meson is denoted as

$$M''_0 = \sqrt{\frac{m_1''^2 + k_\perp''^2}{x_1} + \frac{m_2''^2 + k_\perp''^2}{x_2}}, \quad (9)$$

with $\mathbf{k}'_\perp = \mathbf{k}' - x_2 \mathbf{q}_\perp$. The detailed formalism for the CLFQM is described in Refs. [46, 50–52, 58–60].

In general, the transition form factors $B_c \rightarrow M''$ (where $M'' = P, V$), corresponding to the Feynman diagram of Figure 1, are obtained from explicit expressions for matrix elements of currents between meson states [42],

$$\mathcal{B} \equiv \langle M''(p'') | V_\mu - A_\mu | B_c(p') \rangle, \quad (10)$$

where V_μ and A_μ are the vector and axial vector (A) currents, respectively. The form factors for B_c meson to P and V transitions are defined by the following matrix elements [50],

$$\langle P(p'') | V_\mu | B_c(p') \rangle = p_\mu f_+(q^2) + q_\mu f_-(q^2), \quad (11)$$

$$\langle V(p'', \varepsilon'') | V_\mu | B_c(p') \rangle = \epsilon_{\mu\nu\alpha\beta} \varepsilon''^{*\nu} p^\alpha q^\beta g(q^2), \quad (12)$$

$$\langle V(p'', \varepsilon'') | A_\mu | B_c(p') \rangle = -i \{ \varepsilon''^{*\mu} f(q^2) + \varepsilon''^{*\nu} \cdot \mathbf{p} [p_\nu a_+(q^2) + q_\nu a_-(q^2)] \}, \quad (13)$$

where, $p_\mu = p' + p''$ and $q_\mu = p' - p''$. The polarization of the outgoing vector meson is denoted by ε_μ and the convention $\epsilon_{0123} = 1$ is adopted. The matrix element expressions, Eqs. (11)-(13), are conventionally represented in terms of the BSW [63] form factors as,

$$\langle P(p'') | V_\mu | B_c(p') \rangle = (p_\mu - \frac{M_{B_c}^2 - M_P^2}{q^2} q_\mu) F_1^{B_c P}(q^2) + \frac{M_{B_c}^2 - M_P^2}{q^2} q_\mu F_0^{B_c P}(q^2), \quad (14)$$

$$\langle V(p'', \varepsilon'') | V_\mu | B_c(p') \rangle = -\frac{1}{M_{B_c} + M_V} \epsilon_{\mu\nu\alpha\beta} \varepsilon''^{*\nu} p^\alpha q^\beta V^{B_c V}(q^2), \quad (15)$$

$$\begin{aligned} \langle V(p'', \varepsilon'') | A_\mu | B_c(p') \rangle &= i \{ (M_{B_c} + M_V) \varepsilon''^{*\mu} A_1^{B_c V}(q^2) - \frac{\varepsilon''^{*\nu} \cdot \mathbf{p}}{M_{B_c} + M_V} p_\nu A_2^{B_c V}(q^2) \\ &\quad - 2M_V \frac{\varepsilon''^{*\nu} \cdot \mathbf{p}}{q^2} q_\nu [A_3^{B_c V}(q^2) - A_0^{B_c V}(q^2)] \}, \end{aligned} \quad (16)$$

where the meson masses are denoted by M_{B_c} and $M_{P(V)}$. The BSW-type form factors can be related to the CLFQM form factors as [50],

$$\begin{aligned} F_1^{B_c P}(q^2) &= f_+(q^2), & F_0^{B_c P}(q^2) &= f_+(q^2) + \frac{q^2}{q} f_-(q^2), \\ V^{B_c V}(q^2) &= -(M_{B_c} + M_V) g(q^2), & A_1^{B_c V}(q^2) &= -\frac{f(q^2)}{M_{B_c} + M_V}, \\ A_2^{B_c V}(q^2) &= (M_{B_c} + M_V) a_+(q^2), & A_3^{B_c V}(q^2) - A_0^{B_c V}(q^2) &= \frac{q^2}{2M_V} a_-(q^2), \end{aligned} \quad (17)$$

with

$$\begin{aligned}
F_1^{B_c P}(0) &= F_0^{B_c P}(0), \\
A_3^{B_c V}(0) &= A_0^{B_c V}(0), \quad \text{and} \\
A_3^{B_c V}(q^2) &= \frac{M_{B_c} + M_V}{2M_V} A_1^{B_c V}(q^2) - \frac{M_{B_c} - M_V}{2M_V} A_2^{B_c V}(q^2).
\end{aligned} \tag{18}$$

In contrast to LFQM, the quark and antiquark within a meson system are off-shell in CLFQM. Aforementioned, the CLFQM provides a systematic way to handle zero-mode contributions. The light-front matrix element obtained in CLFQM receives additional spurious contributions proportional to the light-like vector $\omega^\mu = (0, 2, 0_\perp)$ which violates the covariance [46]. However, these spurious contributions are canceled out by the addition of zero-mode contributions, restoring the covariance of current matrix elements in CLFQM. Thus, allowing the calculation of physical quantities in terms of manifestly covariant Feynman momentum loop-integrals. Customarily, for the $B_c(p') \rightarrow M''(p'')$ transition, it is convenient to use the Drell–Yan–West frame, $q^+ = 0$, which implies that the form factors are known only for space-like momentum transfer, $q^2 = -q_\perp^2 \leq 0$, and for the time-like region ($q^2 = -q_\perp^2 \geq 0$), an additional q^2 extrapolation is needed. Furthermore, we consider a Lorentz frame in which $\mathbf{p}'_\perp = 0$ and $\mathbf{p}''_\perp = -\mathbf{q}_\perp$ leads to $\mathbf{k}''_\perp = \mathbf{k}'_\perp - x_2 \mathbf{q}_\perp$ [61]. Note that $q^2 = q_{max}^2 = (M_{B_c} - M_{P(V)})^2$ corresponds to zero-recoil of the final meson in the initial meson rest frame and the $q^2 = 0$ indicates the maximum recoil of the final meson [62]. Following the CLF approach [46, 58, 59], the form factors in Eqs. (11), (12), and (13) can be extracted from one-loop approximation as a momentum integral given by

$$\mathcal{B} = N_c \int \frac{d^4 k'_1}{(2\pi)^4} \frac{H_{M'} H_{M''}}{N'_1 N''_1 N_2} iS_B, \tag{19}$$

where N_c denotes the number of colors, $d^4 k'_1 = \frac{1}{2} dk'_1{}^- dk'_1{}^+ d^2 \mathbf{k}'_\perp$, and $H_{M^{(\prime\prime)}}$ is the bound-state vertex functions. The terms $N'_1{}^{(\prime\prime)} = k'_1{}^{(\prime\prime)2} - m_1{}^{(\prime\prime)2} + i\varepsilon$ and $N_2 = k_2^2 - m_2^2 + i\varepsilon$, arise from the quark propagators, and the trace S_B can be directly obtained by using the Lorentz contraction,

$$S_B = \text{Tr}[\Gamma(\mathbf{k}'_1 + m'_1)(i\Gamma_{M'})(-\mathbf{k}_2 + m_2)(i\gamma^0 \Gamma_{M''}^\dagger \gamma^0)(\mathbf{k}''_1 + m''_1)], \tag{20}$$

where the vertex operator $\Gamma_{M^{(\prime\prime)}}$ corresponds to the relevant meson, and have the forms

$$i\Gamma_P = -i\gamma_5 \quad \text{and} \quad i\Gamma_V = i \left[\gamma^\mu - \frac{(k_1 - k_2)^\mu}{D_{V,con}} \right], \tag{21}$$

for P and V mesons, respectively [59].

In practice, we use the light-front decomposition of the loop momentum and perform integration over the minus component that transforms to the standard LFQM from the covariant BS approach. This requires the following replacements:

$$N_1{}^{(\prime\prime)} \rightarrow \hat{N}_1{}^{(\prime\prime)} = x_1(M^{(\prime\prime)2} - M_0^{(\prime\prime)2}), \tag{22}$$

and

$$\chi_{M^{(\prime\prime)}} = \frac{H_M{}^{(\prime\prime)}}{N_1{}^{(\prime\prime)}} \rightarrow \frac{h_M{}^{(\prime\prime)}}{\hat{N}_1{}^{(\prime\prime)}}, \quad D_{V,con}{}^{(\prime\prime)} \rightarrow D_{V,LF}{}^{(\prime\prime)}, \quad (\text{Type-I}) \tag{23}$$

where the D factor $D_{V,con}{}^{(\prime\prime)} = M^{(\prime\prime)} + m_1{}^{(\prime\prime)} + m_2$ present in the vertex operator are substituted with $D_{V,LF}{}^{(\prime\prime)} = M_0^{(\prime\prime)} + m_1{}^{(\prime\prime)} + m_2$ [51, 60]. The LF forms of vertex functions, $h_{M'}$ for P and V mesons

are given by

$$\frac{h_P}{\hat{N}_1^{(\prime\prime)}} = \frac{h_V}{\hat{N}_1^{(\prime\prime)}} = \frac{1}{\sqrt{2N_c}} \sqrt{\frac{x_2}{x_1}} \frac{\psi(x_1, \mathbf{k}'_{\perp})}{\hat{M}_0^{(\prime\prime)}}, \quad (24)$$

where $\hat{M}_0^{(\prime\prime)} \equiv \sqrt{M_0^{(\prime\prime)} - (m_1^{(\prime\prime)} - m_2)^2}$. It should be noted that there are some debates regarding the self-consistency of the CLFQM [50, 51, 60]. The explicit validity of replacing $D_{V,con}^{(\prime\prime)}$ with $D_{V,LF}^{(\prime\prime)}$ leads to inconsistency issues in Type-I correspondence. Qin Chang *et al.* [59] found that the resulting $P \rightarrow V$ form factors extracted with the longitudinal ($\lambda = 0$) and transverse ($\lambda = \pm$) polarization states are not consistent with each other. This is because the $P \rightarrow V$ form factors obtained from the longitudinal polarization state receive an additional contribution characterized by the coefficients $B_1^{(2)}$ and $B_3^{(3)}$, which is noticeable in the B_c to V form factor expressions of $f(q^2)$ and $a_-(q^2)$. Furthermore, the manifest covariance of the matrix element in CLFQM is also violated in the Type-I correspondence scheme because of the residual ω -dependencies associated with $B_j^{(i)}$ functions, which are independent of zero-mode contributions. Therefore, a proposed solution to address these inconsistencies observed in the Type-I CLF form factors is to modify the relationship between the manifestly covariant BS approach and the standard LFQM [46, 50, 51]. In regard to this, Choi and Ji [51] suggested the replacement of $M^{(\prime\prime)}$ with kinetic invariant mass $M_0^{(\prime\prime)}$ in every term that contains $M^{(\prime\prime)}$ within the integrand, in addition to the D factor. As a result, the correspondence given by Eq. (23) can be generalized to

$$\chi_{M^{(\prime\prime)}} = \frac{H_M^{(\prime\prime)}}{N_1^{(\prime\prime)}} \rightarrow \frac{h_M^{(\prime\prime)}}{\hat{N}_1^{(\prime\prime)}}, \quad M^{(\prime\prime)} \rightarrow M_0^{(\prime\prime)}. \quad (\text{Type-II}) \quad (25)$$

Thus, by employing Type-II correspondence from Eq. (25), the matrix element \mathcal{B} in Eq. (19) shall reduce to the LF form,

$$\hat{\mathcal{B}} = N_c \int \frac{dx_1 d^2 \mathbf{k}'_{\perp}}{2(2\pi)^3} \frac{h_{M'} h_{M''}}{x_2 \hat{N}'_1 \hat{N}''_1} \hat{S}_{\mathcal{B}}. \quad (26)$$

Essentially, by embracing the Type-II correspondence described by Eq. (25), the manifest covariance of the CLFQM can be restored, which in turn should yield numerically equal form factors for $\lambda = 0$ and $\lambda = \pm$ polarization states. Therefore, it can be inferred that Type-II correspondence offers a potentially self-consistent framework that resolves the issues connected to the covariance of the matrix elements and the inconsistencies.

The determination of transition form factors for the B_c to ground-state s -wave meson for $q^2 = -q_{\perp}^2 \leq 0$ is a straightforward process, since the calculation of the zero-mode contribution is obtained in a frame where the momentum transfer q^+ becomes zero. As a result, the form factors are only known for space-like momentum transfer $q^2 = (p' - p'')^2 = -q_{\perp}^2 \leq 0$ [46]. Nevertheless, the transition form factors in the time-like region can be obtained through extrapolation, which will be discussed in the following subsection.

Furthermore, the B_c to $P(V)$ transition form factors are explicitly expressed as [59],

$$F(q^2) = N_c \int \frac{dx_1 d^2 \mathbf{k}'_{\perp}}{(2\pi)^3} \frac{\chi'_{B_c} \chi''_{P(V)}}{2x_2} \tilde{F}(q^2), \quad (27)$$

where

$$\chi'_{B_c} = \frac{1}{\sqrt{2N_c}} \sqrt{\frac{x_2}{x_1}} \frac{\psi(x_1, \mathbf{k}'_{\perp})}{\hat{M}'_0}, \quad \text{and} \quad \chi''_{P(V)} = \frac{1}{\sqrt{2N_c}} \sqrt{\frac{x_2}{x_1}} \frac{\psi(x_1, \mathbf{k}''_{\perp})}{\hat{M}''_0}. \quad (28)$$

The form factor function $\tilde{F}(q^2) \equiv \{\tilde{f}_\pm(q^2), \tilde{g}(q^2), \tilde{f}(q^2), \tilde{a}_\pm(q^2)\}$ corresponding to B_c to $P(V)$ transitions are defined as follows:

(i) B_c to P form factors [50, 60],

$$\tilde{f}_+(q^2) = x_1 M_0'^2 + x_1 M_0''^2 + x_2 q^2 - x_1 (m_1' - m_2)^2 - x_1 (m_1'' - m_2)^2 - x_2 (m_1' - m_1'')^2, \quad (29)$$

$$\begin{aligned} \tilde{f}_-(q^2) = & -2x_1 x_2 M'^2 - 2k_\perp'^2 - 2m_1' m_2 + 2(m_1'' - m_2)(x_2 m_1' + x m_2) \\ & - 2 \frac{\mathbf{k}'_\perp \cdot \mathbf{q}_\perp}{q^2} \left[(x_1 - x_2) M'^2 + M''^2 + x_2 (q^2 + q \cdot p) + 2x_1 M_0'^2 \right. \\ & \left. - 2(m_1' + m_1'')(m_1' - m_2) \right] + a \frac{p \cdot q}{q^2} \left[k_\perp'^2 + \frac{2(\mathbf{k}'_\perp \cdot \mathbf{q}_\perp)^2}{q^2} \right] + 4 \frac{(\mathbf{k}'_\perp \cdot \mathbf{q}_\perp)^2}{q^2}. \end{aligned} \quad (30)$$

(ii) B_c to V form factors [50, 59],

$$\tilde{g}(q^2) = -2 \left\{ x_2 m_1' + x_1 m_2 + (m_1' - m_1'') \frac{\mathbf{k}'_\perp \cdot \mathbf{q}_\perp}{q^2} + \frac{2}{D_{V,con}''} \left[k_\perp'^2 + \frac{(\mathbf{k}'_\perp \cdot \mathbf{q}_\perp)^2}{q^2} \right] \right\}, \quad (31)$$

$$\begin{aligned} \tilde{f}(q^2) = & -2 \left\{ - (m_1' + m_1'')^2 (m_1' - m_2) + (x_1 m_2 - x_2 m_1') M'^2 + (x_1 m_2 + x_2 m_1') M''^2 \right. \\ & - x_1 (m_2 - m_1') (M_0'^2 + M_0''^2) + 2x_1 m_1'' M_0'^2 - 4(m_1' - m_2) \left(k_\perp'^2 + \frac{(\mathbf{k}'_\perp \cdot \mathbf{q}_\perp)^2}{q^2} \right) \\ & - m_2 q^2 - (m_1' + m_1'') (q^2 + q \cdot p) \frac{\mathbf{k}'_\perp \cdot \mathbf{q}_\perp}{q^2} + 4(m_1' - m_2) B_1^{(2)} + \frac{2}{D_{V,con}''} \left[\left(k_\perp'^2 \right. \right. \\ & \left. \left. + \frac{(\mathbf{k}'_\perp \cdot \mathbf{q}_\perp)^2}{q^2} \right) \left((x_1 - x_2) M'^2 + M''^2 - 2(m_1' - m_1'')(m_1' - m_2) + 2x_1 M_0'^2 \right. \right. \\ & \left. \left. - q^2 - 2(q^2 + q \cdot p) \frac{\mathbf{k}'_\perp \cdot \mathbf{q}_\perp}{q^2} \right) - \left(M'^2 + M''^2 - q^2 + 2(m_1' - m_2)(m_1'' \right. \right. \\ & \left. \left. + m_2) \right) B_1^{(2)} + 2B_3^{(3)} \right] \left. \right\}, \end{aligned} \quad (32)$$

$$\begin{aligned} \tilde{a}_+(q^2) = & 2 \left\{ (m_1'' - 2x_1 m_1' + m_1' + 2x_1 m_2) \frac{\mathbf{k}'_\perp \cdot \mathbf{q}_\perp}{q_\perp^2} + (x_1 - x_2)(x_2 m_1' + x_1 m_2) \right. \\ & \left. + \frac{2}{D_{V,con}''} \frac{\mathbf{k}'_\perp \cdot \mathbf{q}_\perp}{x_2 q_\perp^2} \left[\mathbf{k}'_\perp \cdot \mathbf{k}''_\perp + (x_1 m_2 - x_2 m_1'')(x_1 m_2 + x_2 m_1') \right] \right\}, \end{aligned} \quad (33)$$

$$\begin{aligned} \tilde{a}_-(q^2) = & -2 \left\{ (3 - 2x_1)(x_2 m_1' + x_1 m_2) - \left[(6x_1 - 7)m_1' + (4 - 6x_1)m_2 + m_1'' \right] \frac{\mathbf{k}'_\perp \cdot \mathbf{q}_\perp}{q^2} \right. \\ & + 4(m_1' - m_2) \left[2 \left(\frac{\mathbf{k}'_\perp \cdot \mathbf{q}_\perp}{q^2} \right)^2 + \frac{k_\perp'^2}{q^2} \right] - 4 \frac{(m_1' - m_2)}{q^2} B_1^{(2)} + \frac{1}{D_{V,con}''} \left[-2(M'^2 + M''^2 \right. \\ & - q^2 + 2(m_1' - m_2)(m_1'' + m_2)) (A_3^{(2)} + A_4^{(2)} - A_2^{(1)}) + \left(2M'^2 - q^2 - x_1(M'^2 \right. \\ & - M_0'^2) + x_1(M''^2 - M_0''^2) - 2(m_1' - m_2)^2 + (m_1' + m_1'')^2 \right) (A_1^{(1)} + A_2^{(1)} - 1) \\ & + 2Z_2(2A_4^{(2)} - 3A_2^{(1)} + 1) + 2 \frac{q \cdot p}{q^2} (4A_2^{(1)} A_1^{(2)} - 3A_1^{(2)}) + \frac{2}{q^2} \left((M'^2 + M''^2 \right. \\ & \left. - q^2 + 2(m_1' - m_2)(m_1'' + m_2)) B_1^{(2)} - 2B_3^{(3)} \right) \left. \right] \left. \right\}. \end{aligned} \quad (34)$$

The coefficients $A_j^{(i)}$ and $B_j^{(i)}$ are given as [50, 59],

$$A_1^{(1)} = \frac{x_1}{2}, \quad A_1^{(2)} = -k_\perp'^2 - \frac{(\mathbf{k}'_\perp \cdot \mathbf{q}_\perp)^2}{q^2}, \quad A_2^{(1)} = A_1^{(1)} - \frac{\mathbf{k}'_\perp \cdot \mathbf{q}_\perp}{q^2},$$

$$A_3^{(2)} = A_1^{(1)} A_2^{(1)}, \quad A_4^{(2)} = (A_2^{(1)})^2 - \frac{1}{q^2} A_1^{(2)}, \quad (35)$$

$$B_1^{(2)} = A_1^{(1)} Z_2 - A_2^{(1)}, \quad B_3^{(3)} = B_1^{(2)} Z_2 + \left(p^2 - \frac{(q \cdot p)^2}{q^2}\right) A_1^{(1)} A_1^{(2)}, \quad \text{and}$$

$$Z_2 = x_1(M'^2 - M_0'^2) + m_1'^2 - m_2^2 + (1 - 2x_1)M'^2 + (q^2 + q \cdot p) \frac{\mathbf{k}'_\perp \cdot \mathbf{q}_\perp}{q^2}. \quad (36)$$

It should be noted that the above given expressions for the form factors correspond to the traditional Type-I scheme, for which Type-II correspondence can be obtained by an additional replacement of $M'^{(\prime\prime)}$ to $M_0'^{(\prime\prime\prime)}$ [59]. Moreover, the above form factor expressions are for the case of $\lambda = 0$ (*i.e.*, longitudinal polarization state); and the results for the case of $\lambda = \pm$ (*i.e.*, transverse polarization states) can be obtained from these expressions by omitting the terms associated with $B_j^{(i)}$ functions.

B. q^2 dependence of the form factors

The numerical evaluation of B_c to $P(V)$ transition form factors requires an understanding of the momentum dependence of these form factors over the entire q^2 region in the CLFQM. Conventionally, the meson transition in the Drell-Yan-West frame with $q^+ = 0$ restricts the evaluation of the form factors for the momentum transfer $q^2 = -q_\perp^2 \leq 0$, *i.e.*, space-like region [42, 46, 52, 64]. However, only the form factors in the time-like region ($q^2 = -q_\perp^2 \geq 0$) are relevant for physical decay processes [46, 50]. Therefore, to evaluate the total decay rate of B_c decays, the momentum dependence of the form factors should be reproduced in the space-like region and extrapolated to the time-like region using simplified parameterizations.

Jaus [42] suggested to estimate the invariant form factors as functions of q^2 , extending them analytically from space-like ($q^2 \leq 0$) to time-like regions ($q^2 \geq 0$) [29, 50, 59, 62, 64]. This reformulation relies on the assumption that the form factors are continuously differentiable with respect to q^2 , emphasizing the importance of understanding their behavior near $q^2 = 0$ [42]. Therefore, understanding wave function overlaps between the initial and final state mesons near $q^2 = 0$ are significant. Furthermore, it has been argued that the form factors obtained directly in the time-like region ($q^+ > 0$) are equivalent to those from analytic continuation from the space-like region [55]. Consequently, uncertainties arise in transition form factors calculated for $q^2 \geq 0$ (with $\mathbf{q}_\perp = 0$) due to nonvalence configurations; particularly, contributions from the Z-graph representing quark-antiquark pair creation from the vacuum. However, the estimation of these Z-graph contributions are still lacking within the CLFQM formalism. Nevertheless, recent efforts have been made to estimate them, including through a VMD-like decay mechanism [65]. Parameterizing form factors as meromorphic functions of q^2 , with analytic continuation from $q^2 < 0$ to $q^2 > 0$, is proposed to reasonably describe form factors at time-like momentum transfers [66]. Therefore, considering a frame with purely transverse momentum transfer ($q^+ = 0$) is suggested to reduce nonvalence contributions. Additionally, zero-mode contributions affecting these transition

form factors are addressed by the Type-II self-consistent CLF approach. The literature suggests numerous functions of q^2 dependence influenced by the VMD approach, which has been used to parameterize the form factors [67–69]. In our analysis, we reproduce the q^2 dependence of form factors in the space-like region and extrapolate them to the time-like region using the following parameterization [69],

$$F(q^2) = \frac{F(0)}{\left(1 - \frac{q^2}{M_{pole}^2}\right) \left(1 - a \frac{q^2}{M_{pole}^2} + b \frac{q^4}{M_{pole}^4}\right)}, \quad (37)$$

where M_{pole} is the transition pole mass. The q^2 dependence of the form factors defined by Eq. (37) involve contributions from resonances of particular spin in the available q^2 range, for example, the form factors $F_1(q^2)$ and $V(q^2)$ exhibit a pole at $q^2 = M_{1-}^2$, while $A_0(q^2)$ contains a pole at $q^2 = M_{0-}^2$. It is important to note that the remaining form factors, namely, $F_0(q^2)$, $A_1(q^2)$, and $A_2(q^2)$, do not receive contributions from the lowest lying negative parity states [70]. The form factor $F_0(q^2)$ include the pole mass corresponding to 0^+ state, whereas $A_1(q^2)$ and $A_2(q^2)$ incorporates 1^+ state; interestingly, both have significantly higher masses [69, 71, 72], as shown in Table III. As a result, these form factors are expected to show less variation in the decay region for the available q^2 .

Notably, the available q^2 range for the bottom-conserving $B_c \rightarrow P(V)$ transitions is $0 \leq q^2 \lesssim 1$ GeV². However, for bottom-changing transitions, the q^2 range is considerably larger, *i.e.*, $0 \leq q^2 \lesssim 20$ GeV². Since the M_{pole}^2 is greater than available q^2 in heavy to heavy meson transitions, the contributing poles lie farther from the kinematic region. Therefore, it is important to accurately determine the q^2 dependence in decay amplitudes across the entire kinematic range [73], which justifies the use of the three-parameter form given by Eq. (37). The phenomenological accuracy and reliability of q^2 dependence, given in Eq. (37), have been extensively discussed in Refs. [69, 71–73]. The physical interpretation of the slope parameters, a and b , is that they signify an effective pole mass and capture the effects of higher-order resonances [13]. The parameters a , b , and $F(0)$ are determined by fitting Eq. (37) in the space-like region and extrapolating to the physical region $q^2 \geq 0$.

Alternatively, many experimental and lattice observations are made using a model-independent parameterization following the general QCD constraints, which is known as z -series (expansion) parameterization. In order to establish a clear understanding of q^2 dependence and comparison among different q^2 formulations, we also incorporate z -series expansion form. Furthermore, the z -series parameterization is given in terms of a complex parameter z , which is the analytic continuation of q^2 into the complex plane [13]. This parametrization of the form factor is based on the power series expansion around the value $q^2 = t_0$. Thus, the form factor is expressed as [74],

$$F(q^2) = \frac{1}{1 - \frac{q^2}{M_{pole}^2}} \sum_{k=0}^K a'_k [z(q^2) - z(0)]^k, \quad (38)$$

where a_k are real coefficients and $z(q^2) \equiv z(q^2, t_0)$ is the function

$$z(q^2) = \frac{\sqrt{t_+ - q^2} - \sqrt{t_+ - t_0}}{\sqrt{t_+ - q^2} + \sqrt{t_+ - t_0}}, \quad (39)$$

which maps the q^2 -plane cut for $q^2 \geq t_+$ onto the disk $|z(q^2, t_0)| < 1$ in the z -complex plane, such that $|z(t_+, t_0)| = -1$ and $|z(\infty, t_0)| = 1$. The arbitrary parameter $t_0 < t_+$ determines the point

q^2 mapped onto the origin in the z -plane, *i.e.*, $|z(t_0, t_0)| = 0$ corresponding to $q^2 = t_0$, and the physical region extends in either direction up to $\pm|z|_{max}$ [75]. The parameters t_+ and t_0 are $(M_{B_c} + M_{P(V)})^2$ and $(M_{B_c} + M_{P(V)})(\sqrt{M_{B_c}} - \sqrt{M_{P(V)}})^2$, respectively [74, 75]. In comparison to other phenomenological approaches, the fitted coefficients a'_k have no physical interpretation [13]. Since the higher order terms in the z -series parameterization given in Eq. (38) have trivial contribution, we restrict ourselves to the power $K = 2$, which contains the free parameters a'_0 ($\approx F(0)$), a'_1 , and a'_2 .

Furthermore, it should be noted that for the calculation of transition form factors, several other theoretical studies have employed the following q^2 dependence [50, 59, 76],

$$F(q^2) = \frac{F(0)}{1 - a \frac{q^2}{M_{B_c}^2} + b \frac{q^4}{M_{B_c}^4}}, \quad (40)$$

where mass of the parent meson $M_{B_c} = 6274.47$ MeV [12] is taken as the pole mass. We use this parameterization in the Type-I correspondence for the sake of comparison. It is expected that the parameterization presented in Eq. (40) is also valid for the physical decay region [73].

C. Semileptonic decay widths and other physical observables

The differential decay width of B_c to $P(V)$ semileptonic decays is expressed in terms of the helicity components as [27],

$$\frac{d\Gamma(B_c^+ \rightarrow P(V)l^+\nu_l)}{dq^2} = \frac{G_F^2}{(2\pi)^3} |V_{q_1 q_2}|^2 \frac{q^2 \sqrt{\lambda}}{24M_{B_c}^3} \left(1 - \frac{m_l^2}{q^2}\right)^2 \mathcal{H}_{\text{total}}, \quad (41)$$

where G_F is the Fermi constant and $V_{q_1 q_2}$ is the relevant CKM matrix element for $q_1 \rightarrow q_2$ transition. The term $\lambda \equiv \lambda(M_{B_c}^2, M_{P(V)}^2, q^2) = (M_{B_c}^2 + M_{P(V)}^2 + q^2)^2 - 4M_{B_c}^2 M_{P(V)}^2$ is the Källén function, and m_l is the lepton mass ($l = e, \mu, \tau$). The total helicity structure, $\mathcal{H}_{\text{total}}$, is given by,

$$\mathcal{H}_{\text{total}} = (\mathcal{H}_U + \mathcal{H}_L) \left(1 + \frac{m_l^2}{2q^2}\right) + \frac{3m_l^2}{2q^2} \mathcal{H}_S, \quad (42)$$

and the helicity components \mathcal{H}_U , \mathcal{H}_L , and \mathcal{H}_S can be defined as,

$$\mathcal{H}_U = |H_+|^2 + |H_-|^2, \quad \mathcal{H}_L = |H_0|^2, \quad \text{and} \quad \mathcal{H}_S = |H_t|^2, \quad (43)$$

where H_\pm , H_0 , and H_t are the helicity amplitudes. These helicity amplitudes are related to the corresponding invariant form factors by the following relations:

(i) For B_c to P meson transitions,

$$H_\pm(q^2) = 0, \quad H_0(q^2) = \frac{\sqrt{\lambda}}{\sqrt{q^2}} F_1(q^2), \quad \text{and} \quad H_t(q^2) = \frac{1}{\sqrt{q^2}} (M_{B_c}^2 - M_P^2) F_0(q^2). \quad (44)$$

(ii) For B_c to V meson transitions,

$$H_\pm(q^2) = (M_{B_c} + M_V) A_1(q^2) \mp \frac{\sqrt{\lambda}}{M_{B_c} + M_V} V(q^2), \quad (45)$$

$$H_0(q^2) = \frac{1}{2M_V \sqrt{q^2}} (M_{B_c} + M_V) (M_{B_c}^2 - M_V^2 - q^2) A_1(q^2) - \frac{\lambda}{M_{B_c} + M_V} A_2(q^2), \quad (46)$$

$$H_t(q^2) = \frac{\sqrt{\lambda}}{\sqrt{q^2}} A_0(q^2). \quad (47)$$

Following Eq. (41) the longitudinal and transverse differential decay widths are given by

$$\frac{d\Gamma_L(B_c^+ \rightarrow Vl^+\nu_l)}{dq^2} = \frac{G_F^2}{(2\pi)^3} |V_{q_1 q_2}|^2 \frac{q^2 \sqrt{\lambda}}{24M_{B_c}^3} \left(1 - \frac{m_l^2}{q^2}\right)^2 [\mathcal{H}_L \left(1 + \frac{m_l^2}{2q^2}\right) + \frac{3m_l^2}{2q^2} \mathcal{H}_S], \text{ and} \quad (48)$$

$$\frac{d\Gamma_T(B_c^+ \rightarrow Vl^+\nu_l)}{dq^2} = \frac{G_F^2}{(2\pi)^3} |V_{q_1 q_2}|^2 \frac{q^2 \sqrt{\lambda}}{24M_{B_c}^3} \left(1 - \frac{m_l^2}{q^2}\right)^2 [\mathcal{H}_U \left(1 + \frac{m_l^2}{2q^2}\right)], \quad (49)$$

respectively.

In order to gain a deeper understanding of semileptonic decays beyond just the branching ratio, it is valuable to investigate the influence of the lepton mass. Moreover, by defining additional physical observables that are experimentally measurable, we can obtain a more comprehensive and intricate depiction of the underlying physics in these decays. Some of these physical observables are FB asymmetry ($A_{FB}(q^2)$), leptonic convexity parameter ($C_F^l(q^2)$), longitudinal (transverse) ($P_{L(T)}^l(q^2)$) polarization of the charged lepton, and asymmetry parameter ($\alpha^*(q^2)$). These observables can be expressed by the above helicity structure functions as [27, 77]

$$A_{FB}(q^2) = \frac{3}{4} \frac{\mathcal{H}_P - 2\frac{m_l^2}{q^2} \mathcal{H}_{SL}}{\mathcal{H}_{\text{total}}}, \quad (50)$$

$$C_F^l(q^2) = \frac{3}{4} \left(1 - \frac{m_l^2}{q^2}\right) \frac{\mathcal{H}_U - 2\mathcal{H}_L}{\mathcal{H}_{\text{total}}}, \quad (51)$$

$$P_L^l(q^2) = \frac{(\mathcal{H}_U + \mathcal{H}_L) \left(1 - \frac{m_l^2}{2q^2}\right) - \frac{3m_l^2}{2q^2} \mathcal{H}_S}{\mathcal{H}_{\text{total}}}, \quad (52)$$

$$P_T^l(q^2) = -\frac{3\pi m_l}{8\sqrt{q^2}} \frac{\mathcal{H}_P + 2\mathcal{H}_{SL}}{\mathcal{H}_{\text{total}}}, \text{ and} \quad (53)$$

$$\alpha^*(q^2) = \frac{\mathcal{H}_U + \tilde{\mathcal{H}}_U - 2(\mathcal{H}_L + \tilde{\mathcal{H}}_L + 3\tilde{\mathcal{H}}_S)}{\mathcal{H}_U + \tilde{\mathcal{H}}_U + 2(\mathcal{H}_L + \tilde{\mathcal{H}}_L + 3\tilde{\mathcal{H}}_S)}, \quad (54)$$

where $\tilde{\mathcal{H}}_i = \frac{m_l^2}{2q^2} \mathcal{H}_i$ for ($i = U, L, S$). The helicity components \mathcal{H}_P and \mathcal{H}_{SL} are defined by $\mathcal{H}_P = |H_+|^2 - |H_-|^2$ and $\mathcal{H}_{SL} = \mathcal{R}(H_0 H_t^\dagger)$.

For $B_c^- \rightarrow Vl^-\bar{\nu}_l$ decays, the physical observables like FB asymmetry, longitudinal and transverse polarization of the charged lepton are altered due to the opposite sign in the leptonic tensor [27]. However, there is no change in the expression for other observables. In this study, we calculate the mean values of all the above mentioned physical observables by separately integrating the numerator and denominator over q^2 , with the inclusion of a kinematic factor $q^2 \sqrt{\lambda} \left(1 - \frac{m_l^2}{q^2}\right)^2$, where $\left(1 - \frac{m_l^2}{q^2}\right)$ represents the velocity-type parameter.

D. Nonleptonic decay widths

The QCD modified weak Hamiltonian generating the B_c^+ decay involving $b \rightarrow c(u)$ transitions is expressed as follows [78]:

$$H_w^{(\Delta b=-1)} = \frac{G_F}{\sqrt{2}} \sum_{Q(q)=u,c} \sum_{q'=d,s} V_{Qb}^* V_{qq'} \left(a_1(\mu) O_1^{qq'}(\mu) + a_2(\mu) O_2^{qq'}(\mu) \right) + h.c. , \quad (55)$$

where a_1 and a_2 are the standard perturbative QCD coefficients, evaluated at renormalization scale $\mu \approx m_b^2$. Local tree-level operators $O_{1,2}$ involving $b \rightarrow q$ transition can be expressed as products of colour-singlet currents are given below:

$$\begin{aligned} O_1^{qd} &= (\bar{b}_\alpha q_\alpha)_{V-A} \cdot (\bar{q}_\beta d_\beta)_{V-A}, & O_2^{qd} &= (\bar{b}_\alpha q_\beta)_{V-A} \cdot (\bar{q}_\beta d_\alpha)_{V-A}, \\ O_1^{qs} &= (\bar{b}_\alpha q_\alpha)_{V-A} \cdot (\bar{q}_\beta s_\beta)_{V-A}, & O_2^{qs} &= (\bar{b}_\alpha q_\beta)_{V-A} \cdot (\bar{q}_\beta s_\alpha)_{V-A}, \end{aligned} \quad (56)$$

where $(\bar{q}q')_{V-A} \equiv \bar{q}\gamma_\mu(1-\gamma_5)q'$, α and β are $SU(3)$ color indices. Selection rules for various decay modes corresponding to the Hamiltonian , (55), are:

- (i) CKM-enhanced modes $\Delta b = -1, \Delta C = -1, \Delta S = 0$; $\Delta b = -1, \Delta C = 0, \Delta S = 1$;
- (ii) CKM-suppressed modes $\Delta b = -1, \Delta C = -1, \Delta S = 1$; $\Delta b = -1, \Delta C = 0, \Delta S = 0$;
- (ii) CKM-doubly-suppressed modes $\Delta b = -1, \Delta C = 1, \Delta S = 1$; $\Delta b = -1, \Delta C = 1, \Delta S = 0$.

In addition to the bottom-changing decays, B_c^+ meson can exhibit bottom-conserving decay modes for the c quark decaying to an s or d quark. The weak Hamiltonian generating the c quark decays, $H_w^{(\Delta C=-1)}$, is expressed by replacing b with c , $Q(q) = d, s$, and $q' = u$ in Eq. (55). The selection rules for various bottom-conserving decay channels are given as,

- (i) CKM-enhanced mode $\Delta b = 0, \Delta C = -1, \Delta S = -1$;
- (ii) CKM-suppressed mode $\Delta b = 0, \Delta C = -1, \Delta S = 0$;
- (ii) CKM-doubly-suppressed mode $\Delta b = 0, \Delta C = -1, \Delta S = -1$.

The factorization scheme expresses the decay amplitudes as a product of the matrix elements of weak currents, *i.e.*,

$$\mathcal{A}(B_c \rightarrow PV) \simeq \langle P | J^\mu | 0 \rangle \langle V | J_\mu | B_c \rangle + \langle V | J^\mu | 0 \rangle \langle P | J_\mu | B_c \rangle, \quad (57)$$

where J^μ stands for $V-A$ current. The matrix element of the J^μ between vacuum and final meson (P or V) is parameterized by the decay constants $f_{P(V)}$ as,

$$\begin{aligned} \langle 0 | J_\mu | P(p') \rangle &= \langle 0 | A_\mu | P(p') \rangle = i f_P p'_\mu, \\ \langle 0 | J_\mu | V(p', \varepsilon') \rangle &= \langle 0 | V_\mu | V(p', \varepsilon') \rangle = M'_V f_V \varepsilon'_\mu. \end{aligned} \quad (58)$$

The values of the decay constants used in our calculations are given in Table VIII.

The nonleptonic B_c decays can be categorized based on the colour-favored and -suppressed contribution into three classes, as follows [79, 80]:

- (i) Class I: Decays primarily governed by color-favored diagrams, which can be generated from the color singlet current and their decay amplitudes are proportional to a_1 , given by $a_1(\mu) = c_1(\mu) + \frac{1}{N_c} c_2(\mu)$, where N_c represents the number of colors, and $c_1(\mu)$ and $c_2(\mu)$ are the QCD coefficients.
- (ii) Class II: Decays primarily influenced by color-suppressed diagrams, which can be generated from the neutral current and their decay amplitudes are proportional to a_2 , defined as $a_2(\mu) = c_2(\mu) + \frac{1}{N_c} c_1(\mu)$.

- (iii) Class III: Decays resulting from a combination of both color-favored and color-suppressed diagrams, which can be generated from the interference of color singlet and color neutral currents, *i.e.*, the a_1 and a_2 amplitudes interfere.

In general, the color-favored decay amplitude can be expressed as [81],

$$\mathcal{A}(B_c \rightarrow PV) = \frac{G_F}{\sqrt{2}} \times \text{CKM factors} \times 2M_V a_1 \times (\text{CG Coeff. } f_V F_1^{B_c P}(M_V^2) + \text{CG Coeff. } f_P A_0^{B_c V}(M_P^2)). \quad (59)$$

For the color-suppressed modes, QCD factor a_1 is replaced by a_2 . It is important to note that a_1 and a_2 are undetermined coefficients assigned to the effective charged current and effective neutral current, respectively [82]. In order to establish consistency with the large N_c limit (*i.e.*, $N_c = \infty$), we adopt the convention of setting the QCD coefficients $a_1 \approx c_1$ and $a_2 \approx c_2$, as suggested in Refs. [79, 80]. The numerical values we employ are as follows:

$$\begin{aligned} \text{For } c \text{ decays (i.e., } \mu \approx m_c^2 \text{): } & c_1(\mu) = 1.26; c_2(\mu) = -0.51, \\ \text{For } b \text{ decays (i.e., } \mu \approx m_b^2 \text{): } & c_1(\mu) = 1.12; c_2(\mu) = -0.26. \end{aligned} \quad (60)$$

The relatively smaller magnitudes of a_2 imply that, unlike in the charm sector, one anticipates a more pronounced pattern of color suppression in B_c meson decays [79]. Since B_c decays primarily occur through tree diagrams or are tree-dominated, we neglect the anticipated small non-factorizable and penguin contributions within our formalism. It may be noted that N_c may be treated as a phenomenological parameter in weak meson decays, which account for nonfactorizable contributions [83, 84]. Therefore, we also use $N_c = 3$ to obtain the effective coefficients $a_1(\mu) = c_1(\mu) + \frac{1}{3}c_2(\mu)$ and $a_2(\mu) = c_2(\mu) + \frac{1}{3}c_1(\mu)$,

$$\begin{aligned} \text{for } c \text{ decays (at } N_c = 3 \text{): } & a_1(\mu) = 1.09; a_2(\mu) = -0.09, \\ \text{for } b \text{ decays (at } N_c = 3 \text{): } & a_1(\mu) = 1.03; a_2(\mu) = 0.11. \end{aligned} \quad (61)$$

We have calculated nonleptonic branching ratios of $B_c \rightarrow PV$ decays both at $N_c = \infty$ and $N_c = 3$. It is worth noting that for bottom-conserving decays, experimental charm decay studies have provided a parameterization for a_1 and a_2 . These results suggest that considering the large N_c limit is appropriate for c quark decays [85]. On the other hand, for bottom-changing decays, phenomenological analyses [86] indicate variations in the magnitudes of the Wilson coefficients a_1 and a_2 , as well as sub-leading contributions from the $1/N_c$ term. This can be accounted for by allowing a certain range of values for these coefficients, as shown in Eq. (61). We would like to emphasize that the decay amplitudes can be expressed as factorizable contributions multiplied by their respective a_i values, which are independent of the (renormalization) scale and process.

Using the decay amplitude defined in Eq. (59), the decay rate for the B_c to PV decay is given by

$$\Gamma(B_c \rightarrow PV) = \frac{\mathbf{k}^3}{8\pi M_V^2} |\mathcal{A}(B_c \rightarrow PV)|^2, \quad (62)$$

where \mathbf{k} is the three-momentum of the final-state particle in the rest frame of B_c meson and is expressed as,

$$\mathbf{k} = \frac{1}{2M_{B_c}} \sqrt{[M_{B_c}^2 - (M_P + M_V)^2][M_{B_c}^2 - (M_P - M_V)^2]}. \quad (63)$$

The numerical results for semileptonic and nonleptonic weak decays of B_c meson are discussed in the following section.

III. NUMERICAL RESULTS AND DISCUSSIONS

In the present work, we calculate the transition form factors for B_c to P and V using the self-consistent CLFQM across the available range of momentum transfer. Furthermore, we provide a comprehensive investigation into their dependence on q^2 and compare our results with other formalisms. We compute the transition form factors for B_c to P and V mesons, using the constituent quark masses and β (Gaussian parameter) values provided in Table II. We use three different q^2 formulations, namely, Type-II, Type-II*, and Type-I schemes following Eqs. (37), (38), and (40), respectively. The transition pole masses given in Table III are used for the calculation of the form factors of q^2 for Type-II(*), while we fix mass of the parent meson as the pole for Type-I. The obtained form factors for bottom-conserving and bottom-changing transitions are tabulated in Tables IV and V, respectively. We plot their q^2 dependence for the available range $0 \leq q^2 \leq q_{max}^2 = (M_{B_c} - M_{P(V)})^2$, as shown in Figures 1–5. We also plot corresponding wave function overlap (Eq. (5)) and overlap integrand (Eq. (27)) at $q^2 = 0$, as shown in Figures 6–9. Using the numerical values of the form factors, we predict the branching ratios for semileptonic decays of the B_c meson². In our calculations, we use the following values for the lepton mass: $m_e = 0.511$ MeV, $m_\mu = 105.66$ MeV and $m_\tau = 1776.86$ MeV; CKM matrix elements: $|V_{ub}| = (3.82 \pm 0.20) \times 10^{-3}$, $|V_{cd}| = 0.221 \pm 0.004$, $|V_{cs}| = 0.975 \pm 0.006$ and $|V_{cb}| = (40.8 \pm 1.4) \times 10^{-3}$, and lifetime of B_c meson: $\tau_{B_c} = 0.51$ ps [12]. Also, we compare our results of semileptonic branching ratios with the existing literature, as shown in Table VII. Besides determining the branching ratios, we also calculate the numerical values of various physical observables, such as $A_{FB}(q^2)$, $C_F^l(q^2)$, $P_{L(T)}^l(q^2)$, and $\alpha^*(q^2)$, as listed in Table VI. Additionally, we plot the differential decay rates and FB asymmetries for $B_c^+ \rightarrow V l^+ \nu_l$ decays in Figures 10 and 11, respectively. Finally, we utilize the obtained form factors and the decay constants listed in Table VIII to predict the branching ratios of nonleptonic B_c to PV decays. The obtained results are presented in Tables IX–XII. We discuss our numerical results as follows.

A. Form factors

In this subsection, we discuss the results for the self-consistent B_c to V transition form factors along with B_c to P for bottom-conserving CKM-enhanced ($\Delta b = 0, \Delta C = -1, \Delta S = -1$) and suppressed ($\Delta b = 0, \Delta C = -1, \Delta S = 0$) modes, as well as bottom-changing CKM-enhanced ($\Delta b = -1, \Delta C = -1, \Delta S = 0$; $\Delta b = -1, \Delta C = 0, \Delta S = 1$) and suppressed ($\Delta b = -1, \Delta C = 0, \Delta S = 0$) modes. We also contrast the form factors in Type-I and Type-II schemes corresponding to different q^2 dependence formulations, as presented in Tables IV and V. Aforementioned, to observe the variation of Type-II(*) form factors with respect to q^2 , we plot these transition form factors, as shown in Figures 2–5. We list our observations as follows.

² The branching ratio is calculated from the decay rate expression given in Eq. (41) by multiplying by $\frac{\tau_{B_c}}{\hbar}$.

1. Bottom-conserving transition form factors

- (i) The bottom-conserving $B_c \rightarrow B_{(s)}$ transitions are governed by c quark decays, for which the observed q^2 range is limited to a narrow interval of $0 \leq q^2 \leq (M_{B_c} - M_{B_{(s)}})^2 \simeq 1 \text{ GeV}^2$. As a result, we expect these form factors to show minimal variations with respect to the available q^2 range, as shown in Figure 2. The Type-II* form factors, corresponding to z -series parameterization, show more deviation than Type-II form factors. It must be noted that although $B_c \rightarrow P$ form factors are free from self-consistency issues, the replacement of $M^{(\prime\prime)} \rightarrow M_0^{(\prime\prime)}$ in Type-II correspondence will result in modified numerical values³. In addition, the choice of q^2 dependence between the two correspondences, *i.e.*, Eqs. (37) and (38) in Type-II and Eq. (40) in Type-I, will also lead to changes in the numerical values of form factors and (a , b , a'_1 , and a'_2) parameters. We noted that the form factors as well as the slope parameters a and b are least affected by the uncertainties in β parameter and, therefore, are ignored. It may be emphasized that in the case of Type-I correspondence scheme, the numerical values are calculated by using the parent pole mass in Eq. (40), as suggested in the literature [50, 60]. However, we calculate the form factors in Type-II correspondence by using transition pole masses for both q^2 formulations, Eqs. (37) and (38). We observe that $B_c \rightarrow B_{(s)}$ form factors in Type-I scheme show marginal change in $F(0)$ values as compared to Type-II scheme. However, the slope parameters in both the correspondences are significantly different⁴. The form factors within Type-I scheme have substantially larger values for slope parameter b , which decreases on account of transition pole masses, as reported in our previous work [61]. However, the slope parameters a and b in Type-II correspondence are less than one. On the other hand, the parameters a'_1 and a'_2 also take significantly larger values for z -series parameterization (in Type-II*), unfortunately, there cannot be any physical interpretation associated with these coefficients [13]. It is important to note that the form factors in Type-I correspondence show a decreasing trend with respect to q^2 variation, in contrast to Type-II correspondence. Furthermore, we wish to emphasize that the Type-II(*) numerical results for the form factors $F_0^{B_c B_{(s)}}(q^2)$ and $F_1^{B_c B_{(s)}}(q^2)$ are in very good agreement with the LQCD observations, for both at $q^2 = 0$ and q_{max}^2 [19]. The form factors for lattice results for both at $q^2 = 0$ and q_{max}^2 are as follows: $F_{0[1]}^{B_c B}(0) = 0.555$ [0.555], $F_{0[1]}^{B_c B}(q_{max}^2) = 0.756$ [0.910]; $F_{0[1]}^{B_c B_s}(0) = 0.621$ [0.621], $F_{0[1]}^{B_c B_s}(q_{max}^2) = 0.817$ [0.911]. Furthermore, the LQCD results also show an increasing trend with respect to the q^2 variation likewise Type-II(*) results. The characteristic feature of bottom-conserving transitions, which has been reported in our previous work [61], is that these form factors in the small available q^2 range show near flat behavior.
- (ii) Similar to $B_c \rightarrow P$ transitions, we calculate the form factors for bottom-conserving $B_c \rightarrow V$ transitions for both Type-I and Type-II correspondences, as shown in Table II. It should be noted that in the $B_c \rightarrow V$ transitions, $V(q^2)$ and $A_2(q^2)$ form factors remain unaffected

³ Note that the numerical values of all the form factors, which are free from self-consistency issues will be updated due to $M^{(\prime\prime)} \rightarrow M_0^{(\prime\prime)}$ transition.

⁴ Note that the sign and magnitude of the slope parameter signifies how sharply the form factor varies with respect to allowed q^2 .

by the spurious contributions associated with the $B_j^{(i)}$ functions. Consequently, the results obtained in CLF approach for $\lambda = 0$ and $\lambda = \pm$ polarization states of vector mesons are in agreement with each other, regardless of whether Type-I or Type-II correspondence schemes are employed. However, in Type-I scheme, these zero-mode contributions lead to inconsistency in $A_0(q^2)$ and $A_1(q^2)$ form factors for $B_c \rightarrow V$ transitions. As described in the methodology in Sec. II, the Type-II scheme effectively resolves the issues corresponding to self-consistency and covariance of the matrix elements [59]. Therefore, in Type-II scheme, zero-mode contributions associated with the $B_1^{(2)}$ and $B_3^{(3)}$ functions vanish in the form factors $A_0(q^2)$ and $A_1(q^2)$, as explained in Sec. II. Therefore, the form factors $A_0(q^2)$ and $A_1(q^2)$ corresponding to longitudinal ($\lambda = 0$) and the transverse ($\lambda = \pm$) polarization states are numerically equal. Furthermore, we plot all the bottom-conserving $B_c \rightarrow B_{(s)}^*$ transition form factors to observe their variation with respect to q^2 , as shown in Figure 3. The form factors $A_0(q^2)$, $A_1(q^2)$, and $A_2(q^2)$ display a nearly flat behavior with respect to q^2 likewise $B_c \rightarrow P$ form factors. In addition, the form factor $V(q^2)$ shows a reasonable variation in magnitude corresponding to the available q^2 . Although the variations in $V(q^2)$ form factors seem to be significant in Figure 3 (due to their higher numerical values), however are only roughly 20% larger with respect to $q^2 = 0$.

- (iii) In general, the transition form factors essentially involve the overlap integral of the initial and final state meson wave functions, which depend upon the internal degrees of freedom, mainly transverse momentum distributions and constituent quark masses. Furthermore, in CLFQM the actual magnitude of these transitions have contributions originating from vertex functions and current operators. Therefore, first we plot the overlap⁵ of initial and final wave functions at $q^2 = 0$, where we have integrated out k_\perp^2 using Eq. (5), as shown in Figure 6 with corresponding overlap factor. The larger wave function overlap can be explained by the internal momentum distribution peaks at $x_1 \sim 0$ for $\psi_{B_{(s)}^*}(x_1)$ and $x_1 \sim 0.25$ for $\psi_{B_c}(x_1)$, as per Eq. (5). The location and width of the peak are governed by constituent quark masses, where heavier quark takes larger fraction of momentum [87–89]. Thus, for $B_c \rightarrow B_{(s)}^*$ transition, the fraction of momentum carried by b quark in the bound-state is roughly same, while the momenta carried by $d(s)$ quark in $c \rightarrow d(s)$ transitions is negligibly small, since the initial meson is at rest. This results in a large overlap between the initial and final states. The overlap factor inside the total integrand, therefore, leads to decisive change in magnitude of the total form factor. For further analysis, we also plot the total integrand defined by Eq. (27) (where we include the mass factors given by Eq. (17)) with respect to the momentum fraction x_1 for the B_c meson to $P(V)$ transition form factors at $q^2 = 0$, as shown in Figures 8 and 9. It should be noted that the total integrand of transition form factors, *e.g.*, $B_c \rightarrow B_{(s)}^*$ follow exactly same overlap region which is governed by the initial and final wave functions. The bottom-conserving transition form factors have larger amplitudes than the bottom-changing form factors (as seen in Figures 8 and 9). The area under the curves gives the magnitude of the form factor for the respective transitions and we observe constructive interference for

⁵ The normalization of Gaussian-type radial wave function of meson is described by Choi *et al.* [62, 89].

most of the transition form factors, except for $A_2^{B_c B^*}$. We observe that the overlap integrand of $A_2^{B_c B^*}$ traverses both positive and negative regions with respect to changes in x_1 . The positive peak and negative peaks are due to the constructive and destructive interference of their corresponding wave functions, and therefore, should be added with their respective signs to give the total magnitude of the overlap integrand. It is worth noting that among the $B_c \rightarrow B^*$ transition form factors, the area under the peak corresponding to the $V(x_1)$ integrand is larger, which leads to the larger the magnitude of the form factor $V^{B_c B^*}(0)$, as listed in the Table IV. Similar conclusions can be made for other transition form factors. Thus, the overlap integrand plots represent the true behavior of form factors at $q^2 = 0$. Furthermore, the magnitude of the overlap is expected to increase with respect to q^2 to reach a maximum at q_{max}^2 . Since the available q^2 range is small, the overlap at q_{max}^2 is expected to be roughly the same as that at $q^2 = 0$. Therefore, a flat behavior of form factor is expected, as seen in Figures 2 and 3.

- (iv) Aforementioned, the choice of $q^+ = 0$ frame of reference restricts the calculation of the form factors only in the space-like region for momentum transfer $q^2 \leq 0$. For understanding the physical decay process, we need to know the form factors in time-like region, *i.e.*, $q^2 > 0$. This can be achieved by extrapolating the form factors as appropriate functions of q^2 (given by Eqs. (37) and (38)), for which the knowledge of form factors at $q^2 = 0$ (see Figures 8 and 9) is crucial. It should be noted that although the two methods are independent to give description of the form factors in space-like and time-like regions but are complementary to each other [64]. Thus, provide complete description of the decay dynamics of the transition process for the full q^2 range. In our work, to determine the form factors over the entire range, we utilize parameterization in Eq. (37) that accommodates the contributions of meson resonances of relevant spin and parity for the entire q^2 -channel. Similarly, the parameterization in Eq. (38) isolates meson resonances below the transition threshold for the corresponding meson poles given in Table III. In the case of B_c to $B_{(s)}^{(*)}$, we use resonances $D_{(s)}^{**}$ as pole masses to analyze q^2 behavior throughout the available range. Since the pole at $M_{D_{(s)}^{**}}^2$ lies far from the q_{max}^2 ($\lesssim 1 \text{ GeV}^2$), which is less than $\sim 25\%$ as compared to $M_{D_{(s)}^{**}}^2$. Therefore, the effect of pole contribution in the q^2 variation of bottom-conserving $B_c \rightarrow B_{(s)}^{(*)}$ form factors are smaller. Furthermore, the form factors $F_1(q^2)$, $V(q^2)$, and $A_0(q^2)$ involving M_{1-} and M_{0-} poles are affected by roughly (22 – 25)% for $B_c \rightarrow B^{(*)}$ transitions, while $B_c \rightarrow B_s^{(*)}$ transitions are less affected, *i.e.*, by (5 – 7)%. Thus, these form factors show very small variations in the $0 \leq q^2 \leq q_{max}^2$. Similarly, $F_0(q^2)$, $A_1(q^2)$, and $A_2(q^2)$ are affected by M_{0+} and M_{1+} poles, which lie farther away from q_{max}^2 , show least variation with q^2 , and therefore, show near flat behavior. In addition, the variation between the numerical values of the form factors at $q^2 = 0$ and q_{max}^2 for $B_c \rightarrow B_{(s)}^{(*)}$ form factors in Type-II* are slightly larger as compared to Type-II. This numerical variation between Type-II and Type-II* is less than 5% corresponding to the parameterizations given by Eqs. (37) and (38). Therefore, we expect that the variation in the form factors over a small q^2 range in bottom-conserving transitions can be reliably estimated by a simple VMD-type pole behavior. However, the parameterizations described by Eqs. (37) and (38) are necessary for the accuracy of the

numerical evaluation of the form factors. Moreover, such extension beyond the available q^2 range is important for the understanding of semileptonic decays. This is due to the distinct feature of the semileptonic decays in which resonances are not only observed within the kinematic range of meson decay, but also extend beyond the available q^2 region.

(v) For $B_c \rightarrow B_{(s)}^*$ transitions, the slope parameters a and b are less than one in magnitude and are positive, except for the form factors $A_2^{B_c B_{(s)}^*}$ in Type-II correspondence for Eq. (37). Interestingly, the magnitude of the parameter a is nearly zero for $A_2^{B_c B_{(s)}^*}$ which explains the flat behavior, as shown in Figure 3. We found that the numerical values of all the form factors for the Type-I scheme (using Eq. (40) and parent pole mass) are less than one, except for $V(q^2)$, the same can be observed for Type-II and Type-II*. Although the numerical values of $V(0)$ between Type-I and Type-II(*) differ roughly by 17%, the slope parameters are substantially different. Interestingly, the slope parameter a is negative and greater than one for most of the form factors, except for $A_1^{B_c B_{(s)}^*}$, and the parameter b has very large values ranging roughly from 120 – 1000 (for $A_0(q^2)$ in Type-I) with positive sign. It may be noted that both slope parameters are exceptionally large for the form factor $A_0^{B_c B_{(s)}^*}$. Similar observations can be made for the remaining form factors, where the slope parameters a and b are typically large for the Type-I scheme. As observed in $B_c \rightarrow P$ bottom-conserving transitions, for $B_c \rightarrow B_{(s)}^*$ form factors, we observe smaller numerical values for the form factors along with a decreasing trend in the Type-I scheme, as compared to Type-II correspondence. In addition, we observe that the form factors $A_0(q^2)$ and $A_1(q^2)$ affected by the zero-mode contributions show a substantial decrease in the numerical values with respect to the Type-I scheme. Furthermore, the $A_1(0)$ form factors change by $\sim 23\%$ for both Type-II and Type-II* schemes in addition to the a and b parameters. We want to emphasize that the numerical values of the form factors in Type-II(*) correspondence exhibit a significant variation in the magnitude of $A_0(0)$ form factors ranging from (70–90)% compared to Type-I scheme. The impact of the spectator quark mass on the numerical values of $B_c \rightarrow B_{(s)}^*$ transition form factors over the available q^2 is negligible, which has also been recently observed by LQCD calculations [19].

(vi) Furthermore, we analyze the z -series parameterization of the form factors at maximum recoil point (a'_0), as given in Eq. (38). The numerical results obtained from z -series parameterization are surprisingly consistent with those obtained from the q^2 dependence used in Eq. (37). In addition, the free parameters a'_1 and a'_2 take very large values, as shown in Table IV. However, the sign for a'_1 parameter is consistently negative, and a'_2 parameter is positive, except for $A_2^{B_c B_{(s)}^*}(q^2)$. Further, the magnitude of a'_2 parameter is exceedingly larger than a'_1 parameter due to the fact that the coefficients take large values for smaller $\pm|z|_{max}$ (*i.e.*, $\approx \pm 0.0008$ for B_c to $B_{(s)}^*$ transition). As already pointed out, the q^2 behavior of power series expansion, as shown by Type-II* in Figures 2 and 3, are consistent with the q^2 behavior corresponding to Eq. (37). However, it shows relatively larger variation towards the maximum q^2 , particularly for $V(q^2)$ form factors. Therefore, we reemphasize that both q^2 formulations for Type-II(*) scheme appear to be consistent with each other within very

small numerical variations.

2. Bottom-changing transition form factors

- (i) The bottom-changing transitions typically exhibit a wider range of q^2 compared to bottom-conserving transitions. In the case of $B_c \rightarrow D^{(*)}$ transition form factors, it is expected that the q^2 range will be considerably broader with respect to $B_c \rightarrow \eta_c(J/\psi)$ form factors, spanning from $0 \leq q^2 \lesssim 20 \text{ GeV}^2$. This extended range offers an opportunity to examine how the form factors are influenced by the dependence on q^2 and to highlight the importance of the resonance pole contribution below the threshold. We plot the bottom-changing B_c to P and V transition form factors to observe their variation with respect to q^2 , as shown in Figures 4 and 5, respectively. The form factors remain the same at $q^2 = 0$ for all the bottom-changing transitions in both Type-II and Type-II*. For bottom-changing transitions, both the slope parameters of $B_c \rightarrow P$ and $B_c \rightarrow V$ form factors are positive and in the range of $a, b \in (0, 2)$ and $a, b \in (1, 3)$, respectively.
- (ii) Similar to the bottom-conserving case, in order to understand the dynamics of the $B_c \rightarrow D^{(*)}$ transitions, we plot the wave function overlap between the initial $\psi_{B_c}(x_1)$ and final $\psi_{D^{(*)}}(x_1)$ wave functions at $q^2 = 0$, as shown in Figure 7a. Due to the limited overlap near $q^2 = 0$, the numerical values of the form factors are expected to be smaller as compared to $B_c \rightarrow B_{(s)}^{(*)}$ and $B_c \rightarrow \eta_c(J/\psi)$ transitions. Since the fraction of momentum carried by the spectator c quark is of the order of the decaying b quark, and u quark takes minimal momentum, where the B_c meson is at rest. Consequently, $\psi_{D^{(*)}}(x_1)$ exhibits its maximum near $x_1 \sim 1/4$ with a larger width, while the peak for $\psi_{B_c}(x_1)$ lies at $x_1 \sim 3/4$. Since the available q^2 for B_c to $D^{(*)}$ transitions is significantly large ($0 \leq q^2 \lesssim 20 \text{ GeV}^2$), these $b \rightarrow u$ transitions involves B^{**} poles fluctuating in the weak current $b\bar{u}$. Moreover, the q_{max}^2 is around 65% of the $M_{B^{**}}^2 \lesssim 34 \text{ GeV}^2$, which is not far away from the q_{max}^2 as observed in $B_c \rightarrow B_{(s)}^{(*)}$ transitions. Thus, we expect reasonable contributions from the resonance poles in the available q^2 range, as shown in Figures 4 and 5. As a result, the form factors will have larger numerical values at q_{max}^2 , as can be seen from Table V. Similar to $B_c \rightarrow B_{(s)}^{(*)}$ form factors, we also plot the total integrand for bottom-conserving transition form factors, as shown in Figures 8 and 9. Note that the total integrand of bottom-changing transition form factors show a substantial decrease in magnitude, as compared to bottom-conserving transition form factors. Additionally, we observe constructive interference for all the bottom-changing transition form factors. Among bottom-conserving and bottom changing transitions, $B_c \rightarrow \eta_c(J/\psi)$ form factor have intermediate amplitude due to the largest wave function overlap factor. As stated before, we wish to emphasize that our numerical values of form factors $F_0^{B_c D^{(s)}}(q^2)$ and $F_1^{B_c D^{(s)}}(q^2)$ are consistent with the LQCD predictions [20]. The form factors for lattice results for both at $q^2 = 0$ and q_{max}^2 are as follows: $F_{0[1]}^{B_c D}(0) = 0.186 [0.186]$, $F_{0[1]}^{B_c D}(q_{max}^2) = 0.668 [1.50]$; $F_{0[1]}^{B_c D_s}(0) = 0.217 [0.217]$, $F_{0[1]}^{B_c D_s}(q_{max}^2) = 0.736 [1.45]$. The numerical values of $B_c \rightarrow D$ form factors differ by $\sim 25\%$ at $q^2 = 0$ compared to the LQCD results. However, the consistency improves at q_{max}^2 , where the difference in their and our numerical values

is $\sim 10\%$. Furthermore, for $B_c \rightarrow D_s$ form factors, our results are in good agreement in comparison to the LQCD results, where the results match within $\sim 10\%$. It is interesting to note that the q^2 variation of Type-II* form factors in Figure 4 show a behavior similar to that observed in LQCD [20]. The numerical values of the form factors in Type-II* vary more sharply near the maximum q^2 than the form factors in Type-II. It is significant to note that the pole at $M_{B(s)^{**}}^2$ lie away from q_{max}^2 , *i.e.*, $\sim (50 - 70)\%$ of $M_{B(s)^{**}}^2$ for $B_c \rightarrow D_{(s)}^{(*)}$ transitions. Furthermore, the form factors $F_0(q^2)$ and $F_1(q^2)$ receive pole contributions from M_{0+} and M_{1-} , respectively, which result in visibly different behavior corresponding to the squared mass of resonances. We observe similar q^2 behavior for $B_c \rightarrow D_{(s)}^*$ form factors. In addition, the form factors $V(q^2)$ and $A_0(q^2)$ which receive pole contributions from M_{1-} and M_{0-} poles show expected behavior. Whereas, the form factors $A_1(q^2)$ and $A_2(q^2)$ that receive contributions from M_{1+} poles vary less sharply, as expected.

- (iii) One of the most peculiar aspects of bottom-changing transition form factors, especially for $B_c \rightarrow V$, is that they have larger values of a and b parameters due to the smaller magnitude of form factors as compared to bottom-conserving ones. It is worth mentioning that even though the numerical values of all the bottom-changing transition form factors at $q^2 = 0$ are similar between Type-I and Type-II schemes (except $A_0(q^2)$ and $A_1(q^2)$), their respective slope parameters as well as values at q_{max}^2 differ significantly with larger magnitudes, observed exclusively for parameter b . This shows that the form factors with q^2 dependence given by Eq. (40) vary more sharply. It should be emphasized that, likewise bottom-conserving transition form factors in the Type-I scheme, we observe significant numerical variation in the magnitudes of the form factor $A_0(0)$ ($A_1(0)$), *i.e.*, $\sim 30\%$ (10%) as compared to both Type-II and Type-II* schemes for $B_c \rightarrow D_{(s)}^*$ transitions. Therefore, the effect of self-consistency cannot simply be determined from the numerical values of the affected form factors at $q^2 = 0$. Particularly, in the z -series parameterization (Type-II*), the form factor at the maximum recoil point (a'_0) have comparable value with the Type-II form factor at $q^2 = 0$; however, they differ significantly at q_{max}^2 . For $B_c \rightarrow D^*$ transition, the numerical values of $A_0(0)$ between Type-I and Type-II* differ by $\sim 33\%$. On the other hand, the free parameters a'_1 and a'_2 have large values and follow the same pattern in all bottom-changing transitions. Among these, B_c to $D_{(s)}^{(*)}$ transitions have smaller value of a'_1 and a'_2 as compared to transitions involving charmonia due to the larger value of $\pm|z|_{max} = \pm 0.039$ for $D_{(s)}^{(*)}$ mesons. In general, a comparison of the numerical values of the form factors between Type-I and Type-II correspondence reveals that the effect of self-consistency and covariance leads to significant changes in the numerical values of $A_0(q^2)$ and $A_1(q^2)$. Such deviations between the two schemes are expected to be decisive for the study of weak semileptonic and nonleptonic decays. We also observe that the effects of self-consistency on bottom-changing transition form factors are smaller than those of bottom-conserving transition form factors.
- (iv) Among the bottom-changing transitions, we observe that B_c decaying to charmonium states have larger numerical values of the form factors. This is due to the fact that in $B_c \rightarrow c\bar{c}$ meson transitions, the fractional momentum of the charm quark in the final state is of the order of the spectator c quark. Therefore, $\psi_{\eta_c(J/\psi)}(x_1)$ have a peak near $x \sim 1/2$ which

shows a larger overlap with $\psi_{B_c}(x_1)$ at $x \sim 3/4$ as compared to the overlap between $\psi_{B_c}(x_1)$ and $\psi_{D_{(s)}^*}(x_1)$ (see Figure 7c), in fact the overlap is even larger than bottom-conserving transitions. Thus, the overlap plot (as shown in Figures 8 and 9) for the total integrand shows the importance of the vertex functions and other factors including masses. This results in an intermediate integrand amplitude of the $B_c \rightarrow \eta_c(J/\psi)$ form factors that lies between $B_c \rightarrow B_{(s)}^*$ and $B_c \rightarrow D_{(s)}^*$. A similar trend can be observed for Type-II* and Type-I results using the q^2 dependence given by Eqs. (38) and Eq. (40), respectively. It may be noted that for $B_c \rightarrow \eta_c(J/\psi)$ the resonance poles $M_{B_c^{**}}^2$ lies much farther as compared to $B_c \rightarrow D_{(s)}^*$ transitions, which is $\sim (21 - 26)\%$ of $M_{B_c^{**}}^2$. Further, we observed that similar to other bottom-changing transition form factors, $B_c \rightarrow \eta_c(J/\psi)$ form factors show an increasing behavior toward the maximum q^2 though less sharply. In addition, both Type-II and Type-II* q^2 formulations show roughly similar behavior, as shown in Figures 4 and 5. Furthermore, it is interesting to note that the effects of self-consistency on bottom-changing $B_c \rightarrow J/\psi$ transition form factors are minimal as compared to both bottom-conserving and other bottom-changing transition form factors.

We have employed the Type-II correspondence to vector emitting transitions for both bottom-changing and bottom-conserving decays. Moreover, we confirm that on the application of Type-II correspondence, the B_c to V transition form factors are self-consistent, *i.e.*, zero-mode contributions vanish numerically. We now proceed to calculate the branching ratios of semileptonic $B_c \rightarrow Pl\nu_l$ and $B_c \rightarrow Vl\nu_l$ decays involving $B_c \rightarrow P$ and V transition form factors, respectively.

B. Semileptonic decays

In this subsection, we study the branching ratios of the semileptonic B_c meson decays obtained by using the transition form factors given in Tables IV and V. We list our predictions of the branching ratios of $B_c^+ \rightarrow Vl^+\nu_l$ in Type-II correspondence as shown in Table VI. We have also computed these branching ratios using CLF form factors by employing Type-I correspondence, and the results are presented in column 3 of Table VII. As already discussed in the form factors, we also employ the q^2 formulation given by Eq. (38) referred to as Type-II*, to obtain the semileptonic branching ratios of B_c decays. Furthermore, we compare these results with other theoretical predictions from [26, 27, 33] and [29], as given in Table VII. In addition, we list relative decay widths, the average values of other observables for the B_c transitions, including the FB asymmetry ($\langle A_{\text{FB}} \rangle$), convexity parameter ($\langle C_F^l \rangle$), longitudinal (transverse) ($\langle P_{L(T)}^l \rangle$) polarization of the charged lepton, and asymmetry parameter (α^*) in Table VI. Furthermore, we plotted the q^2 variation of the differential decay rates and $A_{\text{FB}}(q^2)$ of $B_c^+ \rightarrow Vl^+\nu_l$ decays in Figures 10 and 11, respectively.

1. Bottom-conserving decays

The bottom-conserving CKM-enhanced ($\Delta b = 0, \Delta C = -1, \Delta S = -1$) and CKM-suppressed ($\Delta b = 0, \Delta C = -1, \Delta S = 0$) semileptonic decay modes of B_c mesons undergo kinematic suppres-

sion due to the large mass of the $B_{(s)}^*$ meson in the final states. These semileptonic decay processes provide an excellent opportunity to observe the effects of form factors on the branching ratios and, therefore, to test the theoretical models. In addition to form factors, kinematic and CKM factors play an important role in determining their magnitude. We analyzed $B_c^+ \rightarrow B_{(s)}^{*0} l^+ \nu_l$ decays using the self-consistent CLFQM. We have observed the following.

- (i) We observe that the branching ratios of bottom-conserving decays are of $\mathcal{O}(10^{-2})$ to $\mathcal{O}(10^{-3})$ despite of the kinematic suppression. Among these decays, the CKM-enhanced modes have dominant branching ratios, *i.e.*, $\mathcal{B}(B_c^+ \rightarrow B_s^{*0} e^+ \nu_e) = 3.20 \times 10^{-2}$ and $\mathcal{B}(B_c^+ \rightarrow B_s^{*0} \mu^+ \nu_\mu) = 2.99 \times 10^{-2}$. This is due to the fact that the kinematic suppression is predominated by the CKM factor (V_{cs}). On the other hand, the branching ratios of $B_c \rightarrow B^* l \nu_l$ decays involving $c \rightarrow d$ transition (governed by V_{cd}) are smaller by an order of magnitude. Although we focus on $P \rightarrow V$ semileptonic decays of the B_c meson, we list $B_c^+ \rightarrow P l^+ \nu_l$ decays in CLFQM for both Type-II^(*) and Type-I correspondence, as shown in Table I of Appendix A. In general, the branching ratios of $P \rightarrow V$ semileptonic decays are expected to be larger than $P \rightarrow P$ decays, which can also be observed from our results. We found that our results are in good agreement with recent LQCD predictions [19]. The bottom-conserving branching ratios for lattice results are as follows: $\mathcal{B}(B_c^+ \rightarrow B^0 l \nu_l) = (8.47 \pm 0.31 \pm 0.43 \pm 0.24) \times 10^{-4}$ and $\mathcal{B}(B_c^+ \rightarrow B_s^0 l \nu_l) = (1.348 \pm 0.046 \pm 0.033 \pm 0.043) \times 10^{-2}$ [19]. In order to ensure the reliability of the CLF approach, we compare the decay width ratios of our results with LQCD expectations:

Type-II (Type-II*)	LQCD [19]
$\frac{\Gamma(B_c^+ \rightarrow B_s^{*0} e^+ \nu_e) V_{cd} ^2}{\Gamma(B_c^+ \rightarrow B^0 e^+ \nu_e) V_{cs} ^2} = 0.894 \text{ (0.840)}$	(0.759 ± 0.044) ;
$\frac{\Gamma(B_c^+ \rightarrow B_s^{*0} \mu^+ \nu_\mu) V_{cd} ^2}{\Gamma(B_c^+ \rightarrow B^0 \mu^+ \nu_\mu) V_{cs} ^2} = 0.882 \text{ (0.834)}$	(0.759 ± 0.044) .

Our results are in good agreement with LQCD ratios for Type-II* q^2 formulation; however, are slightly larger for Type-II q^2 formulation. Correspondingly, for $B_c \rightarrow B_{(s)}^* l \nu_l$ decays, we predict

$$\frac{\Gamma(B_c^+ \rightarrow B_s^{*0} e^+ \nu_e) |V_{cd}|^2}{\Gamma(B_c^+ \rightarrow B^{*0} e^+ \nu_e) |V_{cs}|^2} = 0.889 \text{ (0.850);}$$

$$\frac{\Gamma(B_c^+ \rightarrow B_s^{*0} \mu^+ \nu_\mu) |V_{cd}|^2}{\Gamma(B_c^+ \rightarrow B^{*0} \mu^+ \nu_\mu) |V_{cs}|^2} = 0.878 \text{ (0.836)}.$$

- (ii) The $B_c \rightarrow V l \nu_l$ branching ratios are influenced mainly by the form factors $V(q^2)$, $A_1(q^2)$, and $A_2(q^2)$. However, it is worth mentioning that the contribution of the form factor $A_0(q^2)$ to these branching ratios can be considered insignificant (see Eq. (41)). It is well known that in the semileptonic $P \rightarrow V$ weak decays, the contribution from the form factor $A_2(q^2)$ can be ignored due to the negligible coefficient in the decay rates [29, 90]. Furthermore, the branching ratios of the semileptonic decays depend upon the magnitude and signs of the form factors. We want to emphasize that the numerical values of the form factors, especially $A_0(q^2)$ and $A_1(q^2)$ have changed significantly in Type-II correspondence. Therefore, to quantify the

effect of self-consistency on the branching ratios of the semileptonic decay modes, we compare our results with those of Type-I correspondence. We found that the numerical results for Type-II scheme (using Eq. (37)) are larger by (50–60)% as compared to the branching ratios in Type-I scheme. Similar observations can be made for the comparison between Type-II* and Type-I results, because the results between Type-II and Type-II* differ by less than 10% for bottom-conserving modes. As expected the difference between the Type-I and Type-II correspondence results is sufficiently large and thus cannot be ignored. In addition, we also compare our results with other works [26, 27, 29, 33], and we found that our results for bottom-conserving semileptonic decays are of the same order as compared to others, except for $B_c^+ \rightarrow B^{*0}l^+\nu_l$ by Li *et al.*[26] using the CLFQM framework within Type-I scheme.

- (iii) The mass difference between the electrons and muons has minimal impact ($\sim 6\%$) on the branching ratios and other physical observables of bottom-conserving semileptonic $B_c \rightarrow B_{(s)}^*$ decays. Additionally, the comparative variation of bottom-conserving semileptonic differential decay rates for e and μ lepton modes with respect to q^2 are plotted in Figures 10a and 10b. It should be noted that in semileptonic decay processes, the physical observables depend on the mass of the final lepton, with $q_{min}^2 = m_l^2$ (assuming mass of neutrino is negligible). The differential decay rate plots show distinct peaks corresponding to the lepton mass for the available q^2 range, with the same end points at q_{max}^2 as expected. We also have calculated relative longitudinal and transverse decay widths, and their ratios for bottom-conserving $B_c^+ \rightarrow Vl^+\nu_l$ decays, as shown in columns 4, 5, and 6 of Table VI, respectively. It is noteworthy to mention that the longitudinal component of the decay widths dominates the transverse component; however, the difference between their magnitudes is small, *i.e.*, (6–8)%. The longitudinal decay widths of $B_c \rightarrow B_{(s)}^*l\nu_l$ decays decreases with increasing lepton mass but marginally.
- (iv) Also, we calculated the expectation values of FB asymmetry, A_{FB} , using Eq. (50), as shown in column 7 of Table VI. It is noteworthy that all the $A_{FB}(B_c^+ \rightarrow Vl^+\nu_l)$ values are negative without any exceptions. The negative values of A_{FB} in bottom-conserving semileptonic decays reflect the dominance of the parity-violating helicity structure-function, \mathcal{H}_P , particularly with a larger contribution from H_- amplitude. The \mathcal{H}_{SL} contributions are negligible for electron decay modes, and its value increases with increasing lepton mass. We notice that the magnitude of \mathcal{H}_{SL} in $A_{FB}(B_c^+ \rightarrow B_{(s)}^*\mu^+\nu_\mu)$ is larger by (18–20)% leading to more negative value. Addressing the minimal discrepancy between Type-II and Type-II* in form factors and semileptonic branching ratios, a similar trend can be observed for A_{FB} and other observables. As a result, we only present the results of physical observables obtained from Type-II formulation. Furthermore, we plot the q^2 variation of the FB asymmetry of $B_c^+ \rightarrow B_{(s)}^*l^+\nu_l$ decays in Figures 11a and 11b. Notably, A_{FB} shows a distinct rise near q_{min}^2 , particularly in the electron decay mode. The high precision calculation shows that $A_{FB} \rightarrow 0$ as $q^2 \rightarrow 0$. Such behavior can also be seen in other works [28, 91].
- (v) Furthermore, we calculated the mean values of C_F^l , P_L^l , and P_T^l , as shown in columns 8, 9, and 10 of Table VI, respectively. It is noteworthy that the bottom-conserving semilep-

tonic decay modes have a negative lepton-side convexity parameter, C_F^l , which is due to the predominance of the longitudinal helicity component, \mathcal{H}_L . Additionally, the transverse polarization parameter, P_T^l is very small for e decay modes, *i.e.*, $\mathcal{O}(10^{-3})$. Furthermore, we also computed the asymmetry parameter, α^* by using Eq. (54), as illustrated in column 11 of Table VI. The asymmetry parameter, α^* , is consistently negative for all B_c to V semileptonic decays, indicating the dominance of the longitudinal helicity components, \mathcal{H}_L and \mathcal{H}_S . Notably, parameters such as C_F^l , P_L^l and α^* show decrease in magnitude with increases in lepton mass.

2. Bottom-changing decays

In this subsection, we focus on the bottom-changing CKM-enhanced ($\Delta b = -1, \Delta C = -1, \Delta S = 0$) and CKM-suppressed ($\Delta b = -1, \Delta C = 0, \Delta S = 0$) semileptonic decay modes of B_c mesons, which involve the charm mesons in the final states. One notable aspect of bottom-changing semileptonic decays is that they include $\tau^+\nu_\tau$ alongside $e^+\nu_e$ and $\mu^+\nu_\mu$ lepton pairs in the final state. We have analyzed and listed our major findings on $B_c \rightarrow D^*(J/\psi)l\nu_l$ decays as follows:

- (i) The branching ratios of bottom-changing $B_c^+ \rightarrow Vl^+\nu_l$ decays ranges from $\mathcal{O}(10^{-2})$ to $\mathcal{O}(10^{-5})$. Among these decays, $B_c^+ \rightarrow J/\psi e^+\nu_e$ and $B_c^+ \rightarrow J/\psi \mu^+\nu_\mu$ are most dominant with branching ratios 2.60×10^{-2} and 2.59×10^{-2} , respectively, since $B_c^+ \rightarrow J/\psi l^+\nu_l$ decays are both CKM- and kinematically enhanced. On the other hand, the CKM-suppressed $B_c^+ \rightarrow D^{*0}l^+\nu_l$ decays, involving $b \rightarrow u$ transition, have smaller branching ratios, *i.e.*, $\mathcal{O}(10^{-5})$. Similar to bottom-conserving $B_c \rightarrow P$ semileptonic decays, the branching ratios of bottom-changing $B_c^+ \rightarrow Dl^+\nu_l$ decays are of the same order, though small in magnitude as compared to the recent LQCD results [20]. The bottom-changing branching ratios for lattice results are as follows: $\mathcal{B}(B_c^+ \rightarrow D^0 e^+\nu_e) = (3.37 \pm 0.48 \pm 0.08 \pm 0.42) \times 10^{-5}$ and $\mathcal{B}(B_c^+ \rightarrow D^0 \tau^+\nu_\tau) = (2.29 \pm 0.23 \pm 0.06 \pm 0.29) \times 10^{-5}$ [20].
- (ii) In bottom-changing semileptonic B_c transitions, the phase space is usually larger compared to bottom-conserving transitions. Specifically, the semileptonic branching ratios involving $B_c \rightarrow D^*$ and $B_c \rightarrow J/\psi$ have 45% and 75% difference between the e (or μ) and τ semileptonic decays, respectively. It is worth noting that the mass difference between the electron and muon does not significantly affect $b \rightarrow u(c)$ semileptonic decays. As observed before, the branching ratios decrease with increasing lepton mass, *i.e.*, the branching ratios of $B_c \rightarrow J/\psi e(\mu)\nu_{e(\mu)}$ are larger roughly by a factor of 4 of $\mathcal{B}(B_c \rightarrow J/\psi \tau\nu_\tau)$. Similarly, for $B_c \rightarrow D$ semileptonic decays, the corresponding decay modes are ~ 2 times larger than $\mathcal{B}(B_c \rightarrow D^* \tau\nu_\tau)$. Furthermore, as observed in bottom-conserving decays, the relative longitudinal decay widths for all the semileptonic $B_c \rightarrow D^*(J/\psi)$ decays have larger magnitude than the transverse decay widths, except for $B_c \rightarrow J/\psi \tau^+\nu_\tau$ decay mode. In addition, we calculate the LFU ratios between τ and $e(\mu)$ leptons for both Type-II and Type-II* results as follows:

	Type-II	Type-II*	LQCD [18]
$\mathcal{R}_{D^*} = \frac{\mathcal{B}(B_c^+ \rightarrow D^{*0} \tau^+ \nu_\tau)}{\mathcal{B}(B_c^+ \rightarrow D^{*0} e(\mu)^+ \nu_{e(\mu)})} =$	0.545 (0.545)	0.594 (0.599)	— ;

$$\mathcal{R}_{J/\psi} = \frac{\mathcal{B}(B_c^+ \rightarrow J/\psi \tau^+ \nu_\tau)}{\mathcal{B}(B_c^+ \rightarrow J/\psi e(\mu)^+ \nu_{e(\mu)})} = 0.247 \text{ (0.247)} \quad 0.248 \text{ (0.249)} \quad 0.2582 \pm 0.0038.$$

Note that the experimental measurements for the LFU ratios involving $b \rightarrow c \tau \nu_\tau$ for J/ψ in the final state is $\mathcal{R}_{J/\psi} = 0.71 \pm 0.18 \pm 0.17$ [17], which is much larger than the theoretical estimates. We want to emphasize that the current SM predictions for these ratios fall within a range of $0.25 - 0.28$ [23, 92, 93], including ours. It is worth mentioning that the difference between multiple approaches is very small, which also agrees with the LQCD observation [18]. Furthermore, the experimental observation is substantially larger than the theoretical expectations, even though the cumulative uncertainties in the experimental value are of the order of 50%. Thus, more experimental observations would result in a clear picture to establish the scope of new physics beyond the SM in these decays. Similarly, for bottom-conserving $B_c \rightarrow B_{(s)}^*$ semileptonic decays, we found

	Type-II	Type-II*
$\mathcal{R}_{B^*} = \frac{\mathcal{B}(B_c^+ \rightarrow B^{*0} \mu^+ \nu_\mu)}{\mathcal{B}(B_c^- \rightarrow B^{*0} e^+ \nu_e)}$	= 0.946	0.951;
$\mathcal{R}_{B_s^*} = \frac{\mathcal{B}(B_c^+ \rightarrow B_s^{*0} \mu^+ \nu_\mu)}{\mathcal{B}(B_c^+ \rightarrow B_s^{*0} e^+ \nu_e)}$	= 0.934	0.935,

which is in good agreement with Ref. [27].

- (iii) As previously noted, the self-consistency effects are expected to be significant in semileptonic $B_c \rightarrow D^*$ decays. The branching ratios of $B_c^+ \rightarrow D^{*0} l^+ \nu_l$ decays in the Type-II^(*) correspondence scheme show a variation ranging from $\sim (64 - 85)\%$ compared to those in the Type-I scheme. However, self-consistency has a minimal effect on the branching ratios of semileptonic decays of B_c to J/ψ states, with variation of $(24 - 28)\%$ across Type-I results, when compared to Type-II^(*) results. Additionally, to compare our results with other works, we have included the branching ratios from literature [27, 29, 33], as presented in Table VII. Interestingly, a similar order of discrepancy can be observed in Type-I correspondence scheme results from other works as compared to that of Type-II correspondence predictions from our work. For $B_c^+ \rightarrow J/\psi l^+ \nu_l$, numerical results of the branching ratios are consistent with other literature; in fact, all the models yield branching ratios of the same order. In general, we observe substantial differences in the numerical values of branching ratios for bottom-changing semileptonic decays from different models that range up to $\sim 60\%$. Particularly, the discrepancy among $\mathcal{B}(B_c^+ \rightarrow D^{*0} l^+ \nu_l)$ results in the Type-I scheme from other works and Type-II scheme in our work also range from $\sim (35 - 60)\%$. We have also plotted the q^2 variation of the differential decay rates of $B_c^+ \rightarrow D^{*0} l^+ \nu_l$ and $B_c^+ \rightarrow J/\psi l^+ \nu_l$ in Figure 10c and 10d, respectively.

- (iv) Furthermore, we calculated the A_{FB} for bottom-changing semileptonic decays, and listed in column 7 of Table VI. The A_{FB} for bottom-changing decays are consistently negative in numerical values due to the dominant contributions from \mathcal{H}_{SL} , with a larger magnitude for the H_0 helicity amplitude. The exception is evident in the decays that involve the pairing of an electron in the final state, where \mathcal{H}_P is predominantly large because of the larger

magnitude of H_- helicity amplitude. However, the contributions from \mathcal{H}_P decrease with the lepton mass. Further, as the mass of the lepton increases, the $A_{FB}(B_c \rightarrow D^* \tau \nu_\tau)$ increases by approximately 27% as compared to $A_{FB}(B_c \rightarrow D^* e \nu_e)$; however, $A_{FB}(B_c \rightarrow J/\psi \tau \nu_\tau)$ increase up to 40% from $A_{FB}(B_c \rightarrow J/\psi e \nu_e)$.

- (v) We observe a behavior similar to that of A_{FB} for observables such as C_F^l and P_L^l with respect to the lepton mass. Here also, the values of e and μ decays are almost identical and only τ decays show some significant change. Furthermore, the α^* values leads to observable differences especially in the case of τ decays, *i.e.*, D^* and J/ψ have 27% and 34% variation with respect to e decays, respectively. This distinction arises from the influence of the lepton's mass on the decay process.

C. Nonleptonic decays

In this subsection, we give our predictions for the branching ratios of nonleptonic $B_c \rightarrow PV$ decays. Aforementioned, the nonleptonic decays of the B_c meson consist of CKM-enhanced ($\Delta b = 0, \Delta C = -1, \Delta S = -1$; $\Delta b = -1, \Delta C = -1, \Delta S = 0$; and $\Delta b = -1, \Delta C = 0, \Delta S = 1$), CKM-suppressed ($\Delta b = 0, \Delta C = -1, \Delta S = 0$; $\Delta b = -1, \Delta C = -1, \Delta S = 1$; and $\Delta b = -1, \Delta C = 0, \Delta S = 0$), and CKM-doubly-suppressed ($\Delta b = 0, \Delta C = -1, \Delta S = 1$; $\Delta b = -1, \Delta C = 1, \Delta S = 1$; and $\Delta b = -1, \Delta C = 1, \Delta S = 0$) bottom-conserving and bottom-changing decay modes. We calculated the decay amplitude using the decay constants listed in Table VIII. Among the form factors listed in Tables IV and V for $B_c \rightarrow P$ and $B_c \rightarrow V$ transitions, only the form factors $F_1(q^2)$ and $A_0(q^2)$ are relevant for the numerical evaluation of the branching ratios of $B_c \rightarrow PV$ decays. Since the $A_0(q^2)$ form factor is affected by self-consistency issues related to the $B_j^{(i)}$ functions, the study of nonleptonic $B_c \rightarrow PV$ decays provides an excellent opportunity to investigate such effects between Type-I and Type-II correspondence. We determine the branching ratios of nonleptonic B_c decays involving color-favored diagram (Class-I), color-suppressed diagram (Class-II), and their interference (Class-III) for both large N_c limit and $N_c = 3$, as given by Eqs. (60) and (61) in Sec. II C. We list all the possible bottom-conserving $B_c \rightarrow PV$ decays in Table IX, and Tables X, XI, and XII show our predictions for bottom-changing decays. We list our key findings as follows.

- (i) For bottom-conserving decay modes, the branching ratios of B_c meson decays into $B^{(*)}$ and $B_s^{(*)}$ mesons in the final state ranges from $\mathcal{O}(10^{-2})$ to $\mathcal{O}(10^{-6})$ for the Type-II formulation and up to $\mathcal{O}(10^{-5})$ for Type-II*, as shown in Table IX. It is well known for the case of CKM-favored decays that the CKM-enhancement dominates the kinematic suppression, resulting in branching ratios of $\mathcal{O}(10^{-2}) \sim \mathcal{O}(10^{-3})$ for $N_c = \infty$. Among them, the most dominant CKM and color-favored (Class I) decays are $B_c^+ \rightarrow \pi^+ B_s^{*0}$ and $B_c^+ \rightarrow B_s^0 \rho^+$, which have branching ratios of 4.86×10^{-2} and 3.65×10^{-2} , respectively. It is worth noting that for $B_c \rightarrow B_{(s)}^{(*)}$ transition, the mass of the spectator b quark is significantly larger than that of the decaying c quark, and the whole momentum is carried by the b quark. Therefore, the transition form factors at $q^2 = 0$ in such case differ up to $\sim 25\%$ from those at maximum momentum transfer between the initial and final states. This variation in the form factor at q_{max}^2 leads to an increase of $\sim (22 - 40)\%$ in the branching ratio of $B_c^+ \rightarrow \pi^+ B_s^{*0} / \bar{K}^0 B^{*+}$

decays (involving $A_0(q^2)$ form factors) for both Type-II and Type-II* formulations. However, the decays involving the form factors $F_1(q^2)$ are affected by less than 10% at maximum momentum transfer.

- (ii) We want to emphasize that $A_0(q^2)$ transition form factors are affected by the self-consistency problems, and their contribution to semileptonic decays involving vector meson in the final state are suppressed in general. However, nonleptonic $B_c \rightarrow PV$ decays that explicitly involve $A_0(q^2)$ form factors would give quantitative measure of self-consistency effects between Type-II and Type-I correspondence schemes. Therefore, we compare our predictions in Type-II(*) with the results in Type-I correspondence, as listed in columns 2, 4, and 6 of Table IX. It may be noted that the results in the tables follow the order in which decays involving $A_0(q^2)$ are listed first, decays involving $F_1(q^2)$ are listed thereafter, and Class-III decays involving both (if allowed) are given last for each CKM mode. We found that the results of the Type-I scheme for CKM-favored bottom-conserving modes are significantly smaller for $B_c^+ \rightarrow \pi^+ B_s^{*0} / \bar{K}^0 B^{*+}$ decays. The branching ratio of color-favored $B_c^+ \rightarrow \pi^+ B_s^{*0}$ decay in the Type-I scheme is $\sim 60\%$ smaller than that of the Type-II scheme. However, the branching ratio of color-suppressed $B_c^+ \rightarrow \bar{K}^0 B^{*+}$ decay changes by $\mathcal{O}(10^{-3})$ in Type-II scheme as compared to Type-I predictions. Moreover, when we compare the numerical results of Type-I and Type-II schemes for exactly same q^2 formulation⁶, *i.e.*, for Eq. (40), we found that $\mathcal{B}(B_c^+ \rightarrow \pi^+ B_s^{*0})$ decay decrease by $\sim 40\%$, while $\mathcal{B}(B_c^+ \rightarrow \bar{K}^0 B^{*+})$ decay still decreases by $\mathcal{O}(10^{-3})$. Thus, we found that the effects of self-consistency on such decays are significant and cannot be ignored. Furthermore, the changes in numerical results for decays involving $F_1(q^2)$ can be attributed to the variations due to q^2 formulations.
- (iii) In the bottom-conserving CKM-suppressed modes, the branching ratios for the dominant decays are $\mathcal{B}(B_c^+ \rightarrow B^0 \rho^+) = 2.87 \times 10^{-3}$, $\mathcal{B}(B_c^+ \rightarrow K^+ B_s^{*0}) = 2.64 \times 10^{-3}$, and $\mathcal{B}(B_c^+ \rightarrow \pi^+ B^{*0}) = 2.26 \times 10^{-3}$. All these decays involve color-favored (Class-I) process. The next order branching ratios are of the order of $\mathcal{O}(10^{-4})$, which correspond to the color-suppressed process, as shown in Table IX. As observed in CKM-enhanced decays, apart from the variation due to different q^2 formulations, the branching ratios of the decays involving $A_0(q^2)$ form factors change substantially as compared to those of the Type-I scheme. We wish to emphasize that the branching ratios of the decays involving $A_0(q^2)$ form factors and color-favored processes in CKM-suppressed modes are more seriously affected by self-consistency. The branching ratios of these decays change by $\mathcal{O}(10^{-2})$ or more. It is interesting to note that the branching ratios of CKM-doubly-suppressed decays are of $\mathcal{O}(10^{-4}) \sim \mathcal{O}(10^{-6})$ with dominant branching ratio, $\mathcal{B}(B_c^+ \rightarrow K^+ B^{*0}) = 1.40 \times 10^{-4}$ for color-favored decay. Furthermore, the effect of self-consistency in such decay modes is even larger as compared to CKM-enhanced and -suppressed modes.
- (iv) In addition to the large N_c limit, we also predict branching ratios of the results at $N_c = 3$, as shown in columns 3, 5, and 7 of Table IX for Type-II, Type-II*, and Type-I, respectively.

⁶ Note that the numerical results of Type-II correspondence scheme for Eq. (40): $A_0^{B_c B^*}(0) = 0.60$, $a = -4.52$, $b = 271.10$ and $A_0^{B_c B_s^*}(0) = 0.48$, $a = -9.93$, $b = 337.80$ are used.

Aforementioned, we have considered tree-dominated B_c decays and have neglected the small nonfactorizable and penguin contributions within our formalism. As prior mentioned, the number of color degrees of freedom (N_c) is usually treated as a phenomenological parameter in weak meson decays to account for nonfactorizable contributions. In the present case, we have used the $N_c = 3$ based on the model-independent analysis of B decays, which suggests that a_2 have smaller magnitude [79]. We get $a_1 = 1.09$ and $a_2 = -0.09$ at $N_c = 3$ for bottom-conserving B_c decays (Eq. (61)). Since, the bottom-conserving weak decays does not involve any Class-III decays, we expect an overall decrease in the branching ratios of these decays corresponding to smaller values of a_1 and a_2 at $N_c = 3$. We observe that the numerical values of color-suppressed decays at $N_c = 3$ are more seriously affected on account of substantial reduction in the magnitude of coefficient a_2 . Hence, these predictions can be seen as a reasonable range of numerical predictions in the current formalism.

- (v) In the case of bottom-changing B_c decays to $D^{(*)}$, $D_s^{(*)}$, and $\eta_c(J/\psi)$ mesons in the final state, we enlist the branching ratio predictions in Tables X, XI, and XII. The most dominant CKM-enhanced decay modes, $B_c^+ \rightarrow \eta_c \rho^+$, $B_c^+ \rightarrow D_s^+ J/\psi$, $B_c^+ \rightarrow \pi^+ J/\psi$, and $B_c^+ \rightarrow \eta_c D_s^{*+}$ have branching ratios 4.31×10^{-3} , 3.00×10^{-3} , 1.91×10^{-3} , and 1.88×10^{-3} , respectively, at large N_c limit. Among these, $B_c^+ \rightarrow \eta_c \rho^+$ and $B_c^+ \rightarrow \pi^+ J/\psi$ decays are color-favored (Class-I) decays, while $B_c^+ \rightarrow D_s^+ J/\psi$ and $B_c^+ \rightarrow \eta_c D_s^{*+}$ are Class III type decays. We wish to emphasize that the $B_c^+ \rightarrow D_s^+ J/\psi$ and $B_c^+ \rightarrow \eta_c D_s^{*+}$ decays receive contributions from both color-favored and -suppressed diagrams and interfere destructively at large N_c limit. However, at $N_c = 3$, color-favored and -suppressed contributions for both of these decays interfere constructively, yielding larger branching ratios due to the positive values of a_1 and a_2 (as shown in Eq.(61)). In the CKM-enhanced ($\Delta C = -1, \Delta S = 0$) mode, the branching ratios of $B_c^+ \rightarrow \bar{D}^0 D^{*+}$ and $B_c^+ \rightarrow D^+ \bar{D}^{*0}$ are of $\mathcal{O}(10^{-5})$, which falls within the experimental upper limits [12]. In contrast, for ($\Delta C = 0, \Delta S = 1$) mode, the branching ratios of the next order of decays, *e.g.*, $B_c^+ \rightarrow \pi^0 D_s^{*+}$, $B_c^+ \rightarrow K^+ D^{*0}$, $B_c^+ \rightarrow D^0 K^{*+}$, and $B_c^+ \rightarrow D_s^+ \rho^0$, remain highly suppressed. The branching ratios of these decays range from $\mathcal{O}(10^{-7}) \sim \mathcal{O}(10^{-10})$ as they occur through CKM-suppressed $b \rightarrow u$ weak transitions. Furthermore, the branching ratios of dominant bottom-changing decays are smaller as compared to the dominant bottom-conserving decays. As expected, due to the smaller values of a_1 and a_2 at $N_c = 3$, the branching ratios of all the decays show a decreasing trend, except for Class-III decays.
- (vi) In the CKM-suppressed ($\Delta C = -1, \Delta S = 1$) decay mode, the dominant $B_c^+ \rightarrow \eta_c K^{*+}$ and $B_c^+ \rightarrow K^+ J/\psi$ decays have branching ratios of $\mathcal{O}(10^{-4})$, and the branching ratios for the rest of the decays are of $\mathcal{O}(10^{-6})$. In the CKM-suppressed ($\Delta C = 0, \Delta S = 0$) mode, the branching ratios are of $\mathcal{O}(10^{-4}) \sim \mathcal{O}(10^{-9})$, where the dominant modes $B_c^+ \rightarrow D^+ J/\psi$ and $B_c^+ \rightarrow \eta_c D^{*+}$ belong to Class III decays. These decays arise from destructive interference between color-favored and color-suppressed processes, and have the branching ratios of $\mathcal{O}(10^{-4})$. Aforementioned, at $N_c = 3$, both coefficients a_1 and a_2 become positive, which enhances their branching ratios as compared to the values at $N_c = \infty$. Furthermore, B_c meson decaying to $D^0 \rho^+$ and $\pi^+ D^{*0}$ in the final states are the only decays that involve the color-favored diagram and have branching ratios of $\mathcal{O}(10^{-6})$. In addition, $\mathcal{B}(B_c^+ \rightarrow$

$\overline{D}^0 D_s^{*+}) = 1.77 \times 10^{-6}$ and $\mathcal{B}(B_c^+ \rightarrow D_s^+ \overline{D}^{*0}) = 2.09 \times 10^{-6}$ at large N_c limit, which are within the experimental upper limit [12].

- (vii) Since we have focused on the discrepancies arising because of the self-consistency problem in form factors and consequently on the decays of B_c meson, we compare our results of the Type-II scheme with those of the Type-I bottom-changing decays. We found that CKM and color-favored bottom-changing decays suffer a change in branching ratios between (30 – 70)%. However, the branching ratios of dominant Class-III decays, which involve $F_1(q^2)$ and $A_0(q^2)$ form factors, change by (15 – 33)%. A change in branching ratios of similar order of magnitude is also observed for CKM-suppressed dominant modes. It may be noted that, in the above mentioned changes corresponding to self-consistency, we have only considered the branching ratios up to $\mathcal{O}(10^{-6})$. Thus, we construe that likewise for bottom-conserving decays, the bottom-changing decays are significantly affected by self-consistency issues, especially for color-favored decays, and therefore cannot be ignored.
- (viii) It is worth noticing that all of the CKM-doubly-suppressed B_c decays belong to the Class-III category. The color-favored and color-suppressed amplitudes interfere destructively to give the branching ratios $\mathcal{O}(10^{-6}) \sim \mathcal{O}(10^{-8})$ for these decays. As intended, the branching ratios of these modes are enhanced at $N_c = 3$. However, the effects of self-consistency on the branching ratios of these decays are roughly (20 – 90)%. Furthermore, all the bottom-changing CKM-doubly-suppressed $B_c \rightarrow PV$ decays such as, $B_c^+ \rightarrow D^0 D_{(s)}^{*+}$ and $B_c^+ \rightarrow D_{(s)}^+ D^{*0}$ are within the observed experimental upper limit [12].

- (ix) It should be noted that the recent experimental observations provide the ratios of branching fractions of nonleptonic B_c decays involving a J/ψ meson in the final state. Therefore, we compared our results with the experimental values reported by LHCb and ATLAS [13–16]. The ratios of the branching fractions determined theoretically are expressed as follows:

Type-II	Type-II*	Experimental value
$\frac{\mathcal{B}(B_c^+ \rightarrow J/\psi D_s^+)}{\mathcal{B}(B_c^+ \rightarrow J/\psi \pi^+)} = 2.350$ (1.571)	2.356 (1.571)	$2.76 \pm 0.33 \pm 0.33$ [14];
$\frac{\mathcal{B}(B_c^+ \rightarrow J/\psi K^+)}{\mathcal{B}(B_c^+ \rightarrow J/\psi \pi^+)} = 0.075$ (0.076)	0.075 (0.076)	$0.079 \pm 0.007 \pm 0.003$ [15],

where the values in the parentheses are obtained for large N_c limit. We wish to point out that our results for $N_c = 3$ match well with the experimental values within the uncertainties. Similarly, we compare the ratio of the branching fractions for the nonleptonic $B_c^+ \rightarrow J/\psi \pi^+$ decay to the semileptonic $B_c^+ \rightarrow J/\psi \mu^+ \nu_\mu$ decay with the experiment, as given below,

Type-II	Type-II*	Experimental value
$\frac{\mathcal{B}(B_c^+ \rightarrow J/\psi \pi^+)}{\mathcal{B}(B_c^+ \rightarrow J/\psi \mu^+ \nu_\mu)} = 0.063$ (0.074)	0.062 (0.073)	$0.0469 \pm 0.0028 \pm 0.0046$ [94].

We note that our results though larger in magnitude are very close to experimental observation including the errors.

Finally, we compare our numerical results of the branching ratios with those of other theoretical models, such as RIQM [36, 37], RCQM [33], RQM [31], QCDF [40], pQCD [38, 39], and CLFQM (Type-I) [28]. All branching ratio predictions from different models are of the same order, with a few exceptions. Among them, our numerical results for the bottom-conserving branching ratios of B_c decays involving a B meson in the final state match well with the QCDF [40] results. We observe that our Type-II predictions for the most dominant bottom-changing CKM-favored B_c decays, *i.e.*, involving $\eta_c\rho^+$, D_s^+J/ψ , π^+J/ψ , and $\eta_c D_s^{*+}$ in the final state, match very well with the predictions of RCQM [33], except $B_c^+ \rightarrow \eta_c D_s^{*+}$. Notably, for these decays, the predictions from other theoretical models are larger as compared to our results. We also compared our Type-I results with CLFQM (Type-I) [28] and observed that their values are of the same order but larger than ours by roughly (30 – 70)%, due to the different input parameters and the exponential q^2 formulation used in their work.

IV. SUMMARY AND CONCLUSIONS

In this paper, we provide a comprehensive analysis of weak transition form factors, semileptonic decays, and nonleptonic decays of the B_c meson involving P and V mesons in CLFQM. We employed Type-II correspondence in the CLF approach to resolve the self-consistency issues due to the presence of $B_j^{(i)}$ functions. It may be noted that the issues of inconsistency and violation of covariance in Type-I correspondence, which affect the $A_0(q^2)$ and $A_1(q^2)$ form factors, can be simultaneously resolved by $M^{(n)} \rightarrow M_0^{(n)}$ considered in Type-II correspondence [60]. However, the quantitative measure of these effects in Type-II correspondence has never been studied in semileptonic as well as nonleptonic decays of the B_c meson. The main focus of the current work is to establish the effects of self-consistency originating from the transition form factors to the weak decays in a quantitative manner. The self-consistency affects the numerical results of the form factors $A_0(q^2)$ and $A_1(q^2)$, which in turn appear in the semileptonic and nonleptonic decays of the B_c meson. It is well known that the coefficient of $A_0(q^2)$ form factor is suppressed in the semileptonic decay rates; therefore, semileptonic decays only provide a comprehensive picture that corresponds to the effects originating from $A_1(q^2)$ form factor. Thus, to observe the effect of $A_0(q^2)$ form factor, we calculated the $B_c \rightarrow PV$ decays which involve $F_1(q^2)$ and $A_0(q^2)$ form factors. Therefore, we calculated the transition form factors in CLFQM formalism in Tables IV and V. In the current work, we thoroughly examined the appropriate q^2 formulations, especially for bottom-conserving transitions involving $B_c \rightarrow V(P)$ form factors. Therefore, we have analyzed two different q^2 formulations in Type-II correspondence referred to as Type-II and Type-II* by using Eqs. (37) and (38), respectively. We also compared our results with Type-I correspondence for the q^2 formulation in Eq. (40) to assess the effects of self-consistency quantitatively. Consequently, we observed their implications on semileptonic and nonleptonic weak decays of B_c meson. In addition, we calculated the experimentally significant physical observables, namely, the FB asymmetry, lepton-side convexity parameter, longitudinal (transverse) polarization of the charged lepton, and asymmetry parameter. We list our major conclusions as follows.

- We reconfirmed that the form factors $A_0(q^2)$ and $A_1(q^2)$ in CLFQM Type-I correspondence

scheme acquire zero-mode contributions through $B_j^{(i)}$ functions, which results in different numerical values for the longitudinal and transverse polarization states. These issues are resolved within Type-II correspondence, which ensures self-consistency and covariance of matrix elements. It may be emphasized that the zero-mode contributions in Type-II correspondence vanish numerically, though exist formally in the analytical relations of the form factors. For bottom-conserving transitions, the numerical results of the Type-II^(*) form factors, $A_0(0)$ and $A_1(0)$, show a significant change of (70 – 90)% and $\sim 23\%$, respectively, as compared to those of the Type-I scheme. Similarly, for bottom-changing transitions, we observed that the numerical values of the form factor $A_0(0)(A_1(0))$ in Type-II correspondence, for both Eqs. (37) and (38), roughly vary by $\sim 30\%$ (10%) as compared to Type-I for $B_c \rightarrow D_{(s)}^*$ transitions. We also observe that these form factors are sensitive to q^2 formulations, resulting in significantly different slope parameters (coefficients). Therefore, we conclude that the improvement in the numerical results of Type-II correspondence cannot simply be determined from the variation of form factors at $q^2 = 0$; the modification in the numerical values of slope parameters also plays a significant role in the quantitative evaluation of these effects. Furthermore, the Type-II correspondence influences $B_c \rightarrow J/\psi$ transition form factors minimally, as compared to both bottom-conserving and other bottom-changing transition form factors.

- We also found that the $M^{(\prime\prime)} \rightarrow M_0^{(\prime\prime)}$ transformation, in general, affects the numerical values of all the transition form factors irrespective of the spin-parity of the final state meson. Therefore, the numerical values of the form factors which do not suffer from self-consistency issues have also been modified. We found that the numerical results for the Type-II^(*) form factors $F^{B_c B_{(s)}}(q^2)$ are in very good agreement with the LQCD observations for both at $q^2 = 0$ and q_{max}^2 . On the other hand, the numerical values of the form factors $F^{B_c D_s}(q^2)$ ($F^{B_c D}(q^2)$) are consistent with the LQCD predictions within $\sim 10\%$ ($\sim 25\%$).
- We found that $\mathcal{B}(B_c \rightarrow B_s^{(*)} l \nu_l)$ and $\mathcal{B}(B_c \rightarrow J/\psi(\eta_c) l \nu_l)$ are the most dominant among the $B_c \rightarrow V(P) l \nu_l$ semileptonic decays. Our results for $\mathcal{B}(B_c^+ \rightarrow B_{(s)}^0 l^+ \nu_l)$ are in good agreement with the recent LQCD predictions. In addition, the decay width ratios of semileptonic decays with B_s^0 to B^0 in final state for Type-II* match well with LCQD expectations. Furthermore, the decays involving the τ lepton have the lowest branching ratios among all the decays because of the significantly larger mass of the τ lepton. We quantified the effect of self-consistency on the branching ratios of the semileptonic decay modes by comparing our results with those of Type-I correspondence. We found that the numerical results for the Type-II scheme are larger by (50 – 60)%, (64 – 85)%, and (24 – 28)% as compared to the branching ratios in the Type-I scheme involving $B_c \rightarrow B_{(s)}^*$, $B_c \rightarrow D^*$, and $B_c \rightarrow J/\psi$ semileptonic decays, respectively. Furthermore, we found that our LFU ratio involving $b \rightarrow c \tau \nu_\tau$ for J/ψ in the final state match well with LQCD and other theoretical models; however, are smaller than the experimental measurement.
- For the nonleptonic B_c decays, branching ratios will be affected by the self-consistency issues for decays involving $A_0(q^2)$ transition form factors. These decays presented an excellent

opportunity to observe these effects in a quantitative manner. Interestingly, the branching ratios of CKM and color-favored $B_c \rightarrow PV$ decays are roughly affected by $\sim (30 - 70)\%$. However, the color-favored CKM-suppressed and doubly-suppressed modes are more seriously affected, where some of the branching ratios are changing by more than 100%. Therefore, we conclude that the self-consistency effects are predominant in $B_c \rightarrow PV$ decays.

In conclusion, the agreement between our predictions and the LQCD results assures the reliability of our numerical results for B_c meson decays. We wish to remark that we have ignored nonfactorizable processes, for example, W-exchange, W-annihilation, penguin processes in our analysis of nonleptonic B_c weak decays. However, the study of nonfactorizable contributions and CP-symmetries can more reliably be carried out in model-independent manner that requires huge amount of experimental data. We hope that the experimental observation of these B_c weak decays can help to shed some light on the underlying physics of the B_c meson.

ACKNOWLEDGMENT

The authors are pleased to express their thanks to H. Y. Cheng, C. K. Chua, H. M. Choi, C. R. Ji, and Gautam Bhattacharyya for their helpful comments and discussions. The author (RD) gratefully acknowledge the financial support by the Department of Science and Technology (SERB:CRG/2018/002796), New Delhi.

REFERENCES

- [1] S. S. Gershtein, V. V. Kiselev, A. K. Likhoded and A. V. Tkabladze, Phys. Usp. **38**, 1-37 (1995) doi:10.1070/PU1995v038n01ABEH000063 [arXiv:hep-ph/9504319 [hep-ph]].
- [2] I. P. Gouz, V. V. Kiselev, A. K. Likhoded, V. I. Romanovsky and O. P. Yushchenko, Phys. Atom. Nucl. **67**, 1559-1570 (2004) doi:10.1134/1.1788046 [arXiv:hep-ph/0211432 [hep-ph]].
- [3] G. Chen, C. H. Chang and X. G. Wu, Phys. Rev. D **97**, no.11, 114022 (2018) doi:10.1103/PhysRevD.97.114022 [arXiv:1803.11447 [hep-ph]].
- [4] R. Aaij *et al.* [LHCb], JHEP **07**, 123 (2020) doi:10.1007/JHEP07(2020)123 [arXiv:2004.08163 [hep-ex]].
- [5] R. Aaij *et al.* [LHCb], Phys. Lett. B **742**, 29-37 (2015) doi:10.1016/j.physletb.2015.01.010 [arXiv:1411.6899 [hep-ex]].
- [6] R. Aaij *et al.* [LHCb], Phys. Rev. Lett. **122**, no.23, 232001 (2019) doi:10.1103/PhysRevLett.122.232001 [arXiv:1904.00081 [hep-ex]].
- [7] A. M. Sirunyan *et al.* [CMS], Phys. Rev. Lett. **122**, no.13, 132001 (2019) doi:10.1103/PhysRevLett.122.132001 [arXiv:1902.00571 [hep-ex]].
- [8] G. Aad *et al.* [ATLAS], Phys. Rev. Lett. **113**, no.21, 212004 (2014) doi:10.1103/PhysRevLett.113.212004 [arXiv:1407.1032 [hep-ex]].

- [9] R. Aaij *et al.* [LHCb], Phys. Rev. Lett. **111**, no.18, 181801 (2013) doi:10.1103/PhysRevLett.111.181801 [arXiv:1308.4544 [hep-ex]].
- [10] R. Aaij *et al.* [LHCb], JHEP **12**, 117 (2021) doi:10.1007/JHEP12(2021)117 [arXiv:2109.00488 [hep-ex]].
- [11] R. Aaij *et al.* [LHCb], Nucl. Phys. B **930**, 563-582 (2018) doi:10.1016/j.nuclphysb.2018.03.015 [arXiv:1712.04702 [hep-ex]].
- [12] R. L. Workman *et al.* [Particle Data Group], PTEP **2022**, 083C01 (2022) doi:10.1093/ptep/ptac097
- [13] Y. S. Amhis *et al.* [HFLAV], Phys. Rev. D **107**, no.5, 052008 (2023) doi:10.1103/PhysRevD.107.052008 [arXiv:2206.07501 [hep-ex]].
- [14] G. Aad *et al.* [ATLAS], JHEP **08**, 087 (2022) doi:10.1007/JHEP08(2022)087 [arXiv:2203.01808 [hep-ex]].
- [15] R. Aaij *et al.* [LHCb], JHEP **09**, 153 (2016) doi:10.1007/JHEP09(2016)153 [arXiv:1607.06823 [hep-ex]].
- [16] G. Aad *et al.* [ATLAS], Eur. Phys. J. C **76**, no.1, 4 (2016) doi:10.1140/epjc/s10052-015-3743-8 [arXiv:1507.07099 [hep-ex]].
- [17] R. Aaij *et al.* [LHCb], Phys. Rev. Lett. **120**, no.12, 121801 (2018) doi:10.1103/PhysRevLett.120.121801 [arXiv:1711.05623 [hep-ex]].
- [18] J. Harrison *et al.* [LATTICE-HPQCD], Phys. Rev. Lett. **125**, no.22, 222003 (2020) doi:10.1103/PhysRevLett.125.222003 [arXiv:2007.06956 [hep-lat]].
- [19] L. J. Cooper *et al.* [HPQCD], Phys. Rev. D **102**, no.1, 014513 (2020) [erratum: Phys. Rev. D **103**, no.9, 099901 (2021)] doi:10.1103/PhysRevD.102.014513 [arXiv:2003.00914 [hep-lat]].
- [20] L. J. Cooper *et al.* [HPQCD], Phys. Rev. D **105**, no.1, 014503 (2022) doi:10.1103/PhysRevD.105.014503 [arXiv:2108.11242 [hep-lat]].
- [21] V. V. Kiselev, A. E. Kovalsky and A. K. Likhoded, Nucl. Phys. B **585**, 353-382 (2000) doi:10.1016/S0550-3213(00)00386-2 [arXiv:hep-ph/0002127 [hep-ph]].
- [22] V. V. Kiselev, O. N. Pakhomova and V. A. Saleev, J. Phys. G **28**, 595-606 (2002) doi:10.1088/0954-3899/28/4/301 [arXiv:hep-ph/0110180 [hep-ph]].
- [23] V. V. Kiselev, [arXiv:hep-ph/0211021 [hep-ph]].
- [24] A. Abd El-Hady, M. A. K. Lodhi and J. P. Vary, Phys. Rev. D **59**, 094001 (1999) doi:10.1103/PhysRevD.59.094001 [arXiv:hep-ph/9807225 [hep-ph]].
- [25] A. Abd El-Hady, J. H. Munoz and J. P. Vary, Phys. Rev. D **62**, 014019 (2000) doi:10.1103/PhysRevD.62.014019 [arXiv:hep-ph/9909406 [hep-ph]].
- [26] X. J. Li, Y. S. Li, F. L. Wang and X. Liu, [arXiv:2308.07206 [hep-ph]].
- [27] R. N. Faustov, V. O. Galkin and X. W. Kang, Phys. Rev. D **106**, no.1, 013004 (2022) doi:10.1103/PhysRevD.106.013004 [arXiv:2206.10277 [hep-ph]].
- [28] Z. Q. Zhang, Z. J. Sun, Y. C. Zhao, Y. Y. Yang and Z. Y. Zhang, Eur. Phys. J. C **83**, no.6, 477 (2023) doi:10.1140/epjc/s10052-023-11576-x [arXiv:2301.11107 [hep-ph]].
- [29] W. Wang, Y. L. Shen and C. D. Lu, Phys. Rev. D **79**, 054012 (2009) doi:10.1103/PhysRevD.79.054012 [arXiv:0811.3748 [hep-ph]].
- [30] W. Wang, Y. L. Shen and C. D. Lu, Eur. Phys. J. C **51**, 841-847 (2007) doi:10.1140/epjc/s10052-007-0334-3 [arXiv:0704.2493 [hep-ph]].

- [31] D. Ebert, R. N. Faustov and V. O. Galkin, Eur. Phys. J. C **32**, 29-43 (2003) doi:10.1140/epjc/s2003-01347-5 [arXiv:hep-ph/0308149 [hep-ph]].
- [32] D. Ebert, R. N. Faustov and V. O. Galkin, Phys. Rev. D **68**, 094020 (2003) doi:10.1103/PhysRevD.68.094020 [arXiv:hep-ph/0306306 [hep-ph]].
- [33] M. A. Ivanov, J. G. Korner and P. Santorelli, Phys. Rev. D **73**, 054024 (2006) doi:10.1103/PhysRevD.73.054024 [arXiv:hep-ph/0602050 [hep-ph]].
- [34] M. A. Ivanov, J. G. Korner and O. N. Pakhomova, Phys. Lett. B **555**, 189-196 (2003) doi:10.1016/S0370-2693(03)00052-2 [arXiv:hep-ph/0212291 [hep-ph]].
- [35] M. A. Ivanov, J. G. Körner and P. Santorelli, doi:10.1007/978-88-470-0530-3_43 [arXiv:hep-ph/0609122 [hep-ph]].
- [36] S. Naimuddin, S. Kar, M. Priyadarsini, N. Barik and P. C. Dash, Phys. Rev. D **86**, 094028 (2012) doi:10.1103/PhysRevD.86.094028
- [37] L. Nayak, P. C. Dash, S. Kar and N. Barik, Phys. Rev. D **105**, no.5, 053007 (2022) doi:10.1103/PhysRevD.105.053007 [arXiv:2202.01167 [hep-ph]].
- [38] Z. Rui, Z. Zhitian and C. D. Lu, Phys. Rev. D **86**, 074019 (2012) doi:10.1103/PhysRevD.86.074019 [arXiv:1203.2303 [hep-ph]].
- [39] Z. Rui and Z. T. Zou, Phys. Rev. D **90**, no.11, 114030 (2014) doi:10.1103/PhysRevD.90.114030 [arXiv:1407.5550 [hep-ph]].
- [40] J. Sun, N. Wang, Q. Chang and Y. Yang, Adv. High Energy Phys. **2015**, 104378 (2015) doi:10.1155/2015/104378 [arXiv:1504.01286 [hep-ph]].
- [41] H. Y. Cheng, C. Y. Cheung, C. W. Hwang and W. M. Zhang, Phys. Rev. D **57**, 5598-5610 (1998) doi:10.1103/PhysRevD.57.5598 [arXiv:hep-ph/9709412 [hep-ph]].
- [42] W. Jaus, Phys. Rev. D **41**, 3394 (1990) doi:10.1103/PhysRevD.41.3394
- [43] W. Jaus, Phys. Rev. D **44**, 2851-2859 (1991) doi:10.1103/PhysRevD.44.2851
- [44] C. R. Ji, P. L. Chung and S. R. Cotanch, Phys. Rev. D **45**, 4214-4220 (1992) doi:10.1103/PhysRevD.45.4214
- [45] H. Y. Cheng, C. Y. Cheung and C. W. Hwang, Phys. Rev. D **55**, 1559-1577 (1997) doi:10.1103/PhysRevD.55.1559 [arXiv:hep-ph/9607332 [hep-ph]].
- [46] W. Jaus, Phys. Rev. D **60**, 054026 (1999) doi:10.1103/PhysRevD.60.054026
- [47] E. E. Salpeter and H. A. Bethe, Phys. Rev. **84**, 1232-1242 (1951) doi:10.1103/PhysRev.84.1232
- [48] E. E. Salpeter, Phys. Rev. **87**, 328-342 (1952) doi:10.1103/PhysRev.87.328
- [49] H. M. Choi and C. R. Ji, Phys. Rev. D **58**, 071901 (1998) doi:10.1103/PhysRevD.58.071901 [arXiv:hep-ph/9805438 [hep-ph]].
- [50] H. Y. Cheng, C. K. Chua and C. W. Hwang, Phys. Rev. D **69**, 074025 (2004) doi:10.1103/PhysRevD.69.074025 [arXiv:hep-ph/0310359 [hep-ph]].
- [51] H. M. Choi and C. R. Ji, Phys. Rev. D **89**, no.3, 033011 (2014) doi:10.1103/PhysRevD.89.033011 [arXiv:1308.4455 [hep-ph]].
- [52] W. Jaus, Phys. Rev. D **67**, 094010 (2003) doi:10.1103/PhysRevD.67.094010 [arXiv:hep-ph/0212098 [hep-ph]].
- [53] B. L. G. Bakker, H. M. Choi and C. R. Ji, Phys. Rev. D **63**, 074014 (2001) doi:10.1103/PhysRevD.63.074014 [arXiv:hep-ph/0008147 [hep-ph]].

- [54] B. L. G. Bakker, H. M. Choi and C. R. Ji, Phys. Rev. D **65**, 116001 (2002) doi:10.1103/PhysRevD.65.116001 [arXiv:hep-ph/0202217 [hep-ph]].
- [55] B. L. G. Bakker, H. M. Choi and C. R. Ji, Phys. Rev. D **67**, 113007 (2003) doi:10.1103/PhysRevD.67.113007 [arXiv:hep-ph/0303002 [hep-ph]].
- [56] H. M. Choi and C. R. Ji, Phys. Rev. D **72**, 013004 (2005) doi:10.1103/PhysRevD.72.013004 [arXiv:hep-ph/0504219 [hep-ph]].
- [57] R. C. Verma, J. Phys. G **39**, 025005 (2012) doi:10.1088/0954-3899/39/2/025005 [arXiv:1103.2973 [hep-ph]].
- [58] Q. Chang, X. L. Wang and L. T. Wang, Chin. Phys. C **44**, no.8, 083105 (2020) doi:10.1088/1674-1137/44/8/083105 [arXiv:2003.10833 [hep-ph]].
- [59] Q. Chang, X. N. Li and L. T. Wang, Eur. Phys. J. C **79**, no.5, 422 (2019) doi:10.1140/epjc/s10052-019-6949-3 [arXiv:1905.05098 [hep-ph]].
- [60] Q. Chang, X. N. Li, X. Q. Li, F. Su and Y. D. Yang, Phys. Rev. D **98**, no.11, 114018 (2018) doi:10.1103/PhysRevD.98.114018 [arXiv:1810.00296 [hep-ph]].
- [61] A. Hazra, T. M. S., N. Sharma and R. Dhir, [arXiv:2309.03655 [hep-ph]].
- [62] H. M. Choi, Phys. Rev. D **103**, no.7, 073004 (2021) doi:10.1103/PhysRevD.103.073004 [arXiv:2102.02015 [hep-ph]].
- [63] M. Wirbel, B. Stech and M. Bauer, Z. Phys. C **29**, 637 (1985) doi:10.1007/BF01560299
- [64] W. Jaus, Phys. Rev. D **53**, 1349 (1996) [erratum: Phys. Rev. D **54**, 5904 (1996)] doi:10.1103/PhysRevD.53.1349
- [65] O. Heger, M. Gómez-Rocha and W. Schweiger, Phys. Rev. D **104**, no.11, 116005 (2021) doi:10.1103/PhysRevD.104.116005 [arXiv:2109.07849 [hep-ph]].
- [66] D. Melikhov, Phys. Rev. D **53**, 2460-2479 (1996) doi:10.1103/PhysRevD.53.2460 [arXiv:hep-ph/9509268 [hep-ph]].
- [67] J. D. Richman and P. R. Burchat, Rev. Mod. Phys. **67**, 893-976 (1995) doi:10.1103/RevModPhys.67.893 [arXiv:hep-ph/9508250 [hep-ph]].
- [68] D. Becirevic and A. B. Kaidalov, Phys. Lett. B **478**, 417-423 (2000) doi:10.1016/S0370-2693(00)00290-2 [arXiv:hep-ph/9904490 [hep-ph]].
- [69] D. Melikhov and B. Stech, Phys. Rev. D **62**, 014006 (2000) doi:10.1103/PhysRevD.62.014006 [arXiv:hep-ph/0001113 [hep-ph]].
- [70] M. Bauer and M. Wirbel, Z. Phys. C **42**, 671 (1989) doi:10.1007/BF01557675
- [71] R. J. Hill, Phys. Rev. D **73**, 014012 (2006) doi:10.1103/PhysRevD.73.014012 [arXiv:hep-ph/0505129 [hep-ph]].
- [72] R. J. Hill, eConf **C060409**, 027 (2006) [arXiv:hep-ph/0606023 [hep-ph]].
- [73] D. Melikhov, Eur. Phys. J. direct **4**, no.1, 2 (2002) doi:10.1007/s1010502c0002 [arXiv:hep-ph/0110087 [hep-ph]].
- [74] N. Gubernari, A. Khodjamirian, R. Mandal and T. Mannel, JHEP **05**, 029 (2022) doi:10.1007/JHEP05(2022)029 [arXiv:2203.08493 [hep-ph]].
- [75] C. Bourrely, I. Caprini and L. Lellouch, Phys. Rev. D **79**, 013008 (2009) [erratum: Phys. Rev. D **82**, 099902 (2010)] doi:10.1103/PhysRevD.82.099902 [arXiv:0807.2722 [hep-ph]].
- [76] P. Colangelo and F. De Fazio, Phys. Rev. D **61**, 034012 (2000) doi:10.1103/PhysRevD.61.034012 [arXiv:hep-ph/9909423 [hep-ph]].

- [77] M. A. Ivanov, J. G. Korner and P. Santorelli, Phys. Rev. D **71**, 094006 (2005) [erratum: Phys. Rev. D **75**, 019901 (2007)] doi:10.1103/PhysRevD.75.019901 [arXiv:hep-ph/0501051 [hep-ph]].
- [78] R. Dhir and C. S. Kim, Phys. Rev. D **88**, no.3, 034024 (2013) doi:10.1103/PhysRevD.88.034024 [arXiv:1307.0216 [hep-ph]].
- [79] T. E. Browder and K. Honscheid, Prog. Part. Nucl. Phys. **35**, 81-220 (1995) doi:10.1016/0146-6410(95)00042-H [arXiv:hep-ph/9503414 [hep-ph]].
- [80] M. Wirbel, Prog. Part. Nucl. Phys. **21**, 33-98 (1988) doi:10.1016/0146-6410(88)90031-2
- [81] R. Dhir and R. C. Verma, Phys. Rev. D **79**, 034004 (2009) doi:10.1103/PhysRevD.79.034004 [arXiv:0810.4284 [hep-ph]].
- [82] T. E. Browder, K. Honscheid and S. Playfer, doi:10.1142/9789814503846_0004 [arXiv:hep-ph/9404314 [hep-ph]].
- [83] F. Jugeau, A. Le Yaouanc, L. Oliver and J. C. Raynal, Phys. Rev. D **72**, 094010 (2005) doi:10.1103/PhysRevD.72.094010 [arXiv:hep-ph/0504206 [hep-ph]].
- [84] R. Dhir and C. S. Kim, Phys. Rev. D **87**, no.3, 034004 (2013) doi:10.1103/PhysRevD.87.034004 [arXiv:1210.7890 [hep-ph]].
- [85] H. Y. Cheng and C. W. Chiang, Phys. Rev. D **81**, 074021 (2010) doi:10.1103/PhysRevD.81.074021 [arXiv:1001.0987 [hep-ph]].
- [86] H. Y. Cheng, C. W. Chiang and A. L. Kuo, Phys. Rev. D **91**, no.1, 014011 (2015) doi:10.1103/PhysRevD.91.014011 [arXiv:1409.5026 [hep-ph]].
- [87] C. W. Hwang, Phys. Rev. D **81**, 114024 (2010) doi:10.1103/PhysRevD.81.114024 [arXiv:1003.0972 [hep-ph]].
- [88] C. Y. Cheung, C. W. Hwang and W. M. Zhang, Z. Phys. C **75**, 657-664 (1997) doi:10.1007/s002880050511 [arXiv:hep-ph/9602309 [hep-ph]].
- [89] H. M. Choi and C. R. Ji, Phys. Rev. D **80**, 054016 (2009) doi:10.1103/PhysRevD.80.054016 [arXiv:0903.0455 [hep-ph]].
- [90] M. Neubert, V. Rieckert, B. Stech and Q. P. Xu, Adv. Ser. Direct. High Energy Phys. **10**, 286-333 (1992) doi:10.1142/9789814503587_0005
- [91] J. N. Pandya, P. Santorelli and N. R. Soni, doi:10.1140/epjs/s11734-023-01006-0 [arXiv:2307.14245 [hep-ph]].
- [92] E. Hernandez, J. Nieves and J. M. Verde-Velasco, Phys. Rev. D **74**, 074008 (2006) doi:10.1103/PhysRevD.74.074008 [arXiv:hep-ph/0607150 [hep-ph]].
- [93] A. Y. Anisimov, I. M. Narodetsky, C. Semay and B. Silvestre-Brac, Phys. Lett. B **452**, 129-136 (1999) doi:10.1016/S0370-2693(99)00273-7 [arXiv:hep-ph/9812514 [hep-ph]].
- [94] R. Aaij *et al.* [LHCb], Phys. Rev. D **90**, no.3, 032009 (2014) doi:10.1103/PhysRevD.90.032009 [arXiv:1407.2126 [hep-ex]].
- [95] R. J. Dowdall, C. T. H. Davies, G. P. Lepage and C. McNeile, Phys. Rev. D **88**, 074504 (2013) doi:10.1103/PhysRevD.88.074504 [arXiv:1303.1670 [hep-lat]].
- [96] A. Bharucha, D. M. Straub and R. Zwicky, JHEP **08**, 098 (2016) doi:10.1007/JHEP08(2016)098 [arXiv:1503.05534 [hep-ph]].
- [97] B. Chakraborty *et al.* [HPQCD], Phys. Rev. D **96**, no.7, 074502 (2017) doi:10.1103/PhysRevD.96.074502 [arXiv:1703.05552 [hep-lat]].

- [98] V. Lubicz *et al.* [ETM], Phys. Rev. D **96**, no.3, 034524 (2017)
doi:10.1103/PhysRevD.96.034524 [arXiv:1707.04529 [hep-lat]].
- [99] M. Ablikim *et al.* [BESIII], Phys. Rev. Lett. **131**, no.14, 141802 (2023)
doi:10.1103/PhysRevLett.131.141802 [arXiv:2304.12159 [hep-ex]].

APPENDIX

Appendix A: Branching ratios of $B_c^+ \rightarrow Pl^+\nu_l$ decays

We list the numerical values of $B_c^+ \rightarrow Pl^+\nu_l$ semileptonic decays using the form factors given in Tables IV and V, and the numerical inputs are discussed in Sec. III.

Table I: Branching ratios of $B_c^+ \rightarrow Pl^+\nu_l$ decays. For the definitions of Type-II, Type-II*, and Type-I, refer to the caption of Table IV.

Decay	Type-II	Type-II*	Type-I
$B_c^+ \rightarrow B^0 e^+ \nu_e$	7.76×10^{-4}	1.07×10^{-3}	2.40×10^{-4}
$B_c^+ \rightarrow B^0 \mu^+ \nu_\mu$	7.46×10^{-4}	1.01×10^{-3}	2.17×10^{-4}
$B_c^+ \rightarrow B_s^0 e^+ \nu_e$	1.35×10^{-2}	1.75×10^{-2}	5.94×10^{-3}
$B_c^+ \rightarrow B_s^0 \mu^+ \nu_\mu$	1.28×10^{-2}	1.64×10^{-2}	5.37×10^{-3}
$B_c^+ \rightarrow D^0 e^+ \nu_e$	1.82×10^{-5}	1.21×10^{-5}	1.41×10^{-6}
$B_c^+ \rightarrow D^0 \mu^+ \nu_\mu$	1.82×10^{-5}	1.21×10^{-5}	1.39×10^{-6}
$B_c^+ \rightarrow D^0 \tau^+ \nu_\tau$	1.35×10^{-5}	7.71×10^{-6}	3.63×10^{-8}
$B_c^+ \rightarrow \eta_c e^+ \nu_e$	7.56×10^{-3}	6.43×10^{-3}	3.06×10^{-3}
$B_c^+ \rightarrow \eta_c \mu^+ \nu_\mu$	7.53×10^{-3}	6.40×10^{-3}	3.03×10^{-3}
$B_c^+ \rightarrow \eta_c \tau^+ \nu_\tau$	2.25×10^{-3}	1.74×10^{-3}	2.80×10^{-4}

Table II: Constituent quark masses and the Gaussian parameters β for P and V mesons.^a

Constituent quark masses (in GeV)					
$m_u = m_d = 0.27; m_s = 0.45; m_c = 1.60; m_b = 4.80$					
Gaussian parameters β (in GeV)					
$^{2S+1}L_J$	1S_0	3S_1	$^{2S+1}L_J$	1S_0	3S_1
$\beta_{c\bar{q}}$	0.4656	0.4255	$\beta_{b\bar{q}}$	0.5547	0.5183
$\beta_{c\bar{s}}$	0.5358	0.4484	$\beta_{b\bar{s}}$	0.6103	0.5589
$\beta_{c\bar{c}}$	0.7690	0.6492	$\beta_{b\bar{c}}$	0.9207	0.8451

^a Note that here q denotes either u or d quark.

Table III: Transition pole masses for $B_c \rightarrow P$ and V form factors (in GeV).

Quark transition	$F_1(q^2), V(q^2)$	$F_0(q^2)$	$A_0(q^2)$	$A_1(q^2), A_2(q^2)$
	$J^P = 1^-$	0^+	0^-	1^+
Bottom-conserving transitions				
$c \rightarrow d$	2.010	2.308	1.870	2.422
$c \rightarrow s$	2.112	2.318	1.968	2.460
Bottom-changing transitions				
$b \rightarrow u$	5.325	5.670	5.279	5.726
$b \rightarrow s$	5.415	5.762	5.367	5.829
$b \rightarrow c$	6.473	6.836	6.274	6.866

Table IV: Form factors of bottom-conserving transitions. Note that Type-II (Type-II*) results represent the transition form factors calculated using q^2 dependence given in Eq. (37) (Eq. (38)) with transition pole masses as listed in Table II. Type-I results represent the transition form factors calculated using q^2 dependence given in Eq. (40) with parent pole mass (M_{B_c}).

Form Factor	Type-II (Type-II*)				Type-I			
	$F(0)$ (a'_0)	$F(q_{max}^2)$	a (a'_1)	b (a'_2)	$F(0)$	$F(q_{max}^2)$	a	b
$B_c \rightarrow P$ transitions								
$F_0^{B_c B}$	0.56 (0.57)	0.72 (0.79)	0.26 (-32.11)	0.68 (442.10)	0.49	0.46	-2.05	174.50
$F_1^{B_c B}$	0.56 (0.57)	0.75 (0.89)	0.24 (-49.84)	0.76 (1279.22)	0.49	0.34	-9.08	318.23
$F_0^{B_c B_s}$	0.66 (0.68)	0.82 (0.86)	0.26 (-32.72)	0.51 (324.65)	0.61	0.63	1.33	128.97
$F_1^{B_c B_s}$	0.66 (0.68)	0.85 (0.93)	0.37 (-54.44)	0.67 (1330.93)	0.61	0.53	-2.40	234.47
$B_c \rightarrow V$ transitions								
$V^{B_c B^*}$	2.54 (2.65)	3.24 (3.98)	0.17 (-253.95)	0.97 (7055.58)	2.18	1.42	-14.64	381.51
$A_0^{B_c B^*}$	0.55 (0.56)	0.75 (0.87)	0.19 (-47.19)	0.54 (1162.64)	0.04	0.01	-138.36	1150.18
$A_1^{B_c B^*}$	0.53 (0.54)	0.65 (0.72)	0.43 (-39.22)	1.02 (864.12)	0.41	0.37	-0.19	158.12
$A_2^{B_c B^*}$	0.26 (0.26)	0.28 (0.30)	-0.40 (1.28)	0.89 (-630.49)	0.24	0.21	-4.51	117.58
$V^{B_c B_s^*}$	2.85 (2.93)	3.51 (3.96)	0.33 (-269.90)	0.93 (7368.86)	2.55	2.04	-7.67	301.89
$A_0^{B_c B_s^*}$	0.66 (0.68)	0.85 (0.93)	0.29 (-55.12)	0.54 (1349.55)	0.19	0.07	-87.95	894.76
$A_1^{B_c B_s^*}$	0.65 (0.66)	0.78 (0.82)	0.52 (-46.59)	0.86 (1026.99)	0.51	0.50	2.20	129.87
$A_2^{B_c B_s^*}$	0.42 (0.42)	0.47 (0.50)	-0.0001 (-15.31)	0.88 (-112.92)	0.40	0.37	-1.25	122.92

Table V: Form factors of bottom-changing transitions. For the definitions of Type-II, Type-II*, and Type-I, refer to the caption of Table IV.

Form Factor	Type-II (Type-II*)				Type-I			
	$F(0)$ (a'_0)	$F(q_{max}^2)$	a (a'_1)	b (a'_2)	$F(0)$	$F(q_{max}^2)$	a	b
$B_c \rightarrow P$ transitions								
$F_0^{B_c D}$	0.14 (0.14)	0.52 (0.73)	1.14 (-1.39)	1.02 (4.07)	0.14	0.15	2.41	4.61
$F_1^{B_c D}$	0.14 (0.14)	0.52 (1.29)	1.55 (-2.15)	1.94 (10.90)	0.14	0.07	2.95	10.40
$F_0^{B_c D_s}$	0.21 (0.21)	0.70 (0.83)	0.92 (-1.69)	0.67 (3.13)	0.21	0.33	2.15	3.00
$F_1^{B_c D_s}$	0.21 (0.21)	0.89 (1.42)	1.39 (-2.86)	1.33 (12.83)	0.21	0.17	2.84	7.18
$F_0^{B_c \eta_c}$	0.61 (0.61)	0.94 (0.95)	0.74 (-3.36)	0.40 (1.71)	0.61	0.91	1.45	0.95
$F_1^{B_c \eta_c}$	0.61 (0.61)	1.15 (1.17)	1.33 (-6.68)	0.87 (26.17)	0.61	1.01	2.11	2.46
$B_c \rightarrow V$ transitions								
$V^{B_c D^*}$	0.17 (0.17)	0.48 (1.41)	1.68 (-3.02)	2.59 (17.34)	0.17	0.07	2.94	13.14
$A_0^{B_c D^*}$	0.18 (0.18)	0.63 (1.37)	1.49 (-2.77)	1.82 (14.31)	0.12	0.01	-3.32	56.88
$A_1^{B_c D^*}$	0.13 (0.13)	0.41 (0.65)	1.38 (-1.61)	1.55 (6.29)	0.12	0.11	2.50	5.59
$A_2^{B_c D^*}$	0.09 (0.09)	0.21 (0.52)	1.71 (-1.35)	2.76 (6.83)	0.09	0.05	2.71	9.84
$V^{B_c D_s^*}$	0.22 (0.22)	0.63 (1.44)	1.68 (-3.74)	2.37 (21.15)	0.22	0.11	2.95	11.38
$A_0^{B_c D_s^*}$	0.22 (0.22)	0.78 (1.38)	1.49 (-3.41)	1.69 (17.39)	0.16	0.02	-0.23	38.66
$A_1^{B_c D_s^*}$	0.17 (0.17)	0.52 (0.72)	1.39 (-2.05)	1.43 (8.05)	0.15	0.17	2.46	4.91
$A_2^{B_c D_s^*}$	0.12 (0.12)	0.30 (0.59)	1.76 (-1.81)	2.65 (9.26)	0.12	0.08	2.73	8.86
$V^{B_c J/\psi}$	0.76 (0.76)	1.45 (1.49)	1.65 (-10.56)	1.49 (53.11)	0.76	1.19	2.35	3.65
$A_0^{B_c J/\psi}$	0.71 (0.71)	1.33 (1.36)	1.37 (-8.72)	1.02 (38.33)	0.59	0.74	2.52	6.67
$A_1^{B_c J/\psi}$	0.62 (0.62)	1.01 (1.03)	1.19 (-5.59)	0.75 (16.55)	0.56	0.85	1.74	1.54
$A_2^{B_c J/\psi}$	0.45 (0.45)	0.82 (0.84)	1.73 (-5.92)	1.63 (27.71)	0.45	0.71	2.18	3.03

Table VI: Branching ratios, relative decay widths and physical observables of $B_c^+ \rightarrow Vl^+\nu_l$ decays in Type-II CLFQM.

Quark Transition	Decay	\mathcal{B}	$\frac{\Gamma_L}{\Gamma}$	$\frac{\Gamma_T}{\Gamma}$	$\frac{\Gamma_L}{\Gamma_T}$	$\langle A_{FB} \rangle$	$\langle C_F^l \rangle$	$\langle P_L^l \rangle$	$\langle P_T^l \rangle$	α^*
$c \rightarrow d$	$B_c^+ \rightarrow B^{*0}e^+\nu_e$	1.85×10^{-3}	0.54	0.46	1.16	-0.16	-0.46	1.00	-1.08×10^{-3}	-0.40
	$B_c^+ \rightarrow B^{*0}\mu^+\nu_\mu$	1.75×10^{-3}	0.53	0.47	1.13	-0.19	-0.37	0.91	-0.14	-0.39
$c \rightarrow s$	$B_c^+ \rightarrow B_s^{*0}e^+\nu_e$	3.20×10^{-2}	0.54	0.46	1.17	-0.13	-0.46	1.00	-1.24×10^{-3}	-0.40
	$B_c^+ \rightarrow B_s^{*0}\mu^+\nu_\mu$	2.99×10^{-2}	0.53	0.47	1.14	-0.16	-0.36	0.90	-0.16	-0.39
$b \rightarrow u$	$B_c^+ \rightarrow D^{*0}e^+\nu_e$	7.73×10^{-5}	0.53	0.47	1.15	-0.21	-0.45	1.00	-1.71×10^{-4}	-0.39
	$B_c^+ \rightarrow D^{*0}\mu^+\nu_\mu$	7.72×10^{-5}	0.53	0.47	1.15	-0.21	-0.45	0.99	-3.28×10^{-2}	-0.39
	$B_c^+ \rightarrow D^{*0}\tau^+\nu_\tau$	4.21×10^{-5}	0.52	0.48	1.06	-0.29	-0.16	0.61	-0.17	-0.36
$b \rightarrow c$	$B_c^+ \rightarrow J/\psi e^+\nu_e$	2.60×10^{-2}	0.54	0.46	1.16	-0.17	-0.46	1.00	-3.09×10^{-4}	-0.40
	$B_c^+ \rightarrow J/\psi \mu^+\nu_\mu$	2.59×10^{-2}	0.54	0.46	1.16	-0.17	-0.44	0.99	-5.62×10^{-2}	-0.40
	$B_c^+ \rightarrow J/\psi \tau^+\nu_\tau$	6.41×10^{-3}	0.46	0.54	0.87	-0.26	-0.07	0.50	-0.15	-0.27

Table VII: Branching ratios of $B_c^+ \rightarrow V l^+ \nu_l$ decays. For the definitions of Type-II, Type-II*, and Type-I, refer to the caption of Table IV.

Decay	Ours		[26]	[27]	[29]	[33]
	Type-II (Type-II*)	Type-I				
$B_c^+ \rightarrow B^{*0} e^+ \nu_e$	1.85×10^{-3} (2.06×10^{-3})	8.35×10^{-4}	7.77×10^{-4}	1.79×10^{-3}	1.41×10^{-3}	6.30×10^{-3}
$B_c^+ \rightarrow B^{*0} \mu^+ \nu_\mu$	1.75×10^{-3} (1.96×10^{-3})	7.59×10^{-4}	7.36×10^{-4}	1.72×10^{-3}	1.34×10^{-3}	-
$B_c^+ \rightarrow B_s^{*0} e^+ \nu_e$	3.20×10^{-2} (3.41×10^{-2})	1.63×10^{-2}	1.42×10^{-2}	2.30×10^{-2}	1.96×10^{-2}	2.37×10^{-2}
$B_c^+ \rightarrow B_s^{*0} \mu^+ \nu_\mu$	2.99×10^{-2} (3.19×10^{-2})	1.47×10^{-2}	1.32×10^{-2}	2.20×10^{-2}	1.83×10^{-2}	-
$B_c^+ \rightarrow D^{*0} e^+ \nu_e$	7.73×10^{-5} (1.15×10^{-4})	2.80×10^{-5}	1.26×10^{-4}	8.40×10^{-5}	4.50×10^{-5}	3.80×10^{-5}
$B_c^+ \rightarrow D^{*0} \mu^+ \nu_\mu$	7.72×10^{-5} (1.14×10^{-4})	2.79×10^{-5}	1.25×10^{-4}	8.40×10^{-5}	4.50×10^{-5}	-
$B_c^+ \rightarrow D^{*0} \tau^+ \nu_\tau$	4.21×10^{-5} (6.83×10^{-5})	1.05×10^{-5}	6.01×10^{-5}	5.50×10^{-5}	2.70×10^{-5}	2.20×10^{-5}
$B_c^+ \rightarrow J/\psi e^+ \nu_e$	2.60×10^{-2} (2.62×10^{-2})	1.97×10^{-2}	2.13×10^{-2}	1.31×10^{-2}	1.49×10^{-2}	2.07×10^{-2}
$B_c^+ \rightarrow J/\psi \mu^+ \nu_\mu$	2.59×10^{-2} (2.61×10^{-2})	1.96×10^{-2}	2.12×10^{-2}	1.30×10^{-2}	1.49×10^{-2}	-
$B_c^+ \rightarrow J/\psi \tau^+ \nu_\tau$	6.41×10^{-3} (6.49×10^{-3})	4.65×10^{-3}	4.89×10^{-3}	3.70×10^{-3}	3.70×10^{-3}	4.90×10^{-3}

Table VIII: Decay constants for P and V mesons (in MeV)^a.

Decay Constants			
f_π	130.56 [12]	f_ρ	210 [96]
f_K	155.7 [12]	f_{K^*}	204 [96]
f_η	(181.14) [95]	f_ϕ	(228.5) [97]
f_D	203.8 [12]	f_{D^*}	(223.5) [98]
f_{D_s}	250.1 [12]	$f_{D_s^*}$	213 [99]
f_{η_c}	335 [12]	$f_{J/\psi}$	416 [12]

^a Available experimental values are listed. The numerical values in the parentheses are from LQCD. Note that we only listed the central values (uncertainties are ignored).

Table IX: Branching ratios of $B_c \rightarrow PV$ bottom-conserving decays. For the definitions of Type-II, Type-II*, and Type-I, refer to the caption of Table IV.

Decay	Type-II		Type-II*		Type-I	
	$N_c = \infty$	$N_c = 3$	$N_c = \infty$	$N_c = 3$	$N_c = \infty$	$N_c = 3$
CKM-favored ($\Delta b = 0, \Delta C = -1, \Delta S = -1$)						
$B_c^+ \rightarrow \pi^+ B_s^{*0}$	4.86×10^{-2}	3.63×10^{-2}	5.18×10^{-2}	3.87×10^{-2}	2.14×10^{-3}	1.60×10^{-3}
$B_c^+ \rightarrow \bar{K}^0 B^{*+}$	8.08×10^{-3}	2.61×10^{-4}	1.00×10^{-2}	3.12×10^{-4}	3.52×10^{-6}	1.09×10^{-7}
$B_c^+ \rightarrow B^+ \bar{K}^{*0}$	3.18×10^{-3}	9.90×10^{-5}	4.34×10^{-3}	1.35×10^{-4}	7.68×10^{-4}	2.39×10^{-5}
$B_c^+ \rightarrow B_s^0 \rho^+$	3.65×10^{-2}	2.73×10^{-2}	4.34×10^{-2}	3.25×10^{-2}	1.50×10^{-2}	1.12×10^{-2}
CKM-suppressed ($\Delta b = 0, \Delta C = -1, \Delta S = 0$)						
$B_c^+ \rightarrow K^+ B_s^{*0}$	2.64×10^{-3}	1.98×10^{-3}	3.01×10^{-3}	2.25×10^{-3}	3.20×10^{-5}	2.40×10^{-5}
$B_c^+ \rightarrow \pi^+ B^{*0}$	2.26×10^{-3}	1.69×10^{-3}	2.48×10^{-3}	1.86×10^{-3}	4.62×10^{-6}	3.46×10^{-6}
$B_c^+ \rightarrow \pi^0 B^{*+}$	1.85×10^{-4}	5.77×10^{-6}	2.03×10^{-4}	6.32×10^{-6}	3.88×10^{-7}	1.21×10^{-8}
$B_c^+ \rightarrow \eta B^{*+}$	3.98×10^{-4}	1.27×10^{-5}	4.94×10^{-4}	1.54×10^{-5}	1.43×10^{-7}	4.45×10^{-9}
$B_c^+ \rightarrow B^+ \rho^0$	2.36×10^{-4}	7.36×10^{-6}	3.09×10^{-4}	9.61×10^{-6}	6.86×10^{-5}	2.13×10^{-6}
$B_c^+ \rightarrow B^+ \omega$	2.04×10^{-4}	6.35×10^{-6}	2.68×10^{-4}	8.33×10^{-6}	5.80×10^{-5}	1.81×10^{-6}
$B_c^+ \rightarrow B^0 \rho^+$	2.87×10^{-3}	2.15×10^{-3}	3.75×10^{-3}	2.81×10^{-3}	8.35×10^{-4}	6.25×10^{-4}
$B_c^+ \rightarrow B_s^0 K^{*+}$	5.89×10^{-5}	4.40×10^{-5}	7.20×10^{-5}	5.39×10^{-5}	2.09×10^{-5}	1.56×10^{-5}
CKM-doubly-suppressed ($\Delta b = 0, \Delta C = -1, \Delta S = 1$)						
$B_c^+ \rightarrow K^+ B^{*0}$	1.40×10^{-4}	1.05×10^{-4}	1.67×10^{-4}	1.25×10^{-4}	5.97×10^{-8}	4.47×10^{-8}
$B_c^+ \rightarrow K^0 B^{*+}$	2.28×10^{-5}	7.11×10^{-7}	2.73×10^{-5}	8.51×10^{-7}	9.58×10^{-9}	2.98×10^{-10}
$B_c^+ \rightarrow B^+ K^{*0}$	8.67×10^{-6}	2.70×10^{-7}	1.18×10^{-5}	3.68×10^{-7}	2.09×10^{-6}	6.52×10^{-8}
$B_c^+ \rightarrow B^0 K^{*+}$	5.26×10^{-5}	3.93×10^{-5}	7.17×10^{-5}	5.37×10^{-5}	1.27×10^{-5}	9.52×10^{-6}

Table X: Branching ratios of CKM-favored $B_c \rightarrow PV$ bottom-changing decays. For the definitions of Type-II, Type-II*, and Type-I, refer to the caption of Table IV.

Decay	Type-II		Type-II*		Type-I	
	$N_c = \infty$	$N_c = 3$	$N_c = \infty$	$N_c = 3$	$N_c = \infty$	$N_c = 3$
$\Delta b = -1, \Delta C = -1, \Delta S = 0$						
$B_c^+ \rightarrow \pi^+ J/\psi$	1.91×10^{-3}	1.63×10^{-3}	1.91×10^{-3}	1.63×10^{-3}	1.33×10^{-3}	1.13×10^{-3}
$B_c^+ \rightarrow \bar{D}^0 D^{*+}$	2.21×10^{-5}	4.62×10^{-6}	2.48×10^{-5}	4.71×10^{-6}	4.79×10^{-6}	9.10×10^{-7}
$B_c^+ \rightarrow D^+ \bar{D}^{*0}$	1.82×10^{-5}	3.46×10^{-6}	1.86×10^{-5}	3.53×10^{-6}	1.66×10^{-5}	3.15×10^{-6}
$B_c^+ \rightarrow \eta_c \rho^+$	4.31×10^{-3}	3.66×10^{-3}	4.31×10^{-3}	3.67×10^{-3}	4.26×10^{-3}	3.63×10^{-3}
$\Delta b = -1, \Delta C = 0, \Delta S = 1$						
$B_c^+ \rightarrow \pi^0 D_s^{*+}$	3.88×10^{-9}	7.37×10^{-10}	3.88×10^{-9}	7.38×10^{-10}	1.92×10^{-9}	3.65×10^{-10}
$B_c^+ \rightarrow \eta D_s^{*+}$	2.52×10^{-9}	4.77×10^{-10}	2.52×10^{-9}	4.79×10^{-10}	1.14×10^{-9}	2.16×10^{-10}
$B_c^+ \rightarrow K^+ D^{*0}$	1.40×10^{-7}	1.19×10^{-7}	1.40×10^{-7}	1.19×10^{-7}	5.23×10^{-8}	4.45×10^{-8}
$B_c^+ \rightarrow \eta' D_s^{*+}$	1.52×10^{-9}	2.87×10^{-10}	1.52×10^{-9}	2.89×10^{-10}	6.16×10^{-10}	1.17×10^{-10}
$B_c^+ \rightarrow D^0 K^{*+}$	1.86×10^{-7}	1.58×10^{-7}	1.87×10^{-7}	1.59×10^{-7}	1.80×10^{-7}	1.53×10^{-7}
$B_c^+ \rightarrow D_s^+ \rho^0$	1.12×10^{-8}	2.13×10^{-9}	1.13×10^{-8}	2.14×10^{-9}	1.06×10^{-8}	2.02×10^{-9}
$B_c^+ \rightarrow D_s^+ \omega$	7.00×10^{-10}	1.33×10^{-10}	7.03×10^{-10}	1.34×10^{-10}	6.63×10^{-10}	1.26×10^{-10}
$B_c^+ \rightarrow D_s^+ \phi$	1.10×10^{-8}	2.08×10^{-9}	1.10×10^{-8}	2.09×10^{-9}	1.03×10^{-8}	1.96×10^{-9}
$B_c^+ \rightarrow D_s^+ J/\psi$	3.00×10^{-3}	3.83×10^{-3}	3.00×10^{-3}	3.84×10^{-3}	1.99×10^{-3}	2.67×10^{-3}
$B_c^+ \rightarrow \eta_c D_s^{*+}$	1.88×10^{-3}	2.41×10^{-3}	1.83×10^{-3}	2.42×10^{-3}	2.14×10^{-3}	2.21×10^{-3}

Table XI: Branching ratios of CKM-suppressed $B_c \rightarrow PV$ bottom-changing decays. For the definitions of Type-II, Type-II*, and Type-I, refer to the caption of Table IV.

Decay	Type-II		Type-II*		Type-I	
	$N_c = \infty$	$N_c = 3$	$N_c = \infty$	$N_c = 3$	$N_c = \infty$	$N_c = 3$
$\Delta b = -1, \Delta C = -1, \Delta S = 1$						
$B_c^+ \rightarrow K^+ J/\psi$	1.45×10^{-4}	1.23×10^{-4}	1.45×10^{-4}	1.23×10^{-4}	1.01×10^{-4}	8.58×10^{-5}
$B_c^+ \rightarrow \bar{D}^0 D_s^{*+}$	1.77×10^{-6}	3.66×10^{-7}	1.96×10^{-6}	3.72×10^{-7}	5.90×10^{-7}	1.12×10^{-7}
$B_c^+ \rightarrow D_s^+ \bar{D}^{*0}$	2.09×10^{-6}	3.97×10^{-7}	2.11×10^{-6}	4.01×10^{-7}	1.90×10^{-6}	3.61×10^{-7}
$B_c^+ \rightarrow \eta_c K^{*+}$	2.22×10^{-4}	1.89×10^{-4}	2.22×10^{-4}	1.89×10^{-4}	2.20×10^{-4}	1.87×10^{-4}
$\Delta b = -1, \Delta C = 0, \Delta S = 0$						
$B_c^+ \rightarrow \pi^0 D^{*+}$	4.78×10^{-8}	9.08×10^{-9}	4.78×10^{-8}	9.09×10^{-9}	2.06×10^{-8}	3.91×10^{-9}
$B_c^+ \rightarrow \pi^+ D^{*0}$	1.78×10^{-6}	1.51×10^{-6}	1.78×10^{-6}	1.51×10^{-6}	7.64×10^{-7}	6.50×10^{-7}
$B_c^+ \rightarrow \eta D^{*+}$	3.10×10^{-8}	5.90×10^{-9}	3.12×10^{-8}	5.92×10^{-9}	1.14×10^{-8}	2.16×10^{-9}
$B_c^+ \rightarrow \eta' D^{*+}$	1.88×10^{-8}	3.57×10^{-9}	1.89×10^{-8}	3.60×10^{-9}	5.76×10^{-9}	1.10×10^{-9}
$B_c^+ \rightarrow D^+ \rho^0$	9.48×10^{-8}	1.80×10^{-8}	9.53×10^{-8}	1.81×10^{-8}	9.22×10^{-8}	1.75×10^{-8}
$B_c^+ \rightarrow D^+ \omega$	5.92×10^{-9}	1.12×10^{-9}	5.95×10^{-9}	1.13×10^{-9}	5.75×10^{-9}	1.09×10^{-9}
$B_c^+ \rightarrow D^+ \phi$	9.31×10^{-8}	1.77×10^{-8}	9.38×10^{-8}	1.78×10^{-8}	8.95×10^{-8}	1.70×10^{-8}
$B_c^+ \rightarrow D^+ J/\psi$	1.17×10^{-4}	1.39×10^{-4}	1.17×10^{-4}	1.40×10^{-4}	7.89×10^{-5}	9.68×10^{-5}
$B_c^+ \rightarrow D^0 \rho^+$	3.52×10^{-6}	3.00×10^{-6}	3.54×10^{-6}	3.02×10^{-6}	3.43×10^{-6}	2.92×10^{-6}
$B_c^+ \rightarrow \eta_c D^{*+}$	1.02×10^{-4}	1.22×10^{-4}	9.93×10^{-5}	1.22×10^{-4}	1.16×10^{-4}	1.11×10^{-4}

Table XII: Branching ratios of CKM-doubly-suppressed $B_c \rightarrow PV$ bottom-changing decays. For the definitions of Type-II, Type-II*, and Type-I, refer to the caption of Table IV.

Decay	Type-II		Type-II*		Type-I	
	$N_c = \infty$	$N_c = 3$	$N_c = \infty$	$N_c = 3$	$N_c = \infty$	$N_c = 3$
$\Delta b = -1, \Delta C = 1, \Delta S = 1$						
$B_c^+ \rightarrow D^0 D_s^{*+}$	1.45×10^{-6}	3.54×10^{-6}	1.50×10^{-6}	3.62×10^{-6}	1.88×10^{-6}	2.86×10^{-6}
$B_c^+ \rightarrow D_s^+ D^{*0}$	3.31×10^{-6}	6.14×10^{-6}	3.39×10^{-6}	6.26×10^{-6}	2.29×10^{-7}	1.45×10^{-6}
$\Delta b = -1, \Delta C = 1, \Delta S = 0$						
$B_c^+ \rightarrow D^+ D^{*0}$	1.30×10^{-7}	2.08×10^{-7}	1.33×10^{-7}	2.12×10^{-7}	1.29×10^{-8}	4.94×10^{-8}
$B_c^+ \rightarrow D^0 D^{*+}$	8.18×10^{-8}	1.65×10^{-7}	8.35×10^{-8}	1.68×10^{-7}	1.06×10^{-7}	1.33×10^{-7}

Table XIII: Branching ratios of $B_c \rightarrow PV$ bottom-conserving decays of other models.

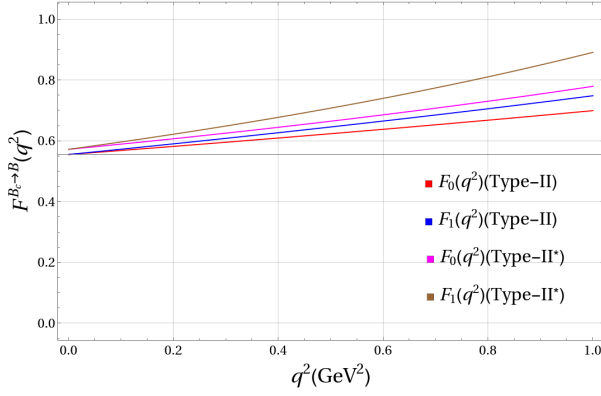
Decay	RIQM [36]	RCQM[33]	RQM[31]	QCDF [40]
$B_c^+ \rightarrow \pi^+ B_s^{*0}$	8.61×10^{-2}	2.1×10^{-2}	1.6×10^{-2}	–
$B_c^+ \rightarrow \bar{K}^0 B^{*+}$	2.26×10^{-2}	8.8×10^{-4}	1.1×10^{-3}	–
$B_c^+ \rightarrow B^+ \bar{K}^{*0}$	1.83×10^{-2}	1.1×10^{-3}	9.0×10^{-4}	3.72×10^{-3}
$B_c^+ \rightarrow B_s^0 \rho^+$	9.97×10^{-2}	2.3×10^{-2}	1.4×10^{-2}	4.44×10^{-2}
$B_c^+ \rightarrow K^+ B_s^{*0}$	4.99×10^{-3}	1.3×10^{-3}	1.1×10^{-3}	–
$B_c^+ \rightarrow \pi^+ B^{*0}$	5.55×10^{-3}	5.7×10^{-4}	2.6×10^{-4}	–
$B_c^+ \rightarrow \pi^0 B^{*+}$	4.70×10^{-4}	2.0×10^{-5}	1.0×10^{-5}	–
$B_c^+ \rightarrow B^+ \rho^0$	1.06×10^{-3}	7.1×10^{-5}	5.0×10^{-5}	2.86×10^{-4}
$B_c^+ \rightarrow B^+ \omega$	–	–	–	2.05×10^{-4}
$B_c^+ \rightarrow B^0 \rho^+$	1.30×10^{-2}	2.0×10^{-3}	1.3×10^{-3}	5.32×10^{-3}
$B_c^+ \rightarrow B_s^0 K^{*+}$	4.00×10^{-4}	1.1×10^{-4}	3.0×10^{-5}	1.25×10^{-4}
$B_c^+ \rightarrow K^+ B^{*0}$	3.90×10^{-4}	3.6×10^{-5}	4.0×10^{-5}	–
$B_c^+ \rightarrow B^+ K^{*0}$	–	–	–	1.07×10^{-5}
$B_c^+ \rightarrow B^0 K^{*+}$	3.20×10^{-5}	4.8×10^{-5}	4.0×10^{-5}	1.06×10^{-4}

 Table XIV: Branching ratios of $B_c^+ \rightarrow D_{(s)}^{(*)+} \bar{D}^{(*)0}$ and $D_{(s)}^{(*)+} D^{(*)0}$ bottom-changing decays of other models.

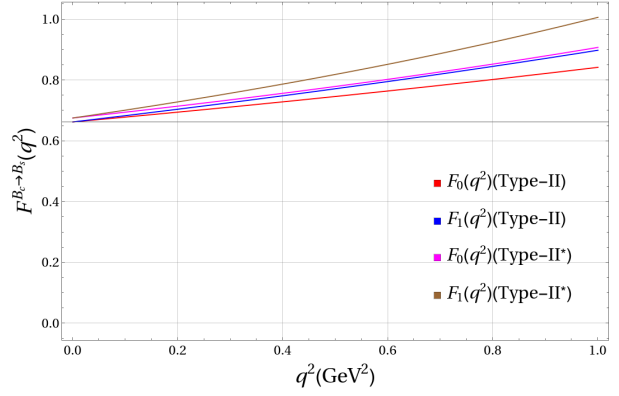
Decay	RIQM [36]	pQCD [38]	RCQM[33]	PDG [12]
$B_c^+ \rightarrow D^0 D_s^{*+}$	4.18×10^{-7}	2.5×10^{-6}	9.3×10^{-6}	$< 9.0 \times 10^{-4}$
$B_c^+ \rightarrow D_s^+ D^{*0}$	2.25×10^{-7}	1.9×10^{-6}	1.3×10^{-6}	$< 6.6 \times 10^{-4}$
$B_c^+ \rightarrow D^+ D^{*0}$	8.00×10^{-9}	7.0×10^{-8}	5.2×10^{-8}	$< 3.7 \times 10^{-4}$
$B_c^+ \rightarrow D^0 D^{*+}$	1.80×10^{-8}	9.0×10^{-8}	4.4×10^{-7}	$< 2.0 \times 10^{-4}$
$B_c^+ \rightarrow \bar{D}^0 D_s^{*+}$	3.15×10^{-7}	7.0×10^{-8}	6.5×10^{-7}	$< 5.3 \times 10^{-4}$
$B_c^+ \rightarrow D_s^+ \bar{D}^{*0}$	4.91×10^{-7}	2.6×10^{-7}	2.4×10^{-6}	$< 4.6 \times 10^{-4}$
$B_c^+ \rightarrow \bar{D}^0 D^{*+}$	1.60×10^{-6}	1.2×10^{-6}	8.8×10^{-6}	$< 3.8 \times 10^{-4}$
$B_c^+ \rightarrow D^+ \bar{D}^{*0}$	2.61×10^{-5}	3.4×10^{-6}	3.8×10^{-5}	$< 6.5 \times 10^{-4}$

 Table XV: Branching ratios of $B_c \rightarrow PV$ bottom-changing decays of other models.

Decay	CLFQM (Type-I)[28]	RIQM [37]	pQCD [39]	RCQM[33]
$B_c^+ \rightarrow D_s^+ J/\psi$	6.09×10^{-3}	1.15×10^{-3}	8.05×10^{-3}	3.4×10^{-3}
$B_c^+ \rightarrow D^+ J/\psi$	2.00×10^{-4}	3.69×10^{-5}	2.80×10^{-4}	1.5×10^{-4}
$B_c^+ \rightarrow K^+ J/\psi$	1.60×10^{-4}	3.00×10^{-5}	1.90×10^{-4}	1.3×10^{-4}
$B_c^+ \rightarrow \pi^+ J/\psi$	1.97×10^{-3}	3.80×10^{-4}	2.33×10^{-3}	1.7×10^{-3}
$B_c^+ \rightarrow \eta_c D_s^{*+}$	6.97×10^{-3}	2.16×10^{-3}	1.65×10^{-2}	3.7×10^{-3}
$B_c^+ \rightarrow \eta_c D^{*+}$	3.10×10^{-4}	7.60×10^{-5}	5.80×10^{-4}	1.9×10^{-4}
$B_c^+ \rightarrow \eta_c K^{*+}$	3.40×10^{-4}	6.30×10^{-5}	5.70×10^{-4}	2.5×10^{-4}
$B_c^+ \rightarrow \eta_c \rho^+$	6.01×10^{-3}	1.20×10^{-3}	9.83×10^{-3}	4.5×10^{-3}

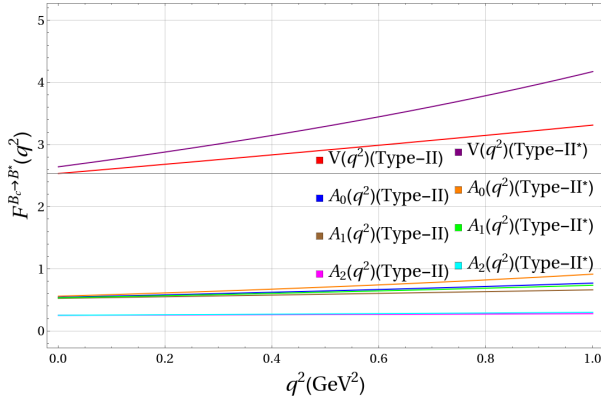


(a) $B_c \rightarrow B$ transition

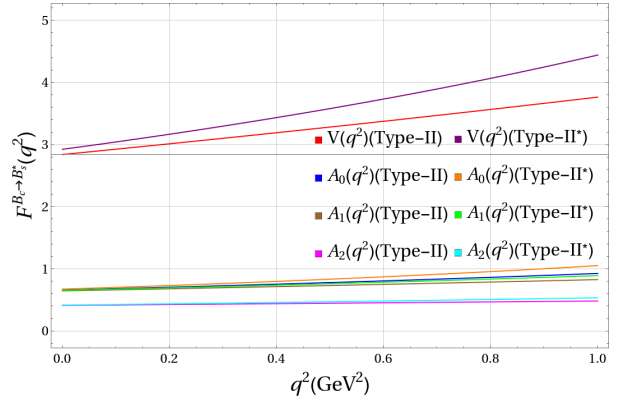


(b) $B_c \rightarrow B_s$ transition

Figure 2: q^2 dependence of bottom-conserving $B_c \rightarrow P$ form factors in Type-II (Type-II*) CLFQM using Eq. (37) (Eq. (38)).

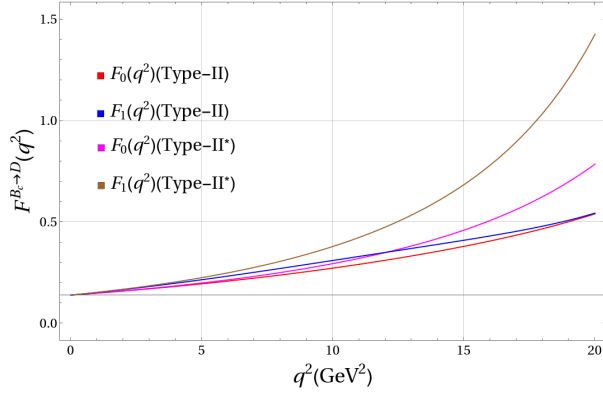


(a) $B_c \rightarrow B^*$ transition

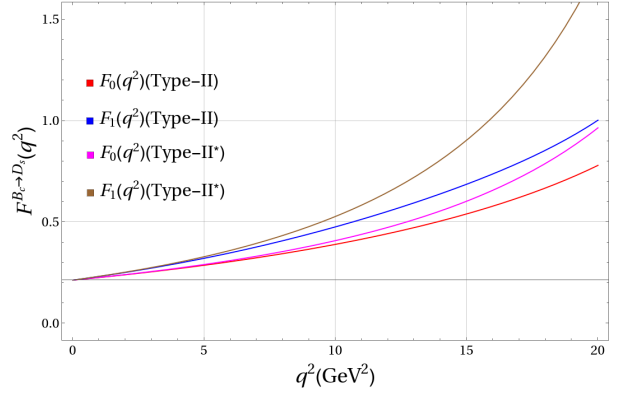


(b) $B_c \rightarrow B_s^*$ transition

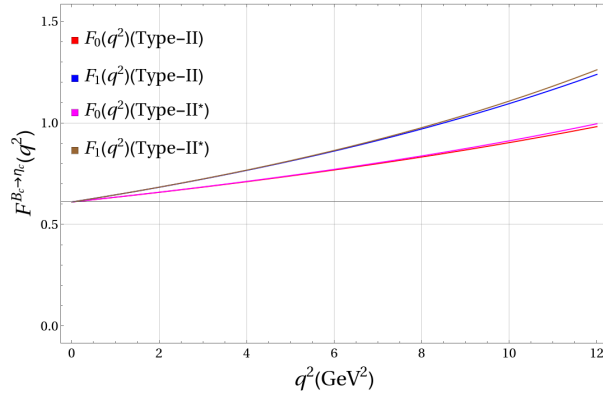
Figure 3: q^2 dependence of bottom-conserving $B_c \rightarrow V$ form factors in Type-II (Type-II*) CLFQM using Eq. (37) (Eq. (38)).



(a) $B_c \rightarrow D$ transition

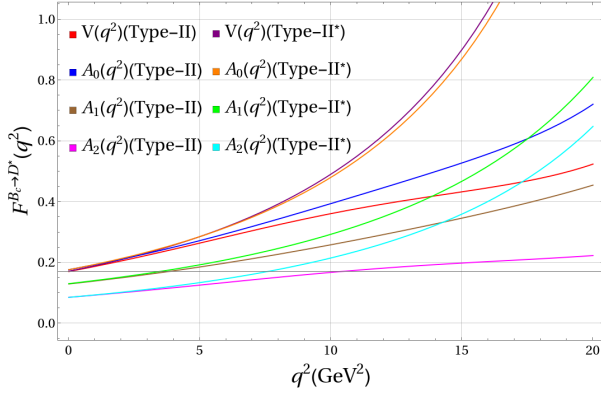


(b) $B_c \rightarrow D_s$ transition

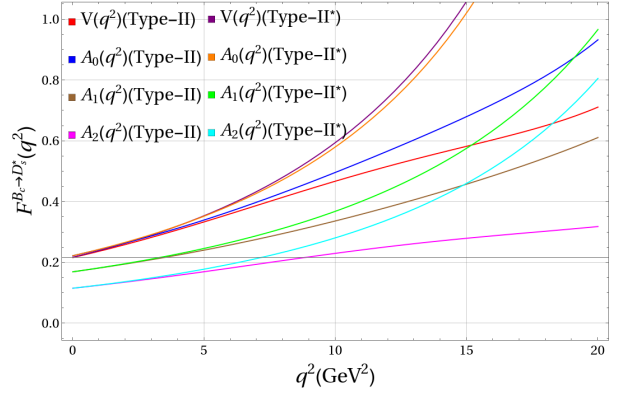


(c) $B_c \rightarrow \eta_c$ transition

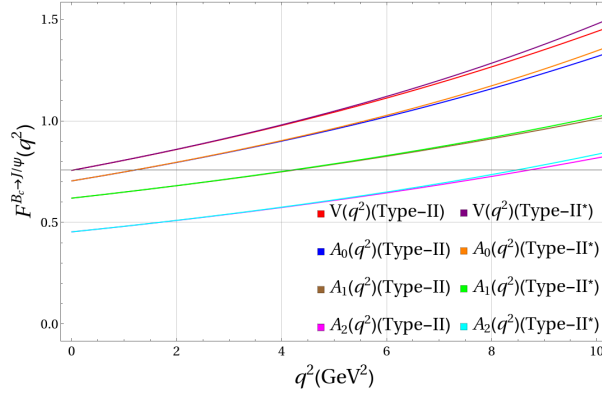
Figure 4: q^2 dependence of bottom-changing $B_c \rightarrow P$ form factors in Type-II (Type-II*) CLFQM using Eq. (37) (Eq. (38)).



(a) $B_c \rightarrow D^*$ transition

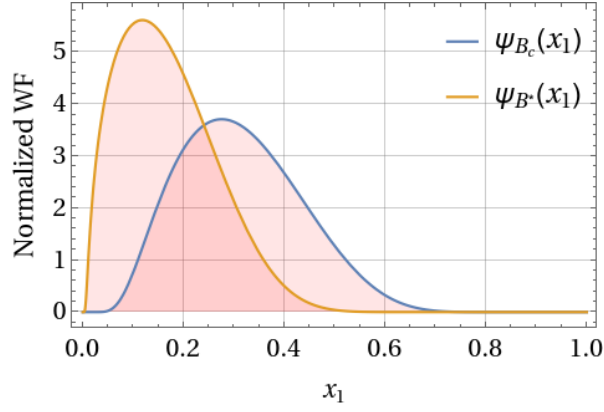


(b) $B_c \rightarrow D_s^*$ transition

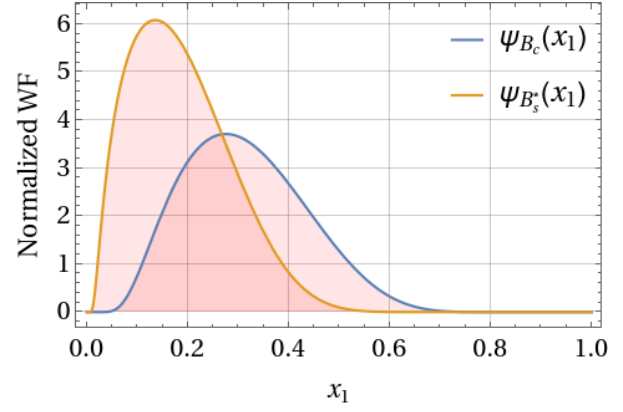


(c) $B_c \rightarrow J/\psi$ transition

Figure 5: q^2 dependence of bottom-changing $B_c \rightarrow V$ form factors in Type-II (Type-II*) CLFQM using Eq. (37) (Eq. (38)).



(a) B_c and B^* (Overlap area = 0.668)



(b) B_c and B_s^* (Overlap area = 0.775)

Figure 6: Overlap plots of B_c and B^* , B_s^* light-front wave function using Eq. (5), in Type-II CLFQM. Note that overlap plots of B_c and B , B_s wave function are similar to B^* , B_s^* , with roughly 10% increase in overlap area.

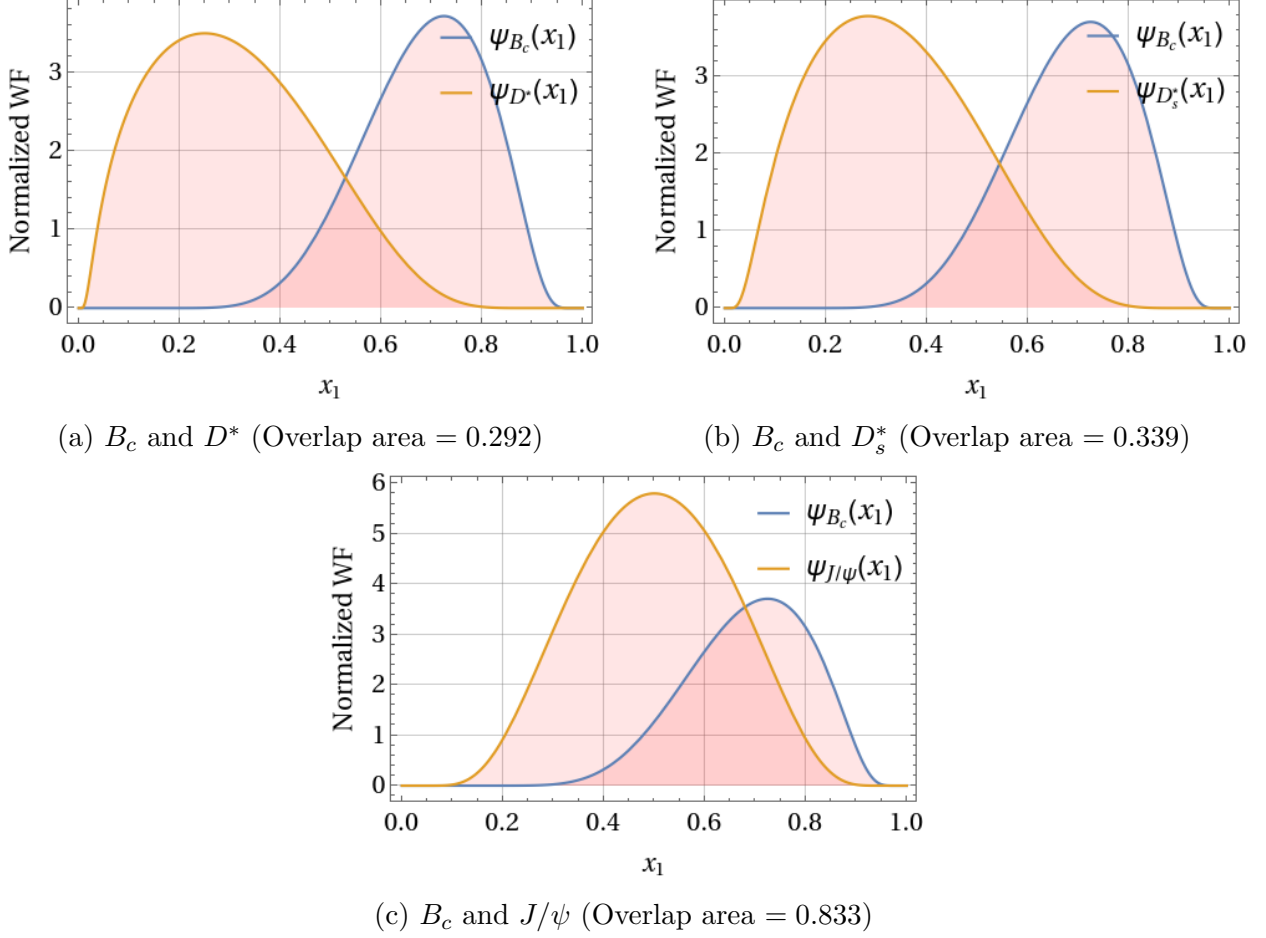


Figure 7: Overlap plots of B_c and D^* , D_s^* , J/ψ light-front wave function using Eq. (5), in Type-II CLFQM. Note that overlap plots of B_c and D , D_s , η_c wave function will be similar; however, we notice approximately 15% and 28% change between B_c and D , η_c , as well as between B_c and D_s , respectively.

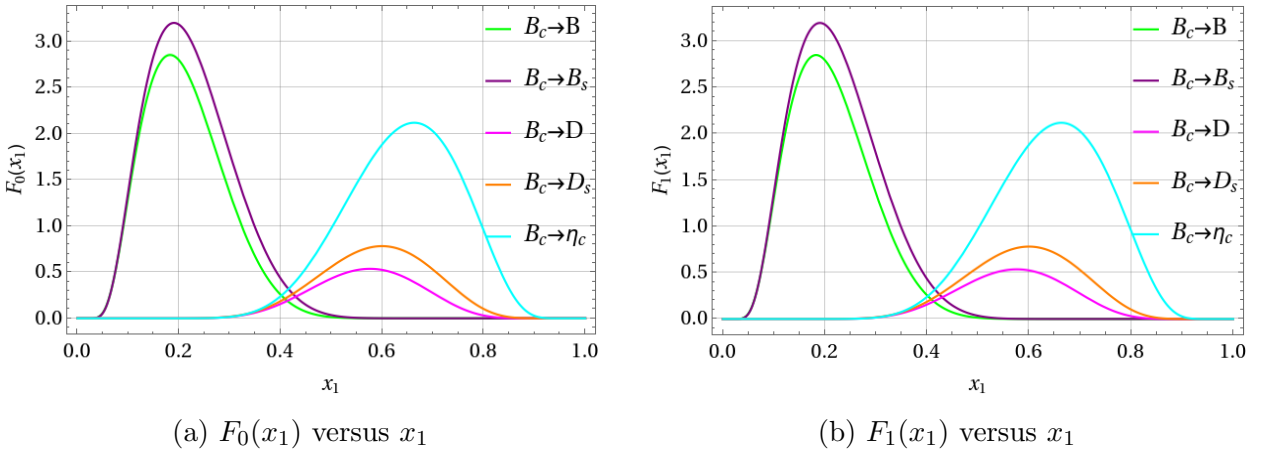
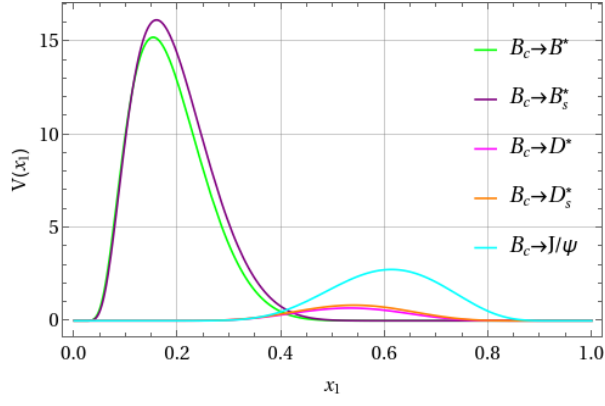
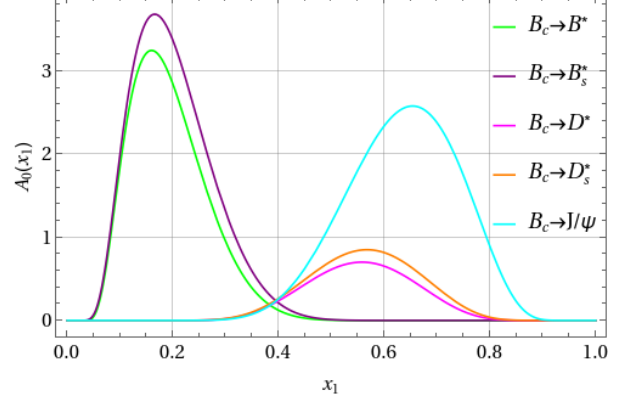


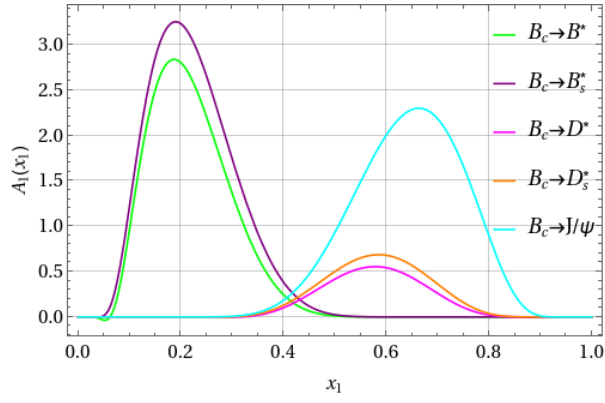
Figure 8: Dependence of form factor, $F(x_1)$ on x_1 for $B_c \rightarrow P$ transition at $q^2 = 0 \text{ GeV}^2$, in Type-II CLFQM using Eq. (27).



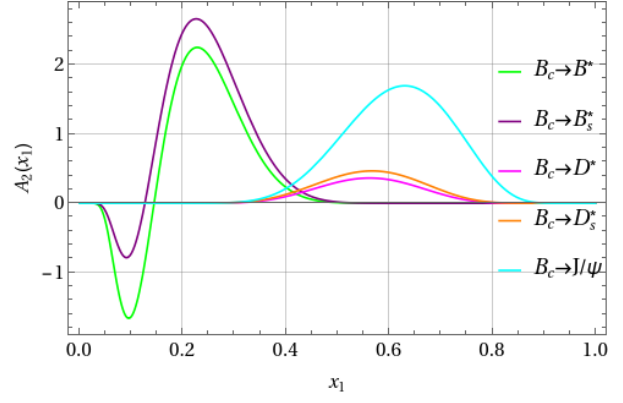
(a) $V(x_1)$ versus x_1



(b) $A_0(x_1)$ versus x_1

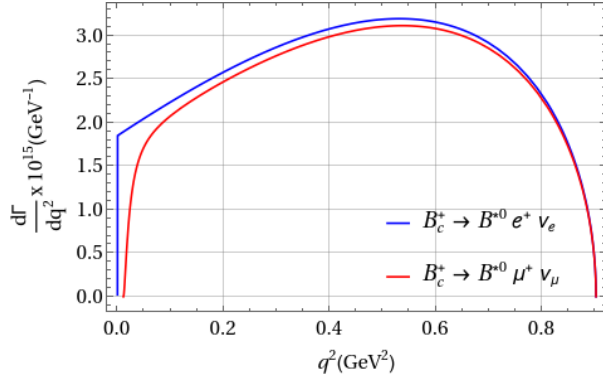


(c) $A_1(x_1)$ versus x_1

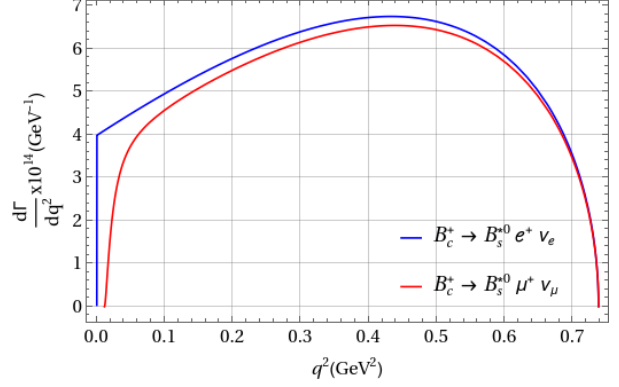


(d) $A_2(x_1)$ versus x_1

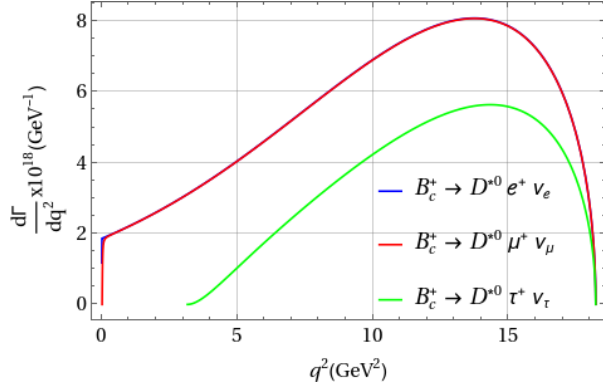
Figure 9: Dependence of form factor, $F(x_1)$ on x_1 for $B_c \rightarrow V$ transition at $q^2 = 0 \text{ GeV}^2$, in Type-II CLFQM using Eq. (27).



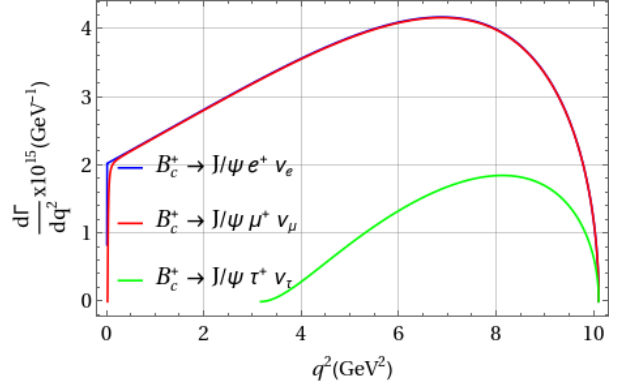
(a) $B_c^+ \rightarrow B^* l^+ \nu_l$



(b) $B_c^+ \rightarrow B_s^* l^+ \nu_l$

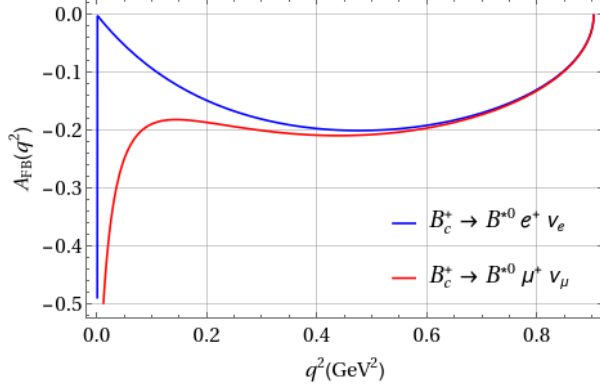


(c) $B_c^+ \rightarrow D^* l^+ \nu_l$

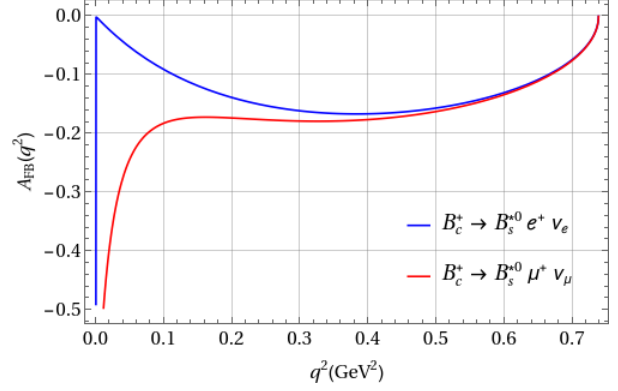


(d) $B_c^+ \rightarrow J/\psi l^+ \nu_l$

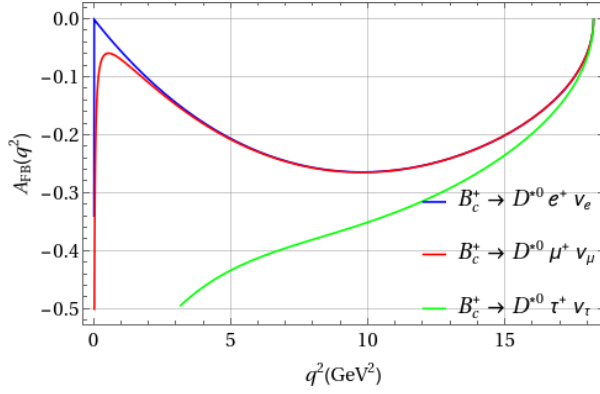
Figure 10: q^2 variation of differential decay rates of $B_c^+ \rightarrow V l^+ \nu_l$ decays in Type-II CLFQM using Eq. (50).



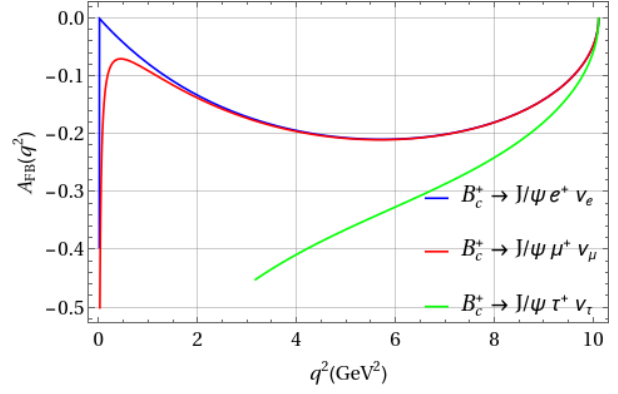
(a) $B_c^+ \rightarrow B^{*0} l^+ \nu_l$



(b) $B_c^+ \rightarrow B_s^{*0} l^+ \nu_l$



(c) $B_c^+ \rightarrow D^{*0} l^+ \nu_l$



(d) $B_c^+ \rightarrow J/\psi l^+ \nu_l$

Figure 11: q^2 variation of forward-backward asymmetries of $B_c^+ \rightarrow V l^+ \nu_l$ decays in Type-II CLFQM using Eq. (50).